Molecular Mechanisms of Aβ Peptide Aggregation and Interaction with Microglia via TREM2

Dissertation

zur

Erlangung des Doktorgrades (Dr. rer. nat.)

der

Mathematisch-Naturwissenschaftlichen Fakultät

der

Rheinischen Friedrich-Wilhelms-Universität Bonn

vorgelegt von

Florian Raphael Riffel

Aus Dahn

Bonn 2023

Angefertigt mit Genehmigung der Mathematisch-Naturwissenschaftlichen Fakultät
der Rheinischen Friedrich-Wilhelms-Universität Bonn

1. Gutachter: Prof. Dr. Jochen Walter

2. Gutachter: Prof. Dr. Thorsten Lang

Tag der Promotion: 02.11.23

Erscheinungsjahr: 2024

Additional Information

Parts of this work have already been published as part of the following publications:

Joshi, P., F. Riffel, S. Kumar, N. Villacampa, S. Theil, S. Parhizkar, C. Haass, M. Colonna, M. T. Heneka, T. Arzberger, J. Herms and J. Walter (2021). "TREM2 modulates differential deposition of modified and non-modified Aβ species in extracellular plaques and intraneuronal deposits." Acta Neuropathol Commun **9**(1): 168. DOI: 10.1186/s40478-021-01263-x

Joshi, P., F. Riffel, K. Satoh, M. Enomoto, S. Qamar, H. Scheiblich, N. Villacampa, S. Kumar, S. Theil, S. Parhizkar, C. Haass, M. T. Heneka, P. E. Fraser, P. St George-Hyslop and J. Walter (2021). "Differential interaction with TREM2 modulates microglial uptake of modified Aβ species." Glia **69**(12): 2917-2932. DOI: 10.1002/glia.24077

Kumar, S., A. Kapadia, S. Theil, P. Joshi, F. Riffel, M. T. Heneka and J. Walter (2020). "Novel Phosphorylation-State Specific Antibodies Reveal Differential Deposition of Ser26 Phosphorylated Aβ Species in a Mouse Model of Alzheimer's Disease." Front Mol Neurosci **13**: 619639. DOI: 10.3389/fnmol.2020.619639

Abstract

Alzheimer's disease (AD) is a progressive neurodegenerative disorder accompanied by a decline in cognitive functions. It is estimated that roughly 50 million people are currently suffering from AD, a number that is thought to triple within the next 20 years, thereby making AD the most common form of dementia. Neuropathological hallmarks of the disease are extracellular senile plaques, formed by neurotoxic amyloid beta peptides (Aβ), and neurofibrillary tangles containing hyperphosphorylated forms of tau. The importance of Aβ in AD pathogenesis is also reflected in the identification of certain rare mutations in the amyloid precursor protein (APP) as well as in proteins involved in its processing, namely presenilin-1 and 2 (PS1, PS2), which lead to early-onset familial AD (FAD). But since these only account for less than 5 % of all cases, a large ambiguity persists about the cause of the more common sporadic form of the disease (SAD). Interestingly, recent genome-wide association studies (GWAS) were able to identify a novel genetic risk factor encoding TREM2 that is involved in microglial function and inflammation. In addition to that, previous studies indicated that phosphorylation of Aβ might be another important factor contributing to SAD by changing the aggregation behaviour, conformation, and stability of Aβ peptides.

This study aimed, therefore, to develop a model to investigate the interaction between TREM2 and differentially modified Aβ species. This was achieved by the recombinant expression and purification of the ligand-binding domain of TREM2 coupled to the Fc region of the human IgG1 heavy chain (sTREM2-Fc).

By using this sTREM2-Fc, it was possible to show that TREM2 preferentially interacts with Aβ in its oligomeric rather than monomeric form. Furthermore, TREM2 showed increased binding to Aβ variants phosphorylated at serine 8 and serine 26 in comparison to its non-phosphorylated form. However, this interaction did not translate to increased activation of downstream signalling but did show a potential effect on Aβ aggregation and subsequent uptake in microglia. Thus, sTREM2-Fc presented as an appropriate model for studying interactions in-vitro, and the resulting observations could underline the importance of TREM2 in sensing and interacting with different Aβ species depending on phosphorylation and aggregation state.

CONTENTS

List of Tables

List of Figures

List of Abbreviations and Acronyms

%	Percent
°C	Degree Celsius
aa	Amino acids
Aβ	Amyloid β peptide
AD	Alzheimer disease
ADAM	A disintegrin and metalloprotease
ApoE	Apolipoprotein E
APP	Amyloid precursor protein
APS	Ammonium persulfate
a.u.	Arbitrary units
BACE	Beta-site APP cleaving enzyme
BSA	Bovine serum albumin
CSF	Cerebrospinal fluid
c-terminus	Carboxy-terminus
CTF	C-terminal fragment
DAP12	DNAX activation protein of 12 kDa
DAPI	4’,6-Diamidin-2-phenyl indol
dH_2O	Distilled water
DMEM	Dulbecco’s Modified Eagle Medium
DMSO	Dimethyl sulfoxide
DNA	Deoxyribonucleic acid
dNTP	Deoxynucleotide triphosphate
DPBS	Dulbecco's phosphate-buffered saline

DTT	Dithiothreitol
E. coli	Escherichia coli
ECL	Enhanced chemiluminescence
EDTA	Ethylenediaminetetraacetic acid
ER	Endoplasmic reticulum
FAD	Familial Alzheimer disease
FBS	Foetal bovine serum
FRT	Flp recombination target
FTD	Frontotemporal dementia
GWAS	Genome-wide association studies
HEK	Human embryonic kidney cells
HRP	Horseradish peroxidase
ICC	Immunocytochemistry
ICD	Intracellular domain
ITAM	Immunoreceptor tyrosine-based activation motif
kDa	Kilodalton
LB	Lysogeny Broth
LOAD	Late-onset AD
MEM	Minimum Essential Medium Eagle
mTOR	Mechanistic target of rapamycin
NaDOC	Deoxycholic acid
NHD	Nasu-Hakola disease
NFT	Neurofibrillary tangles
Nt	Nucleotides
N-terminus	Amino-terminus
PBS	Phosphate buffered saline

PBST	Phosphate buffered saline with 0.05% Tween-20
PCR	Polymerase chain reaction
PFA	Paraformaldehyde
PDL	Poly-L-lysine
PLL	Poly-D-lysine
PSEN	Presenilin
PS	Phosphatidylserine
PTM	Post-translational modification
RNA	Ribonucleic acid
rpm	Revolutions per minute
RT	Room temperature
SAD	Sporadic Alzheimer disease
SD	Standard deviation
SEM	Standard error of the mean
SDS	Sodium dodecyl sulfate
SDS-PAGE	Sodium dodecyl sulphate-polyacrylamide gel electrophoresis
SOC	Super optimal broth with catabolite repression
sTREM	Soluble TREM
SYK	Spleen tyrosine kinase
TCA	Trichloroacetic acid
TEMED	Tetramethyl ethylenediamine
TREM	Triggering receptor expressed on myeloid cells
WB	Western blot
WT	Wild-type

1 INTRODUCTION

1.1 Neurodegenerative diseases (NDs)

Neurodegenerative disease (ND) is an umbrella term for diseases that are defined by a progressive loss of brain function as well as bodily functions controlled by the respective part of the brain. Hereby, neurodegenerative diseases can manifest in impairment or even loss of, for example, speech, movement, stability, and balance (Lamptey, Chaulagain et al. 2022). The loss of brain functions originates from dysfunctional or dying neurons. This effect is especially detrimental considering that the majority of neurons are produced during embryogenesis and the formation of new neurons, which could replace lost neurons, is strongly reduced in adulthood (Ganat, Silbereis et al. 2006). Furthermore, many NDs are characterised by the progressive deposition of misfolded proteins (Taylor, Hardy et al. 2002), as well as dysfunctions in synaptic signalling and plasticity (Hoover, Reed et al. 2010). The most common NDs are Alzheimer's disease (AD), Parkinson's disease (PD), amyotrophic lateral sclerosis (ALS), and Huntington's disease (HD). While there are different underlying genetics and pathophysiological manifestations, all diseases share common hallmarks like neuroinflammation, loss of neurons, and pathological protein aggregation. Whereas the cause of the disease for most of these is not fully understood yet, all of them show a strong correlation between age and onset, making them of uttermost global importance, not just socially but also economically, considering the continuous increase in life expectancy (Ward, Zucca et al. 2014). Predictions are that the population of people over 60 will further rise and will have almost tripled in the span between 2000 (600 million) and 2050 (2.1 billion). As the onset of most ND increases drastically over the age of 60, a large number of those people will have to spend their

lives under the restrictions of a disease, thereby burdening not just the common health care system but also their social environment (Prince, Wimo et al. 2015).

1.2 Alzheimer's disease (AD)

Alzheimer's disease is the most common cause of dementia worldwide. It is estimated that roughly 55 million people were suffering from dementia in the year 2020 (Prince, Wimo et al. 2015). Alzheimer's disease is characterised by progressive memory loss and irreversible cognitive decline. The German psychiatrist Alois Alzheimer was the first to describe and further investigate the disease. Already in 1906, he described two peculiar formations in the brain of his patient, later known as neurofibrillary tangles (NFTs) as well as plaques, which consist of an accumulation of the amyloid beta peptide (Aβ) (Alzheimer 1906). Until today, the formation of extracellular so-called senile plaques from the Aβ peptide is one of the major hallmarks of the disease (Masters, Simms et al. 1985, Goedert, Sisodia et al. 1991, Hardy and Allsop 1991) together with the development of neurofibrillary tangles resulting from intracellular accumulation of hyperphosphorylated tau (Grundke-Iqbal, Iqbal et al. 1986). The accumulation of senile plaques as well as NFTs is usually accompanied by a progressive loss of neurons, most notably in the medial temporal lobe and neocortical structures (De-Paula, Radanovic et al. 2012).

Like other neurodegenerative diseases, age is one of the major risk factors for AD. With the increasing shift in overall age in today's societies comes an increased prevalence of AD. Every year, there are 10 million new confirmed cases worldwide, stating that every 3.2 seconds someone is developing dementia (Prince, Wimo et al. 2015). Furthermore, Alzheimer's Disease International (ADI) published in their recent annual report that 75 % of all dementia cases are probably not even diagnosed. With AD being the second most expensive disease in terms of medical expenditures after cancer, this leads to a huge burden on modern society's healthcare system and also on family members, who are often involved in caretaking especially in the early phases of the disease. After more than a century of ongoing research since its discovery is still a large majority of its underlying biology not understood. So, it is not surprising that so far only a limited number of pharmaceutical therapies have been proposed, even less approved, to intervene with the disease progression (Graham, Bonito-Oliva et al. 2017, Mortada, Farah et al. 2021, Lamptey, Chaulagain et al. 2022). A major problem with AD is the lack of confirmed biological markers, which would help in its early detection, but also because the onset of AD is

usually preceded by a long symptom-free phase before the first clinical symptoms appear. From all the investigations over the past years, for a long time, the amyloid cascade hypothesis and the cholinergic hypothesis had emerged as two of the leading theories to explain AD pathogenesis. The cholinergic hypothesis, which postulated a strong correlation between impaired function of the cholinergic system and decline of cognitive functions in AD, led to quite an increase in the investigation of neurotransmitter and cholinergic therapeutic invention. And while establishing cholinergic therapies proved to be a valid approach for drug development, it still failed to explain overall disease progression (Terry and Buccafusco 2003). For that reason, the amyloid cascade hypothesis became the leading theory for AD.

1.2.1 Proteolytic processing of APP and the amyloid cascade hypothesis

Fundamentally, the amyloid cascade hypothesis states that Aβ deposition is the crucial step in AD initiation. Hereby, Aβ is generated from the amyloid precursor protein (APP) via sequential cleavage by the β-secretase (amyloidogenic pathway) and by γ-secretase releasing Aβ into the extracellular space (**Figure 1**)(Uddin, Kabir et al. 2020).

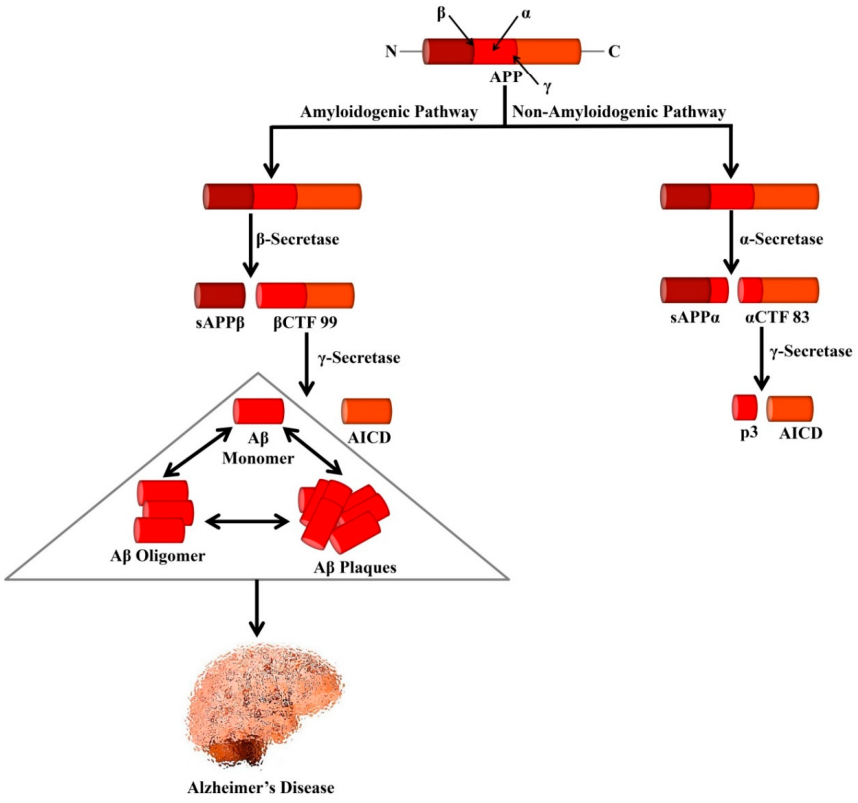

Figure 1 Amyloid precursor protein (APP) cleavage via amyloidogenic or non-amyloidogenic pathway.

In the non-amyloidogenic or non-disease-associated pathway, APP is cleaved sequentially by an α-secretase and a γ-secretase. The former releasing soluble APPα (sAPPα) in the extracellular space, while the latter cleaves the resulting c-terminal fragment (αCTF 83) into the APP intracellular fragment (AICD) and the p3 peptide. In the amyloidogenic pathway, APP is cleaved initially by a β-secretase releasing again a soluble form of APP (sAPPβ) as well as βCTF 99, which is subsequently processed by γ-secretase releasing Aβ as well as the APP intracellular fragment (AICD). The so generated hydrophobic Aβ peptide is prone to aggregation and further plaque formation. Figure adapted from Uddin, Kabir et al. 2020

Because of its hydrophobic nature, Aβ will start to self-aggregate first into aggregates containing a small number of monomers (so-called oligomers), later into full-grown fibres, which will finally deposit as macroscopic plaques (Karran and De Strooper 2016, Selkoe and Hardy 2016).

The accumulation of Aβ, especially of oligomers, the proposed "toxic" species, will eventually provoke an immune response and neuro-inflammation, which will ultimately end in neuronal decay.

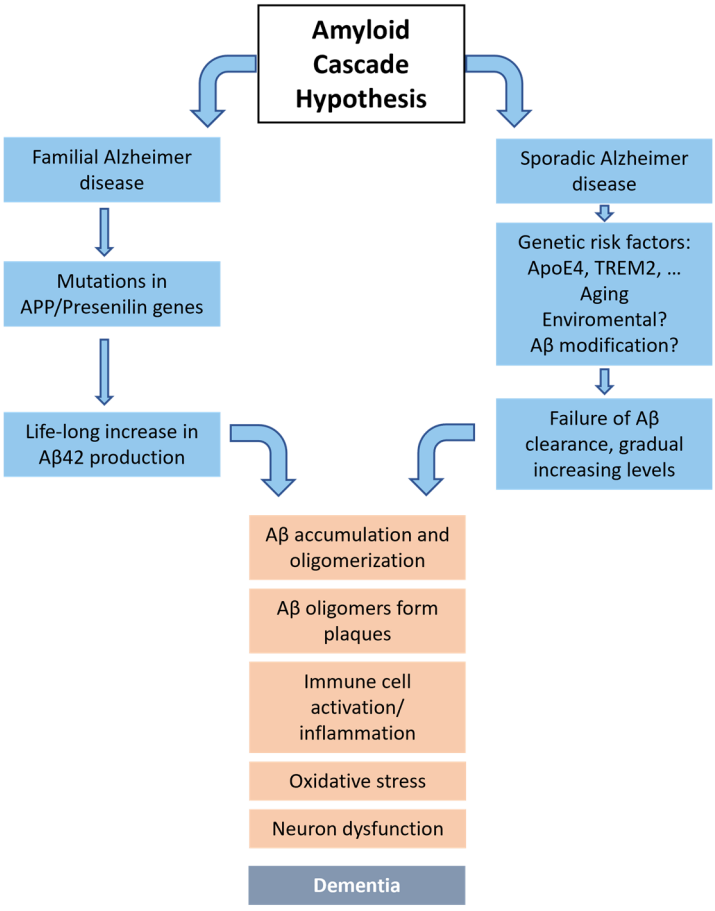

Figure 2 The amyloid cascade hypothesis.

The amyloid cascade hypothesis states that Aβ accumulation in the brain is the crucial step that ultimately leads to AD. In the familial form of AD, which is caused by autosomal dominant mutations occurring in either of three genes: presenilin 1 (PSEN1), PSEN2, or the amyloid precursor protein (APP), Aβ production is increased, leading to a life-long fast accumulation of the peptide. As a result, the peptide is prone to aggregation, which in turn also leads to the activation of immune cells, inflammation, oxidative stress, and finally neuronal dysfunction and death. A similar cascade is also proposed for the sporadic form of AD, but instead of the previously mentioned mutations, other factors like certain genetic risk factors, environmental factors, and aging-induced changes will lead to failure of Aβ clearance and ultimately also to a continuous accumulation of Aβ. Figure adapted from Selkoe and Hardy (2016)

This theory is further supported by the identification of mutations within or close to the Aβ domain, that increase the amount of Aβ produced, and as a result, lead to an early-onset familial form of AD (FAD). Furthermore, missense mutations within presenilin-1 or 2, which are the catalytic subunits of the γ-secretase complex, also increase Aβ production or Aβ 1-42/1-40 ratio significantly and are the leading cause of autosomal dominantly inherited forms of FAD (Goate, Chartier-Harlin et al. 1991, Levy-Lahad, Wasco et al. 1995, Sherrington, Rogaev et al. 1995)(**Figure 2**).

Also independent of these point mutations, the importance of Aβ production is seen when looking at patients with Down syndrome. These carry three identical chromosomes 21 (Trisomie-21) and thereby three copies of APP, leading to an early accumulation of protein deposits and other neuropathological hallmarks of AD (Choong, Tosh et al. 2015). As a result, these patients exhibit a high risk of developing early-onset AD (Prasher, Farrer et al. 1998, Fortea, Zaman et al. 2021). The importance of Aβ further solidifies when looking at the protective effect certain mutations exhibit. So, for example, does the mutation from alanine to threonine at position 673 protect against AD by decreasing the Aβ production and aggregation (Jonsson, Atwal et al. 2012). However, FAD only accounts for less than 10 % of all cases, while the majority of cases are the result of so-called sporadic AD (SAD), whose origin is much more heterogeneous and not fully understood. Nevertheless, SAD also provides evidence to support the amyloid hypothesis. So, show for example ApoE4 carriers, the biggest known genetic risk factor for SAD, decreased Aβ clearance from the brain compared to carriers of the non-disease-associated isoforms ApoE2 and ApoE3 (Corder, Saunders et al. 1993). Finally, during the diagnosis of sporadic AD via amyloid positron emission tomography (PET) and Aβ levels in cerebrospinal fluid (CSF) samples, low Aβ levels in CSF and a positive PET image usually precede other clinically related markers by years (Bateman, Xiong et al. 2012). Nevertheless, the amyloid hypothesis is not at last still under debate since most clinical trials targeting to reduce Aβ burden via pharmacological invention showed no or only very moderate success. This is probably due to the fact that most of the pharmacological studies focused on the disease after the first appearance of cognitive decline, where reduction of plaque load could not reverse neuronal deficits. For successful treatment, it is presumed that the formation of plaques has to be prevented at an early stage, even before clinical symptoms arrive. Finally, it is important to consider that Aβ is a highly heterogeneous protein. This heterogeneity is caused by several variables, such as variations in the protein's length (Aβ length can range from 37 to 49 amino acids), post-translational modifications (such as phosphorylation, glycosylation, and oxidation), and the presence of mutations that change the amino acid sequence of the protein (Kummer and

Heneka 2014). Consequently, it is calling for specific pharmacological agents targeting especially aggregation-prone and toxic species of the protein to unfold their full potential.

1.2.2 Protein misfolding accumulation and aggregation

One of the major characteristics of neurodegenerative diseases is the progressive build-up of toxic protein aggregates. Thereby, different NDs exhibit a different disease-specific protein involved in the pathogenesis and detection of the disease. Most commonly, those are Aβ in Alzheimer's disease (AD), α-synuclein in Parkinson's disease (PD), huntingtin in Huntington's disease (HD), Tau in frontotemporal dementia (FTD), TAR DNA-binding protein 43 (TDP43), and superoxide dismutase 1 (SOD1) in amyotrophic lateral sclerosis (ALS), ataxin proteins in spinocerebellar ataxias (SCAs), and PrP^{sc} in transmissible spongiform encephalopathy (TSEs)(Glenner and Wong 1984, DiFiglia, Sapp et al. 1997, Hutton, Lendon et al. 1998, Spillantini, Crowther et al. 1998, Weissmann 1999, Neumann, Sampathu et al. 2006, Hu, Do et al. 2019). However, there is no obvious relationship in terms of structure, size, or sequence between those proteins. Nevertheless, all of them undergo misfolding during disease progression, which ultimately ends in the formation of protein aggregates with peculiar β-sheet-rich structures (Chiti, Webster et al. 1999). Misfolded proteins usually undergo rapid transmission from small, unordered assemblies (oligomers) to large arrangements of fibrillary structure. Hereby, the individual protein molecules come together and stack on top of each other in a parallel or antiparallel manner, forming extended β-sheets that run perpendicular to the fibril axis, also referred to as cross-β-sheet structure (Sunde, Serpell et al. 1997). These higher-order structures within protein assemblies, which also present them with a peculiar interaction upon binding with Congo red (apple-green birefringence in polarized light (Howie and Owen-Casey 2010), are further defined as amyloids. One of the most investigated amyloids is, of course, the amyloid β peptide, as a key player in AD.

Since its first isolation from vessels (1984) and senile plaques (1985), the Aβ sequence has undergone extensive research (Glenner and Wong 1984, Masters, Simms et al. 1985). Biochemical and biophysical studies on the Aβ monomer have revealed that the peptide, varying in size between 37 and 49 aa, is mainly an intrinsically disordered peptide without a clearly defined three-dimensional structure (Zhang, Iwata et al. 2000, Ball, Phillips et al. 2011). Structurally, it was indicated that the dominant motif within the peptide is often of α-helical

nature, which converts to a β-sheet structure (Talafous, Marcinowski et al. 1994). This conformational change from an α-helical to β-sheet structure, as it is also proposed to happen during disease progression, is considered the initial step in increasing the hydrophobic nature of the peptide and thereby its self-assembly.

Aβ will then rapidly form a variety of different aggregation states, ranging from small oligomers with great heterogeneity in size and structure to protofibrils and fibrils. The latter, largely insoluble in nature in contrast to the very soluble oligomers, will finally deposit in plaques (**Figure 3**)(Faller and Hureau 2021). In vitro, this self-assembly is often described by an initial lag phase, where Aβ mainly exists in its monomeric and smaller oligomeric forms, followed by a rapid growth phase of different Aβ intermediates, and finally, a plateau phase where no further fibril formation can be observed anymore (Arosio, Knowles et al. 2015, Meisl, Kirkegaard et al. 2016). Researchers have identified several markers to track the different stages, mostly by exhibiting fluorescence upon binding to β-sheet-containing structures (Noël, Cadet et al. 2013). The most common of those is thioflavin T (ThT), a benzothiazole dye that increases in fluorescence upon binding to amyloid and will increase in fluorescence intensity relative to the amyloid fibril mass. The extraordinary efforts of researchers throughout the last decades have established that the aggregation of Aβ following its misfolding is a key triggering event in the pathogenesis of AD progression (Glenner and Wong 1984, Masters, Simms et al. 1985, Cleary, Walsh et al. 2005).

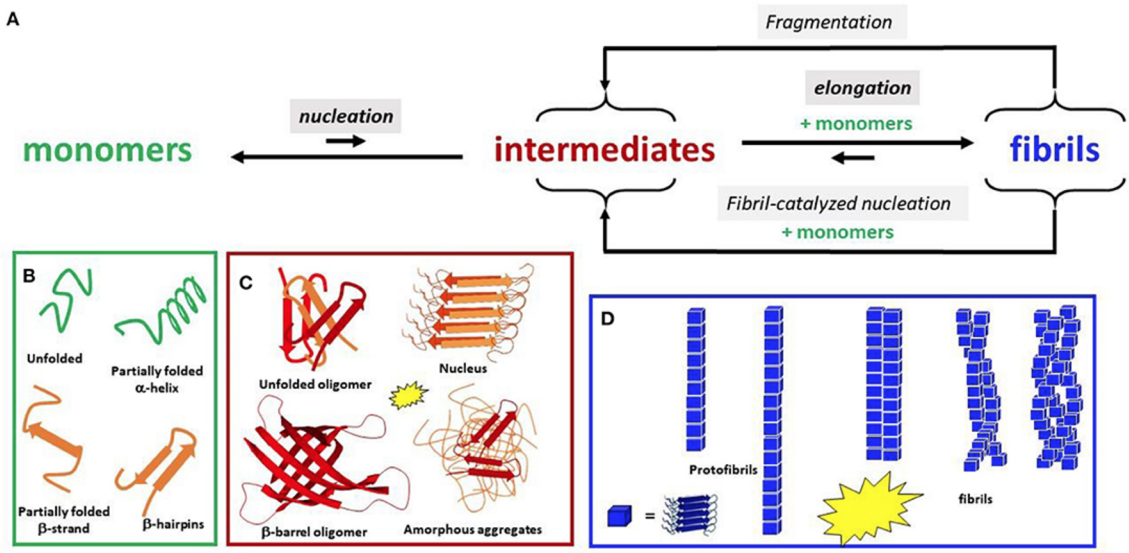

Figure 3 Schematic of the Aβ aggregation process.

A) Schematic overview of the Aβ assembly process. In the beginning, unfolded or partially unfolded Aβ (B) needs a nucleation event to start forming higher assemblies and oligomers (C), which are then able to form fibrils in an elongation phase by the continuous addition of monomers (D). These, in turn, are also able to be fragmented into smaller oligomers again or can catalyse the creation of more oligomers via surface interactions. The intensity of a fluorescent dye that can be used to detect the individual β-sheet conformations is indicated by the yellow stars. Figure adapted from Faller and Hureau 2021.

Nevertheless, the underlying mechanisms that influence misfolding and lead to its initialization or even regulate protein misfolding and aggregation are vast. Thus, it was already demonstrated, that misfolding is influenced by the cellular environment like protein-crowding (Ma, Hu et al. 2013), cellular stress (Weids, Ibstedt et al. 2016) and its chemical and physical environment (Chiti and Dobson 2006). In addition, the amino acid sequence/mutations can alter the propensity of Aβ to misfold and sequentially aggregate, thereby even small changes of a single point mutation can alter the fate of the peptide (de Groot, Aviles et al. 2006). Lastly, posttranslational modifications (PTMs) have proven to be key regulators of a variety of different cellular processes and could be a crucial factor affecting the propensity of Aβ to form aggregates. PTMs can alter the structure, activity, as well as molecular interactions between proteins and might thereby modulate aggregation behaviour.

1.2.3 Posttranslational modification of amyloid β

Even though the human genome covers roughly 20.000–25.000 genes, the human proteome proves to be ultimately more complex, with an estimation of more than 1 million different proteins. This extraordinary difference between transcriptome and proteome can only partly be explained by a variety of mechanisms that create different mRNA transcripts from a reasonable number of genes and involve splicing, recombination, or alternative promoters, to name but a few (Uhlén, Fagerberg et al. 2015).

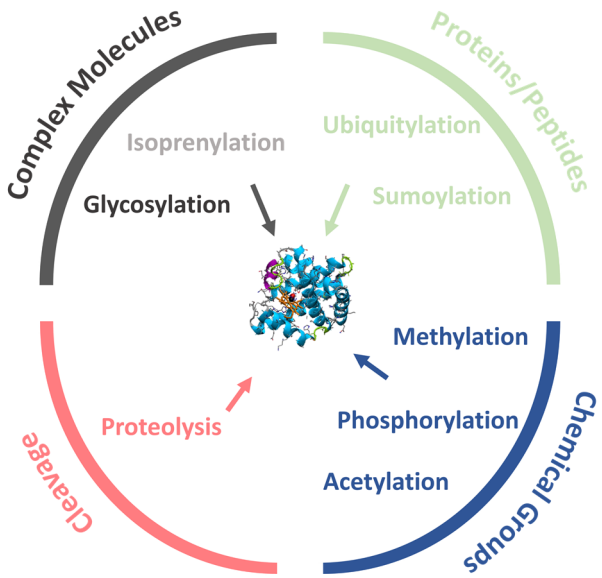

Figure 4 Posttranslational modifications.

Proteins can undergo a variety of different modifications after their translation, which might change their structure, stability, and function. Commonly, those post-translational modifications are grouped into four major changes to the protein: Either complex molecules, proteins/peptides, or chemical groups are added to the protein, or part of the protein is cleaved off. Figure adapted from (Wang, Peterson et al. 2014)

The other factor that vastly increases the complexity of the human proteome is posttranslational modification**.** As the term already implies, PTMs are chemical modifications that happen to proteins after their translation at the ribosome. However, there have been cases described in which modification occurs already during the translation process (co-translational modifications) (Utsumi, Sato et al. 2001, Latousakis and Juge 2018, Ree, Varland et al. 2018). Some of the most common modifications span phosphorylation, truncation, acetylation, ubiquitination, and glycosylation, but with newer and improved detection methods, especially via mass spectrometry (MS), the number of identified PTMs already exceeds 200. In their

complexity, PTMs can range from small additional chemical groups or deletions via cleavage up to the addition of whole proteins or even complex molecules like glycan chains (**Figure 4**)(Wang, Peterson et al. 2014). Originally most known for their involvement in the regulation of kinases (Hunter 2009) or enzymatic reactions (Ciechanover 2005), PTMs over the last decades have proven to be much more versatile than originally believed and are supposed to take part in almost all cellular functions (Deribe, Pawson et al. 2010). Since PTMs also affect protein structure, they are a crucial factor for the correct functionality of a protein. Thereby, even the covalent addition of a phosphoryl group could have significant effects on protein function and might also set out to be a mechanism supporting the misfolding and sequential aggregation of proteins in NDs. The most prominent example is, of course, Tau in AD. It is well known that hyperphosphorylation of the Tau protein, as it is common in AD, leads to dysfunctional Tau, which causes instability of the microtubules, ultimately resulting in neuronal death and the characteristic hallmark of AD, the NFTs (Wang, Yang et al. 2015).
But also, other NDs demonstrate the critical balance between misfolded proteins and PTMs; in ALS, for example, the misfolding of SOD1 and its resulting loss of function can substantially increase the accumulation of reactive oxygen species, which subsequently causes further PTMs, eventually ending in cell death (Deng, Hentati et al. 1993).

Looking at the sequence of Aβ (**Figure 5**) (Kummer and Heneka 2014) and the described post-translational modifications, one quickly concludes that Tau might not be the only protein in AD where PTMs might play an important role. Many studies on the composition of Aβ plaques

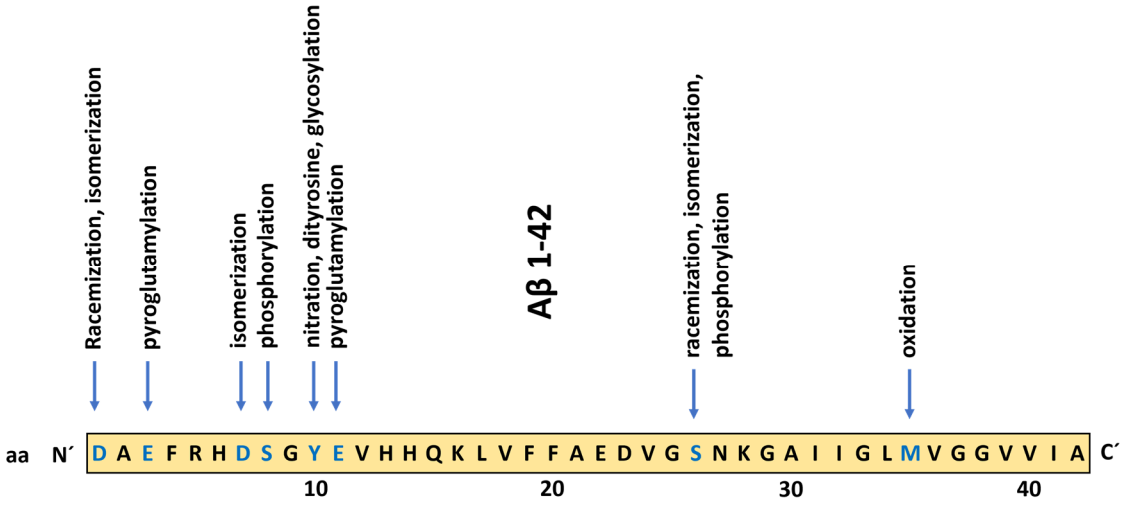

Figure 5 Post-translational modifications (PTMs) in Aβ*.Amino acid sequence of the amyloid beta peptide. Blue letters represent possible posttranslational modification sites. Figure adapted from Kummer and Heneka (2014)*

have confirmed the existence of differently modified Aβ species. While Aβ 1-40 and Aβ 1-42 of course, are still the most abundant species, the appearance of different n-terminal truncated forms of Aβ caught researchers' interest as being the most common modified Aβ species (Moore, Chakrabarty et al. 2012). Indeed, truncation of the n-terminal amino acids showed differential aggregation propensities, which were further reflected in their cellular toxicity (Jawhar, Wirths et al. 2011). A special truncated form of Aβ has been initially described by Saido, Iwatsubo et al. (1995), who identified that after cleavage of the first two amino acids, glutamate at position 3 undergoes dehydration, resulting in the formation of pyroglutamate. Similar to other truncated forms and in line with the assumptions about the importance of PTMs for the structure of proteins, pyroglutamate Aβ (pE3 Aβ) exhibited greater stability, hydrophobicity, and insolubility (Kuo, Webster et al. 1998). All of these seemed to also affect the aggregation propensity (Dammers, Schwarten et al. 2017) as well as the resulting cellular toxicity (Galante, Corsaro et al. 2012). In addition to truncation before position 3, other truncated forms starting at positions 4, 5, 8, or 9 have been described (Sergeant, Bombois et al. 2003).

As displayed in **Figure 5**, Aβ presents with a phosphorylation site at serine 8 (pS8) and serine 26 (pS26). Phosphorylation, even so, described already in 1906 (Levene and Alsberg 1906), only gained importance as a major regulatory cellular mechanism decades later with the discovery of its involvement in enzymatic regulation (Burnett and Kennedy 1954). Nowadays, estimates are that 30-65 % of all proteins are phosphorylated, in part even multiple times (Vlastaridis, Kyriakidou et al. 2017). For Aβ, a protein where structure and folding are of the utmost importance considering its stability and propensity to misfold starting of the aggregation process, phosphorylation might induce a pivotal structural switch. Indeed, researchers were able to show phosphorylation of Aβ in vitro at serine 8 by protein kinase A (PKA) or casein kinase 2 (CK2) and at serine 26 by casein kinase 1 (CK1), cyclin-dependent kinase 1 (CDK1) or protein kinase C (PKC) (Kumar, Rezaei-Ghaleh et al. 2011, Kumar, Wirths et al. 2016). Investigating the biophysical and biochemical properties of synthetic Aβ 1-40 pS8, they confirmed increased stability of the peptide against the insulin-degrading enzyme (Kumar, Singh et al. 2012) and observed a surge in aggregation propensity, resulting in changes in toxicity in cell culture systems as well as the *Drosophila* fly model (Kumar, Rezaei-Ghaleh et al. 2011). Thus, concluding that posttranslational changes of the Aβ peptide via phosphorylation could be key events in the pathogenesis of AD if induced conformational changes interfere with the existing control and degradation mechanisms. As a result, the constant accumulation of a

more stable, potentially highly toxic species of Aβ could further accelerate or even be the initial key triggering event of AD progression.

1.3 Microglia

Microglia, the resident immune cells of the central nervous system (CNS) responsible for its innate immune response, were first defined and described from staining more than 100 years ago, in 1918, by Pio del Rio (Hortega 1918). They cover roughly 5-12 % of all cells in the CNS, varying depending on the area of the brain (Lawson, Perry et al. 1990). The overall responsibility of microglia can be divided into three key functions: sensing their surroundings, housekeeping, and neuroprotection (see **Figure 6**). During sensing, microglia constantly screen their environment for changes, such as the presence of pathogens, damaged or dying cells, abnormal proteins, or changes in neurotransmitter levels, which is achieved via a dense network of branched, so-called ramified microglia distributed all over the CNS (Hickman, Izzy et al. 2018). Each cell is constantly extending its processes to scan its surroundings, and upon detection of injury, cells are even able to migrate towards the affected area (Lawson, Perry et al. 1990). It's suspected that more than 100 genes, also called the sensome, are involved in the constant screening of a variety of different chemical signals. Furthermore, microglia play a strong nurturing role in maintaining overall homeostasis within the CNS, especially during its development. This, of course, requires microglia to interact with a variety of resident cells within the CNS, among them neurons (Zhan, Paolicelli et al. 2014), oligodendrocytes (Peferoen, Vogel et al. 2013), and astrocytes (Liddelow, Guttenplan et al. 2017). The functions they occupy during housekeeping are vast and reach from synaptic remodelling, which plays an important part in creating neuronal plasticity (Zhan, Paolicelli et al. 2014), to maintaining myelin homeostasis (Healy, Perron et al. 2016), to the simple function of migrating towards apoptotic cells and the sequential phagocytosis of such in the developing brain (Ferrer, Bernet et al. 1990). In order to achieve this delicate balance, microglia have to rely on a variety of genes encoding for different chemokines and chemoattractant receptors, phagocytic genes (scavenger receptors, TREM2), as well as genes involved in synaptic remodelling (C1q or Cx3cr1) (Hickman, Kingery et al. 2013, Hickman, Izzy et al. 2018).

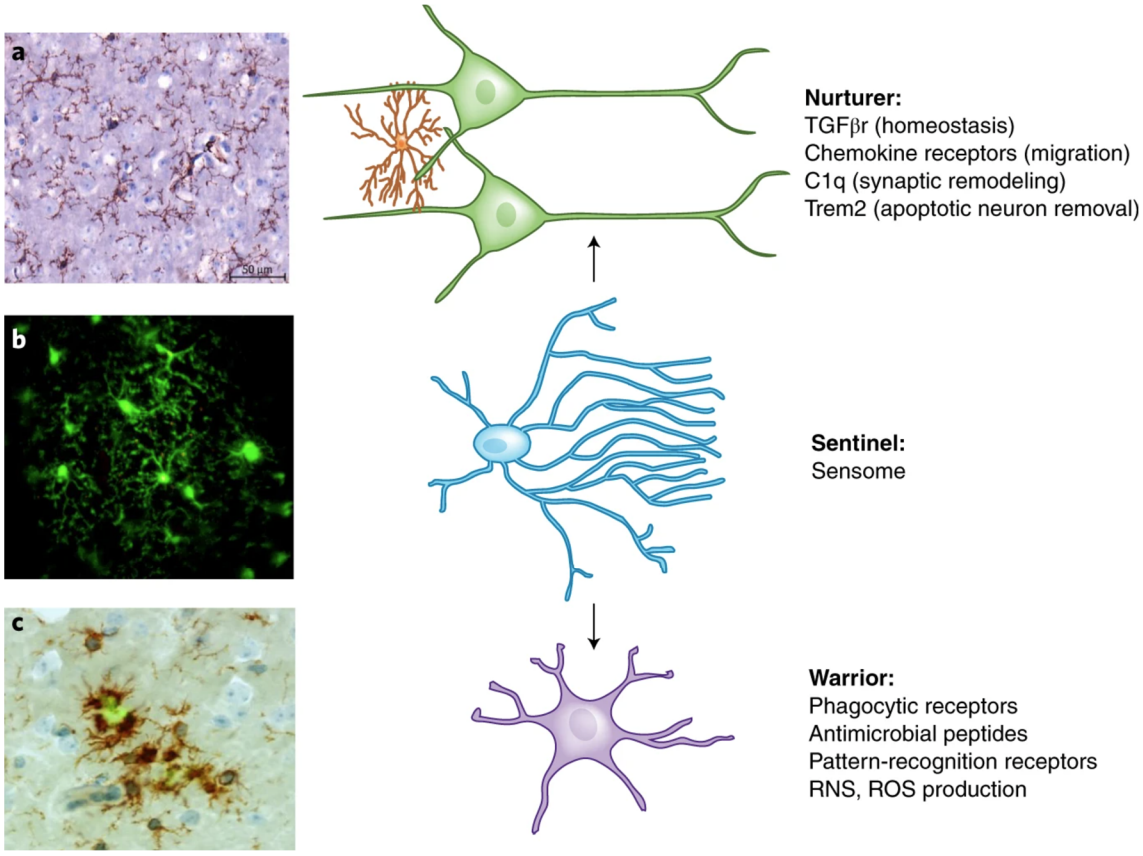

Figure 6 Proposed key functional states of microglia.

A) Microglia in the nurturing state are ramified and distributed throughout the brain in an evenly distributed fashion. Their functions are vast and range from maintaining homeostasis to migration, synaptic remodelling, and even the removal of apoptotic neurons. B) Microglia in the sentinel state are constantly scouting their environment via their abundant processes, which can extend upon injury towards the site of injury. In order to scout the environment, a complex set of proteins (Sensome) is needed, which is encoded by the so-called sensome genes. C) Microglia in the warrior state, reflected by their bulkier size and less ramified appearance, defend against infectious particles, pathogens, or proteins like Aβ, which are sensed via a variety of different surface receptors. Figure adapted from Hickman, Izzy et al. (2018).

Finally, microglia are probably most commonly known for their neuroprotective role, which is why they are commonly referred to as the immune system of the brain. Upon contact with a variety of signals, including damaged cells, injury as well as pathogens, cytokines or even small misfolded proteins (Hickman, Kingery et al. 2013, Anttila, Whitaker et al. 2017), microglia will change into an active state, often accompanied by a change of shape and the retraction of their processes (Gao, Zhu et al. 2013). This response is achieved via the binding of signalling molecules to viral receptors, toll-like receptors (TLRs), and immunoglobulin-like receptors (Fc receptors), resulting in a neuroinflammatory response via the release of cytokines (like TNF;

Il-1) or chemokines (Hickman, Allison et al. 2008). Furthermore, neuroinflammatory responses to a variety of different proteins have been described, including Aβ, α-synuclein, huntingtin, SOD, or prions and thereby suggest the involvement of microglial activation in typical diseases of the CNS, including AD (Frank, Burbach et al. 2008), PD (Barcia, Ros et al. 2013), multiple sclerosis (MS) (Sun, Liang et al. 2006) and ALS (Boillée, Yamanaka et al. 2006). In conclusion, the chronic activation of microglia might be the underlying cause of the age-dependent decline of cognitive functions, where chronic inflammation induces neurotoxicity and eventually neurodegeneration. In general, neurodegeneration might be caused by any imbalance in at least one of the key functional features of microglia: sensing, homeostasis, or neuroprotection.

Microglia in AD

The finding of a disease-modifying therapy for AD has proven itself to be a great challenge, which has led researchers, not at last because of many failures of amyloid-targeting therapeutics, to look out for alternative strategies for AD therapy. Thus, microglia have made their way into the spotlight and given rise to the theory that the over-activation of the innate immune response by microglia might actually represent the true culprit responsible for a great variety of symptoms as observed in NDs. This was further substantiated by genome-wide association studies (GWAS) exposing links between microglial proteins and common neurological diseases (Lambert, Ibrahim-Verbaas et al. 2013). But the involvement of microglia in diseases like AD was already proposed long before when studies showed accumulations of microglia around amyloid plaques not only in disease models but also in post-mortem samples of AD patients (Frautschy, Yang et al. 1998). Furthermore, microglia presented in a constantly activated state as determined by morphological changes as well as pro-inflammatory markers. Intracellular staining of such microglia also confirmed the presence of Aβ, suggesting an active role of microglia in the engulfment of Aβ (D'Andrea, Cole et al. 2004). The active interaction between microglia and Aβ can also be seen by the increased expression of pattern recognition receptors (PPR) upon contact with Aβ. These receptors are used by microglia for the detection of endogenous danger-associated molecular patterns (DAMPs) and exogenous pathogen-associated molecular patterns (PAMPs).

But by far the strongest connection between microglia and AD identified within the last decades came indeed from the previously mentioned GWAS. Independent studies identified an allelic variant of the triggering receptor expressed on myeloid cells (TREM2) associated with a 3- to

4.5-fold increased AD risk (Guerreiro, Wojtas et al. 2013, Jonsson, Stefansson et al. 2013). Since TREM2 is almost exclusively expressed on microglia (Jonsson, Stefansson et al. 2013), it neatly connects AD pathology and microglial function/dysfunction.
In conclusion, microglia present themselves as a delicate topic and a "double-edged sword" when it comes to neuronal health. While on the one hand microglia seem to present as a vital step in the sensing and clearance of Aβ-associated plaques, long-term activation will lead them into a vicious cycle in which the constant activation of microglia via Aβ will spur the production of pro-inflammatory cytokines, which sequentially will reduce cells ability to clear further Aβ. Furthermore, does the activation of the inflammasome via "the NLR family pyrin domain containing 3 protein" (NLRP3) induce the release of "apoptosis-associated speck-like proteins containing CARD" (ASC). The released ASC protein can consequently bind and boost Aβ aggregation, further spreading the pathology (Venegas, Kumar et al. 2017). Nowadays, these dysfunctional microglia are grouped and defined via their transcriptomes as disease-associated microglia (DAMs).

1.4 Triggering receptor expressed on myeloid cells 2 (TREM2)

The membrane receptor and member of the immunoglobulin superfamily, TREM2, is involved in the innate immune response of the brain (Paloneva, Manninen et al. 2002) and is consequently mainly present on microglia. Nevertheless, other cells like macrophages, dendritic cells, and osteoclasts have been described to express TREM2 (Paloneva, Manninen et al. 2002, Jay, Miller et al. 2015). The expression of TREM2 in microglia varies widely and is still under debate but is supposedly dependent on pro- and anti-inflammatory factors, where the latter seem to spur TREM2 expression while pro-inflammatory agents like TNF-α, IL1-β or lipopolysaccharides (LPS) rather dampen its expression (Schmid, Sautkulis et al. 2002, Neumann and Takahashi 2007, Jay, Miller et al. 2015).

Upon binding of an anionic ligand, a signal is triggered through activation of the transmembrane adaptor protein TYROBP/DAP12, leading to a variety of cellular responses, for example, activation of phagocytosis of pathogens and cellular debris, but also anti-inflammatory responses by suppressing secretion and expression of inflammatory cytokines in macrophages or microglia (Campbell and Colonna 1999, Bakker, Wu et al. 2000).
TREM2 is also involved in a rare autosomal recessive disease called Nasu-Hakola, or "polycystic lipomembranous osteodysplasia with sclerosing leukoencephalopathy" (PLOSL).

The disease is characterised by spontaneous bone fractures as well as an AD-like, early-onset form of dementia (Paloneva, Manninen et al. 2002). Observations in AD, on the other hand, have led to the theory that TREM2 might be associated with the recruitment of microglia around amyloid plaques (Perez, Nadeem et al. 2017). This resulted from findings showing increased TREM2 expression in plaque surrounding microglia and was further supported by functional studies in which TREM2-deficient microglia exhibited disrupted clustering around plaques, higher loads of accumulated Aβ, and less dense plagues with a rather diffuse phenotype, as seen by the increased total plaque area and the total number of plaques (Wang, Cella et al. 2015, Wang, Ulland et al. 2016, Jay, Hirsch et al. 2017). Hence, it was concluded that TREM2 is required by plaque-associated microglia to form a protective barrier around plaques to prevent the further spread of Aβ and damage to the brain.

1.4.1 Processing of TREM2

TREM2 is a 230 amino acid (aa) long type I membrane glycoprotein consisting of an 18 aa long signalling peptide, an extracellular (aa 19-173), transmembrane (aa 174-195), and an intracellular domain (aa 196-230). As shown independently in 2017 by three groups, does the extracellular domain undergo proteolytic cleavage by the α-secretases ADAM10 and ADAM17 after amino acid H157. Consequently, resulting in the shedding of the ectodomain, which is released into the extracellular space as soluble TREM2 (sTREM2, see **Figure 7**)(Feuerbach, Schindler et al. 2017, Schlepckow, Kleinberger et al. 2017, Thornton, Sevalle et al. 2017). As a result, a high turnover of the TREM2 receptor is observed, leading to usual half-life times of less than 1 h (Thornton, Sevalle et al. 2017). The driving factor for this shedding of the ectodomain in microglia was proposed to be LPS, while in contrast, the protease meprin β has also been investigated, as it perpetually cleaves TREM2 in macrophages dominantly at aa position 136 (Zhong, Xu et al. 2019, Berner, Wessolowski et al. 2020). The remaining c-terminal parts of TREM2 in the membrane have been described to undergo further cleavage via γ-secretase (Wunderlich, Glebov et al. 2013).

Furthermore, studies also showed that the ectodomains of TREM2 and sTREM2 usually present with strong glycosylation. Hereby, Western blotting and estimations of size suggest that almost half of the molecular weight of the full-length TREM2 is composed of sugars (Ma, Allen et al. 2016).

Together, the strong turnover of TREM2 and the consistent release of sTREM2 suggest that either TREM2 levels have to be quickly controlled or that sTREM2 serves its own distinct

function, in which TREM2 might only present as a precursor. This is further supported by the existence of an alternatively spliced variant of TREM2 lacking the transmembrane domain and making up roughly 25 % of all sTREM2 throughout the brain (Ma, Allen et al. 2016, Del-Aguila, Benitez et al. 2019). In conclusion, this gives rise to the existence of three distinct variants of sTREM2, varying in length from a 219 aa long (alternative splicing), 157 aa long (ADAM10 and 17 cleavage), and a 136 aa long (meprin β cleavage) variant. All of this is, of course, considered before the cleavage of the 18 aa long signal peptide. Thus, it is more likely that sTREM2 has its own distinct function rather than being a simple by-product of TREM2 processing.

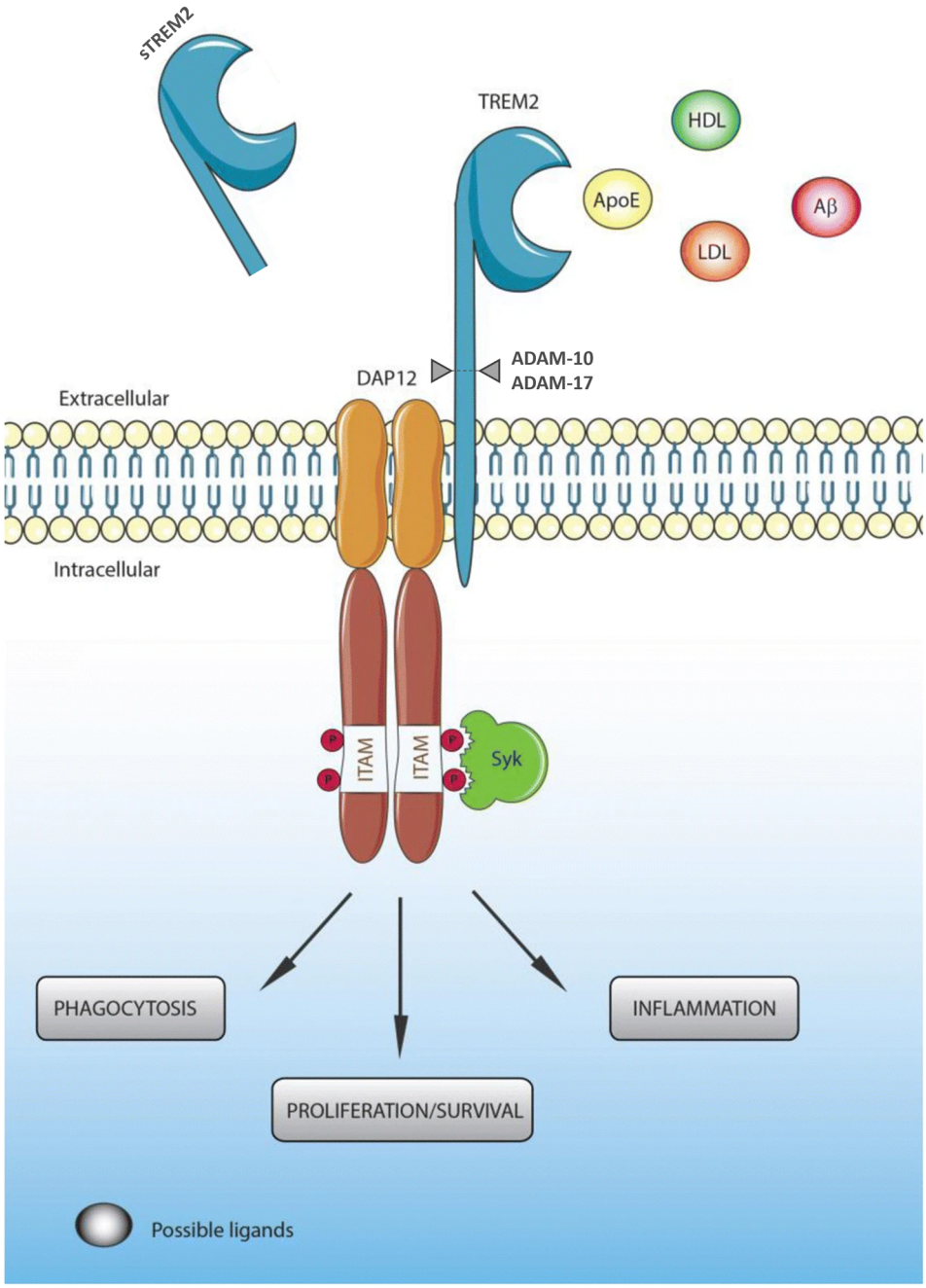

Figure 7 TREM2 receptor binding and subsequent cleavage.

A variety of different ligands have been proposed to bind to TREM2, among them apolipoprotein E4 (ApoE4), amyloid beta (Aβ), and high- and low-density lipoproteins (HDL and LDL). Upon binding, those ligands are supposed to induce the association of TREM2 to its adapter protein DAP12, leading in turn to its phosphorylation within its immunoreceptor tyrosine-based activation motifs (ITAMS). A signalling cascade of different pathway activations will follow in the end, modulating microglial functions like, for example, phagocytosis, proliferation, or inflammation. Furthermore, the extracellular domain will be cleaved by ADAM10/ADAM17 leading to the release of a soluble form of TREM2 (sTREM) into the extracellular space. Figure adapted from Gratuze, Leyns et al. (2018)

Interestingly, sTREM2 can be detected in the cerebrospinal fluid (CSF) and plasma of healthy people as well as in AD patients (Henjum, Almdahl et al. 2016). Supposedly, oligomeric forms of Aβ might present as triggers for increasing TREM2 shedding and release of sTREM2 (Vilalta, Zhou et al. 2021). But there is still a lack of knowledge about the function of sTREM2 or its interactions. Nevertheless, Zhong, Chen et al. (2017) were able to show a protective role of sTREM2 when it comes to the cell viability of microglia. Furthermore, they showed that certain AD-associated variants could also trigger an inflammatory response in microglia. As a conclusion, despite limited evidence in vivo, sTREM2 might present as a clinical marker for microglial activation in AD (Rauchmann, Sadlon et al. 2020, Pascoal, Benedet et al. 2021).

1.4.2 Ligands of TREM2

Signalling via TREM2 upon ligand binding occurs through the cytoplasmic tail of the intracellular adaptor protein DNAX-activation protein 12 (DAP12 or TYROBP), which is pivotal for further downstream signal transduction (Takahashi, Rochford et al. 2005). Ligand binding thereby causes phosphorylation of tyrosine residues within the immunoreceptor tyrosine-based activation motif (ITAM) of the DAP12 protein (**Figure 7**), subsequently creating the binding site for many proteins containing a SRC homology (SH2) domain. Among these most commonly known the spleen tyrosine kinase (Syk), which is involved in the activation of a variety of downstream signalling pathways like the phosphatidylinositol 3-kinase (PI3K) pathway, the mitogen-activated protein kinase (MAPK) pathway, or the regulation of intracellular calcium levels (Takahashi, Rochford et al. 2005, Sun, Zhu et al. 2013).

While the exact ligand interaction with TREM2 remains under investigation, it is known that TREM2 has a high affinity for anionic lipids such as phospho- and glycolipids as well as DNA. Furthermore, a variety of additional ligands, especially those related to dementia, have been proposed. So, it was shown by Atagi, Liu et al. (2015), as well as by Bailey, DeVaux et al. (2015), that the apolipoprotein E (ApoE) can bind TREM2, which, as they proposed, is important for TREM2-related phagocytosis of ApoE-bound debris or plaques. This was also described by Parhizkar, Arzberger et al. (2019) in their recent study. Not only ApoE but also the binding of Aβ, especially to oligomers, has been recently described by Zhao, Wu et al. (2018), suggesting that binding of Aβ induces microglial activation and release of pro-inflammatory cytokines, resulting in enhanced plaque clearance. Since TREM2 undergoes proteolytic cleavage resulting in the release of sTREM2, which is known to promote survival and pro-inflammatory responses (Zhong, Chen et al. 2017), it was furthermore proposed that

sTREM2 might be a putative ligand for yet unknown receptors or could act as a decoy receptor itself. Thereby, binding to TREM2 ligands would inhibit TREM2 signalling through competitive binding (Piccio, Buonsanti et al. 2008, Zhong, Chen et al. 2017).

1.4.3 TREM2 and its genetic variants in AD

Since 2013, research on TREM2 has been on the upswing because of the fact that a genome-wide association study was able to identify certain variants of TREM2 with an increased risk of developing Alzheimer's. Especially the point mutation at position 47 from arginine to histidine, which nearly triples the risk for the development of AD, comparable to having a single APOE4 allele, stood out during this study (Guerreiro, Wojtas et al. 2013, Jonsson, Stefansson et al. 2013). But independently, other studies also found additional mutations, including Q33X, Y38C, T66M, D87N, T96K, R98W, H157Y, R136Q, and L211P, connected to AD or FTD (Benitez, Cooper et al. 2013, Jin, Benitez et al. 2014). After conducting extensive research on different variants of TREM2, researchers identified that most of these point mutations decrease overall TREM2 functions. And while the exact mechanism seems to vary with mutation, quite a few of them interfere with small conformational changes within the basic ligand binding surface of TREM2. Consequently, as shown for R47H, R62H, and D87N, this leads to a disrupted interaction with lipoproteins like ApoE or LDL in vitro (Atagi, Liu et al. 2015, Bailey, DeVaux et al. 2015, Kober, Alexander-Brett et al. 2016). Structure analysis also revealed that arginine 47 plays an important role in the structure of the complementarity-determining region-2 (CDR2) loop as well as the surface characteristics for ligand interaction, thereby enabling the binding of negatively charged ligands to the positively charged ligand-interaction surface. In line with that, the T96K variant shows increased ligand binding, probably due to increasing the basic ligand binding surface (Kober, Alexander-Brett et al. 2016). While decreased ligand binding is usually accompanied by reduced TREM2 activity and signalling, this is not always true, as seen in the case of the D87N variant, which showed increased signalling activation after binding to phosphatidylserine (PS), LDL or HDL (Song, Hooli et al. 2017).

1.5 Aim of this study

Originally, interest in TREM2 as a key protein in Alzheimer's pathology was sparked by the identification of a very rare allelic variant supposedly associated with a 3 to 4.5-fold increased AD risk (Guerreiro, Wojtas et al. 2013, Jonsson, Stefansson et al. 2013), hence almost identical to the risk factor that is conferred by the ApoE4 allele. Even more, with its potential interaction with Aβ (Zhong, Chen et al. 2017, Zhao, Wu et al. 2018) and its effect on aggregation (Vilalta, Zhou et al. 2021, Belsare, Wu et al. 2022), it seemingly connects two important features of AD, namely Aβ and neuroinflammation. On the one hand, TREM2 is important for transformation of microglia into a disease-associated and chronically activated state (Perez, Nadeem et al. 2017). On the other hand, TREM2 can also modulate aggregation, and deposition of Aβ (Hardy and Allsop 1991, Karran, Mercken et al. 2011).

This study was therefore aimed at developing a model system allowing for the investigation of interactions between TREM2 and its soluble form, sTREM2, with Aβ. This was to be achieved by recombinant expression of the ligand-binding domain of TREM2 fused to the Fc-region of the human IgG1 heavy chain. The so-generated fusion protein should allow the investigation of potential ligands and their differential interactions. Since modifications of Aβ species have been recently shown to affect their biophysical properties (Saido, Iwatsubo et al. 1995, Kumar, Rezaei-Ghaleh et al. 2011, Kumar, Wirths et al. 2016), it was sought to investigate how these modifications might affect binding to TREM2.

Furthermore, to address the functional relevance of this binding, thioflavin T aggregation studies were supposed to investigate how the presence of sTREM2 affects the aggregation of differently modified Aβ species. In additional experiments, exposure of microglia to aggregated Aβ species should then determine how the presence of sTREM2 affects Aβ uptake and intracellular signalling pathways. Finally, immunocytochemical, proliferation, and cell viability analyses should elucidate the role of sTREM2 on Aβ uptake in neurons and subsequent neuronal toxicity.

2 MATERIALS AND METHODS

2.1 Biological safety

All procedures were performed in compliance with current safety regulations and instructions described as biosafety level 1 (S1).

2.2 Materials

2.2.1 Buffers and solutions

Table 1 Buffers and solutions

Name	**Composition**
6x OrangeG loading buffer	60 % Glycerine, 0.15 % OrangeG, 60 mM EDTA 10 mM Tris, 1:1.000 Gel Red® (Biotium Inc., Fremont, USA) pH 7.6
1x LAB buffer	10mM Lithium Acetate, 10mM Boric Acid
5x isothermal (ISO) reaction buffer	25 % PEG-8000, 500 mM Tris-HCl, pH 7.5, 50 mM $MgCl_2$, 50 mM DTT, 1 mM each dGTP, dATP, dTTP, dCTP, 5 mM NAD
1.33x ISO assembly mix	320 µl 5x ISO buffer, 0.64 µl T5 exonuclease (10 U/µl), 20 µl Phusion polymerase (2 U/µl), 160 µl Taq Ligase (40 U/µl) add dH_2O to 1.2 ml
Phosphate-buffered saline (PBS)	10mM Phosphate (as sodium phosphates), 2.68 mM Potassium Chloride (KCl), 140

	mM Sodium Chloride (NaCl) pH 7.4 (Invitrogen, Carlsbad, USA)
1x STEN lysis buffer	50 mM Tris-HCl, pH 7.4, 150 mM NaCl, 2 mM EDTA, 1 % Triton X-100, 1 % NP-40 (Igepal CA-630)
5x SDS loading buffer	125 mM Tris, 10 % SDS, 100 mM DTT, 50 % Glycerol, Bromophenol blue
Novex™ NuPAGE™ MES SDS Running Buffer (20x)	1M MES, 1M Tris, 20mM EDTA and 2% SDS (Invitrogen, Carlsbad, USA)
LDS Sample Buffer (4x)	988 mM Tris-HCl, 2.04 mM EDTA, 8 % LDS, 40 % Glycerine, 0.88 % Coomassie-blue and 0.7 mM phenol red pH 8.5 (ThermoFisher, Waltham, USA)
Novex™ Native PAGE™ Running Buffer (20x)	100 mM Bis Tris, 100 mM Tricine pH 6.8 (Invitrogen, Carlsbad, USA)
Novex™ Native PAGE™ Cathode Additive (20x)	8% Coomassie G-250 (Invitrogen, Carlsbad, USA)
Novex™ Native PAGE™ Sample Buffer (4x)	200 mM bistro's, 6 N HCl, 200 mM NaCl, 40% w/v Glycerol, 0.004% Ponceau S pH 7.2 (Invitrogen, Carlsbad, USA)
1x Blotting buffer	20 % Isopropanol, 5 mM Tris, 200 mM Glycine
10x Ponceau	2 % Ponceau S, 30 % TCA
1x TBST	50 mM Tris, 150 mM NaCl, pH 7.6 + 0.05 % Tween20
Blocking buffer	5 % skim milk powder in 1x TBST
Amersham™ ECL™ Prime, Western Blotting Detection Reagent	GE Healthcare, Chicago, USA

2.2.2 Kits

Table 2 Kits

Name	**Supplier**
Gel Extraction Kit, peqGOLD PEQLAB	Biotechnologie, Erlangen, Germany
Quick-change II Site-Directed Mutagenesis Kit	Agilent Technologies, Santa Clara, USA
NucleoSpin Plasmid Kit, Mini	Macherey-Nagel, Düren, Germany
NucleoBond™ Xtra Maxi-Kits	Macherey-Nagel, Düren, Germany
Pierce™ BCA™ Protein Assay Kit	ThermoFisher, Waltham, USA
Caspase-Glo® 3/7 Assay System	Promega, Madison, USA
LDH-Glo™ Cytotoxicity Assay	Promega, Madison, USA

2.2.3 Culture media and cell culture reagents

Table 3 Culture media and reagents

Medium	**Composition**
Lysogeny broth (LB medium)	LB Medium (Luria/Miller, Carl Roth)
LB agar plates	Respective Medium + 15 g/l Agar + Selection antibiotics Blasticidin – 50 µg/ml Zeocin – 25 µg/m
Super optimal broth with catabolite repression (SOC) Medium	0.5 % yeast extract, 2 % Tryptone, 10 mM NaCl, 2.5 mM KCl, 20 mM MgSO4, 20 mM Glucose
Dulbecco's Modified Eagle Medium (DMEM), GlutaMAX™ Supplement	Gibco, Waltham, USA
DMEM/F-12, GlutaMAX™ Supplement	Gibco, Waltham, USA
FreeStyle™ 293 Expression Medium	Gibco, Waltham, USA
Neurobasal™ Plus Medium	Gibco, Waltham, USA
B-27™ Plus Supplement (50x)	Gibco, Waltham, USA
CTS™ (Cell Therapy Systems) N-2 Supplement	Gibco, Waltham, USA
Trypsin-EDTA, 0.05 %	PAN-Biotech, Aidenbach, Germany
Foetal bovine serum (FBS)	PAN-Biotech, Aidenbach, Germany
1 % Penicillin/Streptomycin (P/S)	Gibco, Waltham, USA
Freezing medium	10 % Dimethyl Sulfoxide (DMSO) in FBS
Lipofectamine™ 2000 Transfection	Invitrogen, Carlsbad, USA Reagent
Opti-MEM™ Reduced Serum Media	Gibco, Waltham, USA

Poly-L-Lysine (PLL)	Sigma-Aldrich, Steinheim, Germany
Poly-D-Lysine (PDL)	Gibco, Waltham, USA
Sodium Pyruvate (100 mM)	ThermoFisher, Waltham, USA
MEM Non-Essential Amino Acids Solution (MEAA)(100X)	Gibco, Waltham, USA
40 kDa PEI Max solution	24765–1, Polysciences, Warrington, USA
Pluronic™ F-68 non-ionic surfactant (100x)	Gibco, Waltham, USA
Valproic acid (VPA)	Sigma-Aldrich, Steinheim, Germany
0.4% Trypan blue solution	Gibco, Waltham, USA
Presto Blue	Invitrogen, Carlsbad, USA
LDH Storage Buffer	200mM Tris-HCl (pH 7.3), 10% Glycerol, 1% BSA

2.2.4 Cell lines

Table 4 Cell lines

Cell line	Description	Reference/Source
Escherichia (E.) coli XL10-Gold Ultracompetent cells	High competent bacteria used for transformation during sub-cloning	Agilent Technologies, Santa Clara, USA
Human embryonic kidney (HEK293)	Human embryonic kidney cells	ATCC CRL-1573
HEK 293 Flp-In	HEK293 cells with a Flp-In locus	R75007, Invitrogen, Carlsbad, USA
Expi293F™	HEK293 optimized for high protein expression and culture under non-adhering conditions	A14527, ThermoFisher, Waltham, USA
SH-SY5Y	thrice cloned subline of the neuroblastoma cell line SK-N-SH	ATCC CRL-2266
HEK 293 Flp-In myc-TREM2-FLAG_T2A_DAP12	HEK 293 Flp-In cells stably expressing myc-TREM2-FLAG_T2A_DAP12	Generated previously in the lab by Melanie Ibach
HEK 293 Flp-In myc-TREM2 - R47H - FLAG_T2A_DAP12	HEK 293 Flp-In cells stably expressing myc-TREM2- R47H-FLAG_T2A_DAP12	Generated previously in the lab by Melanie Ibach
HEK 293 Flp-In myc-TREM2 - T66M - FLAG_T2A_DAP12	HEK 293 Flp-In cells stably expressing myc-TREM2- T66M-FLAG_T2A_DAP12	Generated previously in the lab by Melanie Ibach

HEK 293 Flp-In myc-TREM2 - G145W - FLAG_T2A_DAP12	HEK 293 Flp-In cells stably expressing myc-TREM2- G145W-FLAG_T2A_DAP12	Generated previously in the lab by Melanie Ibach
HEK 293 Flp-In myc-TREM2 - H157Y - FLAG_T2A_DAP12	HEK 293 Flp-In cells stably expressing myc-TREM2- H157Y-FLAG_T2A_DAP12	Generated previously in the lab by Melanie Ibach
HEK 293 Flp-In - sTREM2-WT	HEK 293 Flp-In myc-TREM2-FLAG_T2A_DAP12 cells with a stop codon after aa 157, expressing the ectodomain of TREM2 WT	Generated previously in the lab by Pranav Joshi
HEK 293 Flp-In - sTREM2-R47H	HEK 293 Flp-In myc-TREM2-R47H_ FLAG_T2A_DAP12 cells with a stop codon after aa 157, expressing the ectodomain of TREM2 R47H	Generated previously in the lab by Pranav Joshi
HEK 293 Flp-In - sTREM2-T66M	HEK 293 Flp-In myc-TREM2-T66M_ FLAG_T2A_DAP12 cells with a stop codon after aa 157, expressing the ectodomain of TREM2 T66M	Generated previously in the lab by Pranav Joshi
HEK 293 Flp-In - sTREM2-G145W	HEK 293 Flp-In myc-TREM2-G145W_ FLAG_T2A_DAP12 cells	Generated previously in the lab by Pranav Joshi

	with a stop codon after aa 157, expressing the ectodomain of TREM2 G145W	
HEK 293 Flp-In - sTREM2-H157Y	HEK 293 Flp-In myc-TREM2-H157Y_ FLAG_T2A_DAP12 cells with a stop codon after aa 157, expressing the ectodomain of TREM2 H157Y	Generated previously in the lab by Pranav Joshi
HEK 293 Flp-In – Fc2	HEK 293 Flp-In cells stably expressing hIgG1-Fc	Generated in this study
HEK 293 Flp-In - sTREM2-WT-Fc	HEK 293 Flp-In cells stably expressing a fusion protein of the ectodomain of TREM2 WT and hIgG1-Fc	Generated in this study
HEK 293 Flp-In - sTREM2-R47H-Fc	HEK 293 Flp-In cells stably expressing a fusion protein of the ectodomain of TREM2 R47H and hIgG1-Fc	Generated in this study
HEK 293 Flp-In - sTREM2-T66M-Fc	HEK 293 Flp-In cells stably expressing a fusion protein of the ectodomain of TREM2 T66M and hIgG1-Fc	Generated in this study
HEK 293 Flp-In - sTREM2-G145W-Fc	HEK 293 Flp-In cells stably expressing a fusion protein of the ectodomain	Generated in this study

	of TREM2 G145W and hIgG1-Fc	
HEK 293 Flp-In - sTREM2-H157Y-Fc	HEK 293 Flp-In cells stably expressing a fusion protein of the ectodomain of TREM2 H157Y and hIgG1-Fc	Generated in this study
HEK 293 Flp-In – Ef1α-IRES2-EGFP	HEK 293 Flp-In cells stably expressing EGFP	Generated in this study
HEK 293 Flp-In - APP751swe-IRES2-EGFP	HEK 293 Flp-In cells stably expressing APP751swe and reporter EGFP	Generated in this study
HEK 293 Flp-In - APP751swe-S8A-IRES2-EGFP	HEK 293 Flp-In cells stably expressing APP751swe-S8A and reporter EGFP	Generated in this study
HEK 293 Flp-In - APP751swe-S8D-IRES2-EGFP	HEK 293 Flp-In cells stably expressing APP751swe-S8D and reporter EGFP	Generated in this study
HEK 293 Flp-In - APP751swe-S26A-IRES2-EGFP	HEK 293 Flp-In cells stably expressing APP751swe-S26A and reporter EGFP	Generated in this study
HEK 293 Flp-In - APP751swe-S26D-IRES2-EGFP	HEK 293 Flp-In cells stably expressing APP751swe-S26D and reporter EGFP	Generated in this study

2.2.5 Plasmids

Table 5 Plasmids

Name	Source	Description
pcDNA5/FRT sTREM2	Previously generated in the lab by Pranav Joshi	existing mammalian expression vector pcDNA5/FRT (V601020, Invitrogen, Carlsbad, USA) containing the sequence for human TREM2 (NM_018965.3) or variants of such (single point mutation R47H, T66M, G145W and H157Y) and a stop codon after aa 157
pFUSE-hIgG1-Fc1	InvivoGen, San Diego, USA	cloning plasmid for the generation of a Fc-fusion protein expressing the Fc region (CH2 and CH3 domains) of the human IgG1 heavy chain and the hinge region
pFUSE-hIgG1-Fc2	InvivoGen, San Diego, USA	cloning plasmid for the generation of a Fc-fusion protein expressing the Fc region (CH2 and CH3 domains) of the human IgG1 heavy chain and the hinge region with additional IL2 signal sequence for expression of proteins which are not naturally secreted
pFUSE-sTREM2-Fc	Generated in this study	existing mammalian expression vector pFUSE-hIgG1-Fc1 (InvivoGen, San Diego, USA) containing in frame the sequence of the ectodomain of TREM2 (NM_018965.3) or variants of such (single point mutation R47H, T66M, G145W and H157Y
pFUSE-sTREM2-TEV-Fc	Generated in this study	existing mammalian expression vector pFUSE-hIgG1-Fc1 (InvivoGen, San Diego, USA) containing in frame the sequence of

		the ectodomain of TREM2 (NM_018965.3) or variants of such (single point mutation R47H, T66M, G145W and H157Y and a TEV cleavage site between the two
APP751swe-IRES2-EGFP	Generated in this study	lentiviral expression vector containing APP sequence (NM_201413.2) with Swedish mutation (KM670/671NL)
APP751swe-S8A-IRES2-EGFP	Generated in this study	A lentiviral expression vector containing APP sequence (NM_201413.2) with Swedish mutation (KM670/671NL) as well as a single point mutation within the Aβ-sequence (S8A)
APP751swe-S8D-IRES2-EGFP	Generated in this study	A lentiviral expression vector containing APP sequence (NM_201413.2) with Swedish mutation (KM670/671NL) as well as a single point mutation within the Aβ-sequence (S8D)
APP751swe-S26A-IRES2-EGFP	Generated in this study	A lentiviral expression vector containing APP sequence (NM_201413.2) with Swedish mutation (KM670/671NL) as well as a single point mutation within the Aβ-sequence (S26A)
APP751swe-S26D-IRES2-EGFP	Generated in this study	A lentiviral expression vector containing APP sequence (NM_201413.2) with Swedish mutation (KM670/671NL) as well as a single point mutation within the Aβ-sequence (S26D)

2.2.6 Primary antibodies

Table 6 Primary antibodies

Antibody	**Origin**	**Dilution**	**Reference**
Anti-TREM2-NT	Mouse monoclonal	1:1000 WB 1:500 ICC	In-house made
Anti-TREM2 (AF1828)	Goat polyclonal	1:1000 WB 1:500 ICC	R&D Systems, Minneapolis, USA
Anti-Fc-HRP	Goat polyclonal	1:1000 WB 1:500 ICC 1:2000 ELISA	Invitrogen, Carlsbad, USA
Anti-beta-amyloid (17-24) 4G8	Mouse monoclonal	1:1000 WB 1:250 ICC	BioLegend, San Diego, USA
Anti-beta-amyloid 82E1 (n-term.)	Mouse monoclonal	1:100 WB 1:250 ICC	IBL International, Hamburg, Germany
Anti-Aß pSer26 (5H11C10, in-house)	Mouse monoclonal	1:250 WB	In-house made
Anti-Aß pSer8 (1E4E11, in-house)	Mouse monoclonal	1:500 WB	In-house made
Anti-Aß non-phosphorylated (7H3D6, in-house)	Rat monoclonal	1:500 WB	In-house made
Anti-LAMP1 (ab25245)	Rat monoclonal	1:250-1:500 ICC	Abcam, Cambridge, UK
Anti-Trem2 (AF1729)	Sheep monoclonal	1:250-1:500 ICC	R&D Systems, Minneapolis, USA

Anti-Iba1	Rabbit polyclonal	1:250-500 ICC	Synaptic Systems, Göttingen, Germany
Anti-mTOR (7C10)	Rabbit polyclonal	1:1000 WB	Cell Signaling Technologies, Danvers, USA
Anti-pmTOR	Rabbit monoclonal	1:1000 WB	Cell Signaling Technologies, Danvers, USA
Anti-Syk (4D10)	Mouse monoclonal	1:1000 WB	Cell Signaling Technologies, Danvers, USA
Anti-pSyk	Rabbit monoclonal	1:1000 WB	Cell Signaling Technologies, Danvers, USA
Anti-Akt	Rabbit monoclonal	1:1000 WB	Cell Signaling Technologies, Danvers, USA
Anti-pAkt	Rabbit polyclonal	1:1000WB	Cell Signaling Technologies, Danvers, USA
Anti-Erk 1/2	Mouse monoclonal	1:1000 WB	Cell Signaling Technologies, Danvers, USA
Anti-pErk 1/2	Rabbit polyclonal	1:1000 WB	Cell Signaling Technologies, Danvers, USA
MAP2	Guinea-pig monoclonal	1:250 ICC	Synaptic Systems, Göttingen, Germany
cl. Caspase 3	Rabbit polyclonal	1:250 ICC	Cell Signaling Technologies, Danvers, USA

Anti-TGN46 (T7576)	Rabbit polyclonal	1:250 ICC	Sigma-Aldrich, Steinheim, Germany
Anti-LC3	Rabbit polyclonal	1:1000 WB	MBL/Biozol, Eching, Germany
Anti-Lamp2A (ab125068)	Rabbit monoclonal	1:250 ICC	Abcam, Cambridge, UK
Anti-Calnexin (MA3-027)	Mouse monoclonal	1:1000 WB 1:250 ICC	ThermoFisher, Waltham, USA

2.2.7 Secondary antibodies

Table 7 Secondary antibodies

Antibody	**Origin**	**Dilution**	**Reference**
Horseradish peroxidase (HRP) conj. anti-mouse IgG	Rabbit	1:25000	Sigma-Aldrich, Steinheim, Germany
HRP conj. anti-rabbit	Goat	1:25000	Sigma-Aldrich, Steinheim, Germany
HRP conj. anti-goat	Rabbit	1:25000	Sigma-Aldrich, Steinheim, Germany
HRP conj. anti-rat	Goat	1:25000	Rockland, Gilbertsville, USA
IRDye® 680RD conj. Anti-mouse	Goat	1:15000	Li-COR Biosciences, Bad Homburg, Germany
IRDye® 680RD conj. Anti-rabbit	Goat	1:15000	Li-COR Biosciences, Bad Homburg, Germany
IRDye® 680RD conj. Anti-goat	Donkey	1:15000	Li-COR Biosciences, Bad Homburg, Germany
IRDye® 680RD conj. Anti-rat	Goat	1:15000	Li-COR Biosciences, Bad Homburg, Germany

IRDye® 800CW conj. Anti-mouse	Goat	1:15000	Li-COR Biosciences, Bad Homburg, Germany
IRDye® 800CW conj. Anti-rabbit	Goat	1:15000	Li-COR Biosciences, Bad Homburg, Germany
IRDye® 800CW conj. Anti-goat	Rabbit	1:15000	Li-COR Biosciences, Bad Homburg, Germany
IRDye® 800CW conj. Anti-rat	Goat	1:15000	Li-COR Biosciences, Bad Homburg, Germany
IRDye® 800CW anti-Human IgG	Goat	1:15000	Li-COR Biosciences, Bad Homburg, Germany
IRDye® 680CW anti-Human IgG	Goat	1:15000	Li-COR Biosciences, Bad Homburg, Germany
Alexa Fluor 488-conj. Anti-mouse	Goat	1:500	Invitrogen, Carlsbad, USA
Alexa Fluor 488-conj. Anti-rabbit	Goat	1:500	Invitrogen, Carlsbad, USA
Alexa Fluor 488-conj. Anti-rabbit	Donkey	1:500	Invitrogen, Carlsbad, USA
Alexa Fluor 488-conj. Anti-rat	Goat	1:500	Invitrogen, Carlsbad, USA
Alexa Fluor 546-conj. Anti-Guinea pig	Goat	1:500	Invitrogen, Carlsbad, USA

Alexa Fluor 546-conj. Anti-rabbit	Goat	1:500	Invitrogen, Carlsbad, USA
Alexa Fluor 647-conj. Anti-mouse	Goat	1:500	Invitrogen, Carlsbad, USA
Alexa Fluor 647-conj. Anti-mouse	Donkey	1:500	Invitrogen, Carlsbad, USA
Alexa Fluor 647-conj. Anti-sheep	Donkey	1:500	Invitrogen, Carlsbad, USA

2.2.8 Software

Table 8 Software

Software	**Application**	**Origin**
Microsoft Office 2021	Writing, and data analysis	Microsoft Corporation, Redmond, USA
GraphPad Prism 8	Data plotting	GraphPad Software Inc., San Diego, USA
Snap Gene® 3.3.3	Planning of cloning, DNA alignment	GSL Biotech, Chicago, USA
Unicorn 4.12	Control of the Akta purifier system	Amersham Biosciences, Amersham, UK
i-control 1.11	Data acquisition via infinite M200PRO	Tecan, Männedorf, Switzerland
Image Studio Ver 4.0	Data acquisition via Li-cor Odyssey CLx	Li-cor Biosciences GmbH, Bad Homburg, Germany
ImageJ	Image analysis	Wayne Rasband, National Institute of Health, USA

2.2.9 Instruments

Table 9 Instruments

Instrument	**Manufacturer**
Blotting Chamber	Amersham, GE Healthcare, Chicago, USA
Cell culture hoods	Amersham, GE Healthcare, Chicago, USA
Cell culture incubator 37°C/5% CO_2	Binder, Tuttlingen, Germany
Centrifuge 5415 R	Eppendorf, Wesseling, Germany
ChemiDoc XRS	Bio-Rad, Hercules, USA
Electrophoresis power supply	Amersham, GE Healthcare, Chicago, USA
Microscope AxioVert 200 M with AxioCam MR R3 camera	Carl Zeiss, Oberkochen, Germany
Odyssey CLX Imaging system	Li-COR Biosciences, Bad Homburg, Germany
PeqLap electrophoresis system	Peqlab Life Sciences, Erlangen, Germany
Sonicator	Bandelin electronic/Bandelin Sonopuls
Thermomixer	Eppendorf, Wesseling, Germany
VS-Homogenizer	Visitron Systems GmbH, Puchheim, Germany
Yokogawa CSU-W1	Yokogawa Denki, Musashino, Japan
XCell4 SureLock Mini- Cell/ Midi-Cell	ThermoFisher, Waltham, USA
Zeiss Axio Observer	Carl Zeiss, Oberkochen, Germany

2.3 Cloning

2.3.1 Polymerase chain reaction (PCR):

For subsequent sub-cloning, all DNA sequences were amplified via PCR in an Eppendorf Master Cycler personal (Eppendorf, Wesseling, Germany) using the respective set of primers purchased from Eurogentech (Seraing, Belgium, Table 12). Primers, template, and polymerase were prepared in an Eppendorf tube according to recommendations by New England Biolabs (NEB):

Table 10 PCR mix

Component	**Final Concentration**
Q5 High-Fidelity 2X Master Mix	1X
10 µM Forward Primer	0.5 µM
10 µM Reverse Primer	0.5 µM
Template DNA	< 1,000 ng
Nuclease-Free Water	

Samples were then further subjected to a denaturation step followed by an annealing step with the ideal temperature for the respective primer pair as calculated with the help of the Tm calculator (NEB) and finally, the DNA was elongated. These steps were repeated for 30 cycles:

Table 11 PCR program

Step	*Temperature*	*Time*
Initial Denaturation	98°C	30 seconds
30 Cycles	98°C	10 seconds
	50–72°C	30 seconds
	72°C	30 seconds/kb
Final Extension	72°C	2 minutes
Hold	4C	∞

Table 12 Primer

Primer	**Sequence 5' – 3'**	**Method**
sTREM2-AgeI-fwrd	GAGAACCGGTATGGAGCCTCTCCGGCTG	Restriction Cloning
sTREM2-EcoRI-rev	CTCTGAATTCGTGCTCCACATGGGCAT	Restriction Cloning
APP751-SbfI-fwrd	ATACCCTGCAGGATGCTGCCCGGTTTGGC	Restriction Cloning
APP751-NheI-rev	TATGGCTAGCCTAGTTCTGCATCTGCTCAAAG AACTTG	Restriction Cloning
sTREM2-Fc1-H157Y-fwrd	GGATGCCCATGTGGAGTACGAATTCGATATCT CGA	Mutagenesis
sTREM2-Fc1-H157Y-rev	TCGAGATATCGAATTCGTACTCCACATGGGCA TCC	Mutagenesis
sTREM2-Fc1-NheI-fwrd	AGTTGCTAGCATGGAGCCTCTCCGGCT	Restriction Cloning
sTREM2-Fc1-KpnI-rev	TCAAGGTACCTCATTTACCCGGAGACAGGGAG AG	Restriction Cloning
pLenti Vector fwrd	TTGAGCAGATGCAGAACTAGTGATCTACTAGT GCGGATATCTAGTGAACCG	Gibson Assembly
pLenti Vector rev	AGTGCCAAACCGGGCAGCATCCTGCAGGGTCG AAATTCCT	Gibson Assembly

APP Fragment 1 fwrd	AGGAATTTCGACCCTGCAGGATGCTGCCCGGTTTGGC	Gibson Assembly
APP Fragment 1 S8D fwrd	TGATGAACTTCATATCCGTCGTCATGTCGGAA	Gibson Assembly
APP Fragment 2 S8D fwrd	ATGCAGAATTCCGACATGACGACGGATATGAA	Gibson Assembly
APP Fragment 2 rev	ATATCCGCACTAGTAGATCACTAGTTCTGCATCTGCTCAAAGAACTT	Gibson Assembly
APP Fragment 1 S8A rev	TGATGAACTTCATATCCGGCGTCATGTCGGAA	Gibson Assembly
APP Fragment 2 S8A fwrd	ATGCAGAATTCCGACATGACGCCGGATATGAA	Gibson Assembly
APP Fragment 1 S26A rev	ATGATTGCACCTTTGTTGGCACCCACATCTTC	Gibson Assembly
APP Fragment 2 S26A fwrd	TCTTTGCAGAAGATGTGGGTGCCAACAAAGGT	Gibson Assembly
APP Fragment 1 S26D rev	ATGATTGCACCTTTGTTGTCACCCACATCTTC	Gibson Assembly
APP Fragment 2 S26D fwrd	TCTTTGCAGAAGATGTGGGTGACAACAAAGGT	Gibson Assembly

APP Fragment 1 WT rev	TGATGAACTTCATATCCTGAGTCATGTCGGAA	Gibson Assembly
APP Fragment2 WT fwrd	ATGCAGAATTCCGACATGACTCAGGATATGAA	Gibson Assembly
sTREM2-TEV Fragment1 fwrd	TGCTCCTCTGCCACAAAGTGCACGCAGTTGCCGGCCG	Gibson Assembly
sTREM2-TEV Fragment1 rev	ACCCTGGAAGTACAGGTTCTCGTGCTCCACATGGGCATCCT	Gibson Assembly
sTREM2-TEV Fragment2 fwrd	GAGAACCTGTACTTCCAGGGTGACAAAACTCACACATGCCC	Gibson Assembly
sTREM2-TEV Fragment2 rev	GCGTGCACTTTGTGGCAGAGGAGCAGGACTGAGGATAAGC	Gibson Assembly
sTREM2-TEV Frag1 H157Y rev	ACCCTGGAAGTACAGGTTCTCGTACTCCACATGGGCATCCT	Gibson Assembly

2.3.2 Gel electrophoresis

Gel electrophoresis was used to separate negatively charged DNA fragments according to their size and conformation by applying an electric field and letting the samples run through an agarose gel matrix with a defined pore size. The agarose gel was prepared by bringing LAB buffer with 1.5% agarose (AppliChem, Darmstadt, Germany) to boiling temperature and waiting until all the agarose had dissolved. The solution was then poured into a chamber with several combs of the needed size and allowed to cool down until it solidified. Before loading, all DNA samples were mixed with the appropriate amount of OrangeG loading buffer, and for estimation of the size of the fragments, a 1 kbp molecular weight marker (Invitrogen, Carlsbad, USA) consisting of fragments of known sizes was also supplemented with Gel Red™ (Biotium Inc., Fremont, USA) and then loaded in a separate well on the gel. Gel Red™ is a fluorescent dye that intercalates with nucleic acids and can be visualized via ultraviolet (UV) light, showing a strong fluorescent signal upon binding to DNA. Separation of fragments was done by applying a constant voltage of 300 V to the gel matrix for 15-20 min, and the resulting bands were visualized by UV illumination (ChemiDoc™ XRS System, Bio-Rad).

2.3.3 Gel extraction of fragments

The agarose gel with the desired fragments was placed on an UV transilluminator (Trans UV Illuminator GVM 20, Syngene™), and after quickly cutting out the respective bands with a scalpel, the gel pieces were transferred into an Eppendorf tube for further isolation via the Gel Extraction Kit, peqGOLD (Peqlab Life Sciences, Erlangen, Germany), according to the manufacturer's instructions. Afterwards, the purity and concentration of extracted DNA were analysed by UV spectroscopy (NanoPhotometer P-class P330, Implen, Munich, Germany).

2.3.4 Restriction cloning

The generation of the sTREM2-Fc1 construct was done by using the existing mammalian expression vector pcDNA5/FRT (V601020, Invitrogen, Carlsbad, USA) containing the sequence for human TREM2 (NM_018965.3) or variants of such (single point mutations R47H, T66M, and G145W), which were further modified via the introduction of a stop codon after aa

157. Using primers (see Table 12) to introduce a flanking N-terminal AgeI and a C-terminal EcoRI site, sTREM was amplified via PCR, gel purified, digested, and inserted in frame with the fusion tag into the multiple cloning site of a pFUSE-hIgG1-Fc1 expression vector. Digestion of vector and purified sTREM2 was done with Fast Digest EcoRI and Fast Digest BshTI (ThermoFisher, Waltham, USA) in Fast Digest buffer for 10 min at 37 °C. The confirmation and isolation of appropriate fragments were done by another gel extraction. To prevent re-ligation, the isolated vector was further dephosphorylated by the addition of 1 µl Fast AP (ThermoFisher, Waltham, USA) per 1 µg of DNA in Fast AP buffer for 10 min at 37 °C, after which the enzyme was again inactivated by a short incubation of 5 min at 75 °C. Finally, the sticky ends of the vector and sTREM2 insert were ligated in a 3:1 ratio with the T4 ligase (ThermoFisher, Waltham, USA) according to the manufacturer's instructions.

2.3.5 Quick-change site-directed mutagenesis

Introduction of the histidine to tyrosine mutation at aa 157 in the generated sTREM2-Fc fusion construct was achieved via site-directed mutagenesis according to the manufacturer's instructions with respective primers (see Table 12).

2.3.6 Gibson assembly

For the generation of sTREM2 with a cleavable tag, the cleavage site ENLYFQG was introduced between soluble TREM2 and the Fc-fusion tag in the previously generated constructs via site-directed mutagenesis following the Gibson method (Gibson et al., 2009). Similarly, this method was also used for the generation of the lentiviral APP751swe-IRES2-EGFP vector from the in-house existing lentiviral expression vector containing an internal ribosomal entry site (IRES) as well as an EGFP reporter sequence driven by the Ef1α promotor. APP (National Centre for Biotechnology Information reference sequence NM_201413.2) containing the Swedish mutation (KM670/671NL) as well as a single point mutation within the Aβ-sequence (either S8A, S8D, S26A, or S26D) was sub-cloned from pre-existing vectors containing the desired modified APP genes. Therefore, using the respective primer pair (see Table 12), fragments were amplified via PCR, separated by gel electrophoresis, and isolated by gel extraction. Then 5 µl of the fitting fragments in equimolar concentrations were combined with 15 µl of 1.33x ISO assembly mix, not exceeding a total of 200 ng DNA, and incubated for 1 h at 50 °C.

2.3.7 Transformation of competent bacteria

For the transformation of bacteria, 1 ng of DNA plasmid or 5 µl of Gibson/Ligation mix were added to competent XL-10 Gold (Agilent Technologies, Santa Clara, USA) cells on ice for 30 min. The tube was then subjected to a heat pulse at 42 °C for 30 s, followed by a quick cooling period on ice for 2 min. Afterwards, 1 ml of SOC medium was added, and the cells were allowed to recover and grow under shaking (700 rpm) at 37 °C for 1 h. Finally, the cells were pelleted for 5 min at 1.1 g and resuspended in 150 µl of SOC medium before plating them on LB-agar plates containing the respective antibiotics. Bacteria were allowed to grow overnight at 37 °C.

2.3.8 Plasmid isolation and purification

For the isolation of plasmid DNA, a single colony of bacteria grown on an agar plate with the respective antibiotics was picked and used to inoculate 3 ml of LB medium containing the appropriate antibiotics. The liquid culture was then further grown under shaking conditions (250 rpm) at 37 °C till the desired optical density (OD600) was reached, or after 8 h, further diluted in 400 ml of fresh LB medium and cultured overnight under the same conditions. Plasmid DNA was then isolated using the NucleoSpin™ Plasmid Kit, Mini, for 3 ml cultures or the NucleoBond™ Xtra Maxi-Kit for 400 ml cultures, according to the manufacturer's instructions. Afterwards, the purity and concentration of extracted DNA were analysed by UV spectroscopy (NanoPhotometer P-class P330, Implen, Munich, Germany) and the correct sequence was verified via Eurofins Genomics (Ebersberg, Germany).

2.4 Cell Culture

All cell culture handling was done under sterile conditions using a laminar flow cell culture hood (Weiss Pharmatechnik GmbH, Reiskirchen, Germany) with sterile consumables. Cells were kept in a cell incubator (Binder, Tuttlingen, Germany) at 37 °C, 5 % CO2 and constant humidity, unless otherwise stated.

2.4.1 Cultivation and passaging of human embryonic kidney (HEK293) cells

Previously in the lab, established HEK293 Flp-In, as well as HEK293 Flp-In cells with a 2A self-cleaving peptide-based bicistronic expression of TREM2 and DAP12, were cultured in growth medium: DMEM (DMEM containing high glucose (4,5 g/l), phenol red, GlutaMAXTM, 10 mM HEPES, ThermoFisher, Waltham, USA), supplemented with 10% heat-inactivated foetal bovine serum (FBS) (PAN Biotech, Aidenbach, Germany), 1% penicillin and streptomycin solution (P/S) (Gibco, Waltham, USA), and 100 µg/ml hygromycin B. HEK293/HEK293T and generated HEK293/HEK293T-Fc1, Fc2, sTREM2-WT-Fc, sTREM2-R47H-Fc, sTREM2-T66M-Fc, sTREM2-G145W-Fc, and sTREM2-H157Y-Fc cell lines were cultured with and without 100µg/ml Zeocin (ant-zn-1, Invivogen, San Diego, USA) instead of hygromycin. Whenever cells reached 80-90 % confluence, they were split by the detachment of the cells via trypsinization (trypsin/EDTA 0,05 %, PAN-Biotech, Aidenbach, Germany). Briefly, the old medium was removed and the cells were washed with PBS (Invitrogen, Carlsbad, USA) before adding trypsin for 5 min. After that, proteolysis was stopped by the addition of fresh culture medium, and the cells were transferred to a new dish and further diluted in the medium.

The ratio for splitting never exceeded 1/10. Dishes for culturing cell lines were purchased from Sarstedt AG & Co., Nürnbrecht, Germany.

2.4.2 Cultivation and passaging of Expi293F™ cells

Expi293F™ cells (ThermoFisher, Waltham, USA) were grown in suspension with serum-free Freestyle™ expression medium (ThermoFisher, Waltham, USA) and kept at 37 °C and 8 % CO_2. Whenever cells reached a density of 1-3 million viable cells per millilitre (mvc/ml), they were passaged and reseeded at 0.3 mvc/ml. Cultivation of cells was routinely done in 50-ml WHEATON® Erlenmeyer flasks (DWK Life Sciences, Wertheim, Germany) or T-75 cell culture flasks (Sarstedt AG & Co., Nürnbrecht, Germany).

2.4.3 Cultivation and passaging of SH-SY5Y cells

Passaging of SH-SY5Y was done as described for HEK293 cells, but cultured in DMEM/F-12 (DMEM/F-12 containing high glucose, phenol red, GlutaMAX™, ThermoFisher, Waltham, USA), supplemented with 10 % heat-inactivated FBS (PAN Biotech, Aidenbach, Germany), 1 % penicillin and streptomycin solution (Gibco, Waltham, USA), 1 % MEM non-essential amino acids solution (Gibco, Waltham, USA), and 1 % sodium pyruvate (Gibco, Waltham, USA).

Differentiation of SH-SY5Y cells was achieved by the addition of 10 µM all-trans retinoic acid (Sigma-Aldrich, St. Louis, USA) directly to the medium. Medium and retinoic acid were then routinely renewed every 3 days until the start of the experiment.

2.4.4 Isolation and cultivation of primary microglia

Primary microglia were isolated and provided by Hannah Scheiblich and Frederik Eikens (both DZNE, Bonn, Germany) following the described method (Giulian and Baker 1986).

Briefly, the brains of new-born pups were stripped of their meninges and homogenized via trypsinization and mechanical dissociation. The so-generated cell solution from two brains was usually pooled, combined, and seeded in a poly-L-lysine (Sigma-Aldrich, St. Louis, USA) coated T-75 cell culture flask (Gibco, Waltham, USA) in DMEM (Gibco, Waltham, USA) supplemented with 10 % FBS (PAN Biotech, Aidenbach, Germany), and 1 % P/S solution (Gibco, Waltham, USA). After one day, the old medium was aspirated and the cells were washed three times with Dulbecco's PBS (DPBS, Gibco, Waltham, USA). The medium was then renewed and further supplemented with 1 % L929 conditioned medium as a source of

growth factors. The collection of microglia was done after 7-10 days by shaking off the weakly attached mature microglia from the astrocytic layer. This was repeated three times every 2-3 days. For experiments, primary microglia were seeded in serum-free DMEM complemented with 1 % N-2 supplement (Gibco, Waltham, USA) and kept undisturbed overnight.

2.4.5 Cultivation of primary neurons

Cryopreserved primary mouse hippocampal neurons were purchased from Gibco (Waltham, USA) and cultured according to the manufacturer's recommendations. In brief, cells were thawed quickly and transferred drop-wise into a pre-rinsed falcon containing Neurobasal™ medium supplemented with B27™ Plus (Gibco, Waltham, USA). Cells were then plated on poly-D-lysine (Gibco, Waltham, USA) coated wells at a density of 2.5 x 10^4 cells/cm^2. Following the next three weeks, every 3-4 days, half of the old medium was exchanged for fresh medium.

2.4.6 Freezing and thawing of cells

For long-term storage of cells, cells were cryopreserved after trypsinization (see section 2.4.1). Therefore, following trypsinization, cells were centrifuged at 300 x g for 3 min and resuspended in FBS (Gibco, Waltham, USA) supplemented with 10% (v/v) dimethyl sulfoxide (DMSO, Carl Roth, Karlsruhe, Germany) as cryoprotectant. The cell suspension was then transferred to a cryo-vial and stored at -80 °C, or for long-term storage, in liquid nitrogen.

For thawing, the cryo-vials were placed in a water bath at 37 °C until only a small ice crystal in the solution remained. The solution was then mixed with fresh culture medium under the sterile hood and transferred to a cell culture flask/plate for further cultivation.

2.4.7 Counting and seeding of cells

To determine cell number before seeding cells for an experiment and, if needed, also the number of viable cells, 10 µl of the pure cell suspension or a 1:1 mix of cell suspension and Trypan blue (Gibco, Waltham, USA) after trypsinization (see section 2.4.1) was pipetted onto a Neubauer chamber and counted via an automatic cell counter (CytoSMART^{TM}, Corning, New York, USA).

2.4.8 Coating of coverslips and dishes

Coating of labware was always done whenever cell loss as a result of extensive washing steps was expected. Therefore, the surface was incubated with a 50 µg/mL solution of PDL (diluted in DPBS, Gibco, Waltham, USA) for 1 h. Afterwards, the solution was removed and the vessel rinsed with dH_2O three times. Finally, before adding cells, the surface was allowed to dry openly under the sterile hood for at least 2 hours.

2.4.9 Transfection with Lipofectamine 2000

Transfection of cells with Lipofectamine 2000 (Invitrogen, Carlsbad, USA) was done according to the manufacturer's recommendation. Therefore, the appropriate amounts (see Table 13) of Opti-MEM (Gibco, Waltham, USA) and plasmid DNA, as well as Opti-MEM and Lipofectamine 2000, were mixed in separate tubes and then combined within 25 min. After 20 minutes, the solution was added dropwise to the cultured cells. Medium and cells were subsequently collected after 24 or 48 h at 37 °C to test for expression.

For the selection of stable cells, cells were passaged 1:10 after 24 h in fresh growth medium supplemented with an appropriate selection reagent.

Table 13 Transfection mix for different cell culture vessels

Culture vessel	Surf. Area per well	Vol. of plating medium	Volume of dilution medium	DNA	Lipofectamine 2000
96-well	0.3 cm^2	100 µl	2 x 25 µl	0.2 µg	0.5 µl
24-well	2 cm^2	500 µl	2 x 50 µl	0.8 µg	2.0 µl
12-well	4 cm^2	1 ml	2 x 100 µl	1.6 µg	4.0 µl
6-well	10 cm^2	2 ml	2 x 250 µl	4.0 µg	10 µl
6-cm	20 cm^2	5 ml	2 x 500 µl	8.0 µg	20 µl
10-cm	60 cm^2	15 ml	2 x 1.5 ml	24 µg	60 µl

2.4.9.1

2.4.10 Single-cell limited dilution cloning

For the generation of high-expression homozygous stable cell lines, limited dilution cloning was performed. Therefore, previously generated stable cell lines were diluted in a 96-well plate at 0.5 cells per well in selection medium. Growth and verification of single-cell clones were followed via microscopy. After reaching confluency, cells were further expanded and expression levels were analysed via Western blotting (see section 2.5.7).

2.4.11 Recombinant protein expression and purification

Expression of the Fc-fusion proteins (**Figure 8**) was done following the protocol described by Fang, Sehlin et al. (2017). Briefly, one day before transfection, cells were seeded at 1.5 million viable cells (mvc)/ml in fresh medium. The next day, cells were transfected at 3 mvc/ml in half of the final volume with a 1 mg/ml linear 40 kDa PEI Max solution (24765–1, Polysciences, Warrington, USA) and the respective DNA (1 µg/ml) in a 6:1 ratio. The efficiency of transfection was further increased by the addition of 0.1% Pluronic® F-68 (24040032, ThermoFisher, Waltham, USA). After 24 h, the transfection mix was diluted with fresh medium 1:1 and supplemented with 0.5 M valproic acid (VPA, P4543, Sigma-Aldrich, Steinheim,

Germany) at a final concentration of 3.5 mM. The desired protein was collected after 4-5 days. Following centrifugation, filtration, and pH adjustment, the medium was loaded on a HiTrap™ Protein G HP 1 ml column (Cytiva Life Sciences, Marlborough, USA) and affinity purified via fast liquid protein tomography (FPLC). Eluted fractions were neutralized by the addition of 1 M Tris (pH 9.0). Concentration and buffer exchange against PBS were performed by ultrafiltration with a 10 kDa MWCO column (Sartorius, Göttingen, Germany). Originally three variations of this method were compared in their expression of recombinant protein: In Method 1 cells were transfected at 20 million viable cells per ml (mvc/ml)) and diluted to the final volume after 3 h and supplemented with valproic acid after 24 h. For Method 2 and 3 cells were transfected at 3 mvc/ml in half of the final volume and diluted to the final volume after 24 h. However, while cells in the second method were given VPA as an enhancer of expression, cells in the third method were kept untreated.

In order to generate untagged sTREM2 the recombinant protein was further cleaved with Tobacco Etch Virus protease (TEV) (P8112S, New England Biolabs) for 1 h at 30°C. Finally, the protease was simply removed by a nickel-nitrilotriacetic acid (Ni-NTA) column (HisTrap HP 1 ml column, Cytiva Life Sciences, Marlborough, USA) according to the manufacturer's instructions, and the flow-through was subjected to another round of protein-G affinity chromatography, separating the untagged sTREM2 (flow-through) from the hIgG1-Fc or uncleaved protein (eluate).

Since the amino acid sequence of the protein was known, the exact extinction coefficient could be calculated using the Expasy protein parameters software (http://web.expasy.org/protparam/) and used to determine the concentration of the purified proteins via a spectrophotometer (NanoPhotometer P-class P330, Implen, Munich, Germany) measuring the absorbance at 280nm.

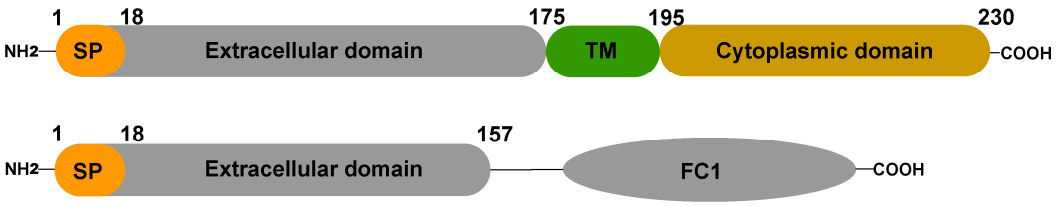

Figure 8 Schematic figure of sTREM-Fc.

2.5 Biochemical and biophysical methods

2.5.1 Preparation of monomeric and oligomeric Aβ

Aβ monomers were purchased from Peptide Specialty Laboratories (Heidelberg, Germany) and prepared as described previously (Kumar, Rezaei-Ghaleh et al. 2011).

Briefly, peptides were dissolved in 10 mM NaOH at a stock concentration of 1 mg/ml (230 µM), sonicated for 5 min, and aliquots flash frozen in liquid nitrogen and stored at -20 °C.

Oligomer-enriched Aβ was prepared in either of two ways.

1st way: Monomeric Aβ stock was diluted to 23 µM in PBS and then incubated at 37 °C for 3 hours.

2nd way: Oligomerization was prepared as previously described by Kim et al. (2013).

Briefly, monomeric Aβ stock was diluted to 100 µM in PBS and incubated at 23 °C for 16 h, followed by incubation at 4 °C for 24 h. The preparation was further centrifuged at 16.000 x g, and the supernatant was aliquoted, flash-frozen in liquid nitrogen, and stored at -20 °C.

2.5.2 Trichloroacetic acid (TCA) precipitation

For further concentration of expressed protein, the supernatant of expressing cells was first centrifuged for 10 min at 2000 x g and 4 °C. Afterwards, the supernatant was collected, and 2 % sodium desoxycholate (NaDOC) was added to reach a final concentration of 0.02 %. Samples were mixed by several inversions of the tubes and incubated for 15 min at room temperature. After that, 100 % trichloroacetic acid (TCA) was added to a final concentration of 10 % and the samples were again mixed by inversion and incubated at room temperature for 1 h. For the collection of the precipitated proteins, the samples were centrifuged for 10 min at 16.000 x g and 4 °C. After aspiration of the supernatant, the pellet was washed with the addition of 700 µl of ice-cold acetone. After 15 minutes of incubation, the samples were centrifuged as described before, and the supernatant was again discarded. This step was repeated two times before the pellet was dried for 1 h at 37 °C.

Finally, samples were resuspended in an appropriate volume of 50 mM Tris/1 % SDS buffer and SDS sample buffer. Samples were boiled at 95 °C for 5 min and further separated via SDS-PAGE (see section 0).

2.5.3 Preparations of cell lysate

For the preparation of whole cell lysates, cells were washed with PBS before collection by scraping off the cells with a rubber policeman on ice. The cell suspension was transferred to a tube and pelleted via centrifugation. For lysis, the cell pellet was resuspended in 1x STEN lysis buffer supplemented with 1x protease inhibitor (cOmplete™ EDTA-free, Roche Diagnostics, Basel, Switzerland) and incubated for 20 min on ice. Finally, lysates were centrifuged at 16.000 x g for 10 min at 4 °C, and the supernatant was collected in a fresh tube, which was used for SDS-PAGE (see section 2.5.5) analysis or stored until use at -20 °C.

2.5.4 Protein estimation by Bicinchoninic acid (BCA) method

For estimating protein concentrations from lysates, the Pierce™ BCA Protein Assay Kit was used according to the manufacturer's instructions. In this assay, bicinchoninic acid is used to visualize the reduction of Cu (II) to Cu (I), which is happening in the presence of proteins in a proportional manner, via measuring the absorbance at 562 nm. Concentrations of unknown samples can then be calculated according to a BSA standard curve.

2.5.5 Sodium dodecyl sulphate – polyacrylamide gel electrophoresis (SDS-PAGE)

SDS-PGAGE was used to separate proteins according to their size and structure. Protein separation was performed using the XCell SureLock® Mini-Cell or XCell4 SureLock® Midi-Cell SDS-PAGE system (Invitrogen, Carlsbad, USA). Therefore, samples were prepared in 5x SDS sample or 4x LDS sample buffer, boiled at 95°C for 5 min (SDS sample buffer) or 75 °C for 10 min (LDS sample buffer), and subsequently separated according to their molecular weight on a pre-casted discontinuous Bis-Tris gel (NuPAGE Novex 4-12%, Invitrogen, Carlsbad, USA). Additionally, a molecular weight marker containing proteins of known sizes (Novex™ See Blue™, Invitrogen, Carlsbad, USA) was loaded onto the gel to track the

separation of the samples. Separation was done using 1x NuPAGE MES SDS Running Buffer and a constant voltage of 120 V. Gels were subsequently analysed by Western blot analysis.

2.5.6 Native-PAGE

For analysis of proteins in their native state and under non-reducing conditions, native PAGE (Novex™ Native PAGE™, Invitrogen, Carlsbad, USA) was performed according to the manufacturer's recommendation. Samples were prepared in a non-reducing sample buffer and then loaded onto a 4 to 16 % Bis-Tris gel. After filling the appropriate chambers with cathode and anode running buffer, proteins were separated solely by size for 60-90 min at 120 V and further analysed via Western blotting.

2.5.7 Western blotting

For the identification and visualization of the previously separated proteins, the wet transfer Western blot technique was used to transfer proteins from the SDS-PAGE or native gel onto a nitrocellulose membrane at a constant current of 400 mA and a transfer time of 2 h. The blotted membrane was then blocked for 1 h at constant agitation with a 5 % blocking solution. The binding of the primary antibody was done by incubation of the membrane overnight at 4 °C and constant agitation with a solution of the primary antibody in 1 x TBST. The next day, the membrane was washed three times for 5 min to remove unbound antibodies and reduce background. Afterwards, the respective secondary antibody conjugated either to horseradish peroxidase or a fluorophore (IRDye 800CW, 680RD, Li-cor Biosciences GmbH, Bad Homburg, Germany) was added and incubated for 1 h at room temperature. Before detection of the protein with a Chemidoc XRS Imager (Bio-Rad, Hercules, USA) or Odyssey® CLx (Li-cor Biosciences GmbH, Bad Homburg, Germany), the membrane was washed again 3 times for 5 min in TBST and then incubated for 1 min with Amersham™ ECL™ Prime Western Blotting Detection Reagent (GE Healthcare, Chicago, USA) (in case of luminescence detection) or directly imaged.

2.5.8 Dot-Blot

For analysis of binding via the dot-blot assay, recombinant proteins or synthetic Aβ peptides (200 ng) were spotted manually onto a nitrocellulose membrane. After 30 min of drying, the membrane was blocked with 5 % BSA (in TBST) for 1 h. For binding, the membrane was incubated with the recombinant proteins or synthetic peptides in 3 % BSA (in TBST) at a concentration of 100 ng/µl (Aβ) or 200 ng/µl (sTREM2-Fc variants). Incubation was done under constant agitation for 1 h at room temperature. The detection of the bound protein was done as described before according to the Western blotting protocol.

2.5.9 Pull-Down assay

For assessing the binding of oligomeric and monomeric Aβ variants to TREM2, 2 µg of recombinant sTREM2-Fc or hIgG1-Fc were pre-coupled to magnetic Protein G beads (Sure Beads™, Bio-Rad, Hercules, USA) for 20 min at 23 °C. The coupled beads were then further incubated with 2 µg of the oligomer-enriched Aβ preparation for 1 h at 23 °C in PBS buffer containing 0.1% Tween-20 (PBST). After precipitation and subsequent thorough washing steps, the bound proteins were eluted from the beads by the addition of 20 mM glycine at pH 2.5. Finally, the eluate was neutralized with 1 M Tris-HCl pH 8 and boiled at 95°C in SDS sample buffer before subjection to Western blot analysis.

For a quantitative assessment, this protocol was slightly altered by reducing the amount of beads (300 µg) and Aβ (1 µg) while increasing the amount of sTREM2-Fc and hIgG1-Fc to 10 µg to ensure full saturation of the beads with recombinant protein.

2.5.10 Solid-phase binding assay

Human recombinant IgG1-Fc and sTREM2-Fc were coated in duplicates onto Nunc MaxiSorp 96-well plates (ThermoFisher, Waltham, USA) by addition of 100 µl of a 500; 100; 50; 25; 12.5; 6.25; 3.125 nM solution in PBS per well at 4 °C overnight. After blocking with 5 % BSA for 2 h at 23 °C and subsequent washing, 100 µl of Aβ in PBST + 0.5 % BSA, equivalent to 100 nM monomers, was added to each well for 1 h at 37 °C. The plates were washed and incubated with 4G8-HRP (1:3000, BioLegend, San Diego, USA) for 1 h at 37 °C. After the final washing steps, plates were developed by the addition of Ultra-TMB solution (ThermoFisher, Waltham, USA) for 6 min before the reaction was stopped by 2 M sulfuric acid. Using a microplate reader (Infinite M200Pro, Tecan, Männedorf, Switzerland) the absorbance was measured at 450nm and for background correction at 620nm.

Alternatively, plates were coated with the oligomeric preparations of the Aβ variants equivalent to 100 nM monomers and incubated with 100 µl of sTREM2-Fc and hIgG1-Fc at 200; 100; 50; 25; 20; 12,5; 10; 6.25; 5; 3.125; 2.5; 0.625; 0.3125 nM. Bound proteins were detected by the addition of anti-human IgG-HRP (1:20000, ThermoFisher, Waltham, USA) and developed for 3 min as described above.

2.5.11 Size exclusion chromatography (SEC)

Gel-filtration chromatography, also known as size exclusion chromatography, was used as a method to separate protein solutions according to their size in a native environment for further characterisation or as a purification step in the production of recombinant proteins. Therefore, the protein solution was injected into an appropriately sized loop on a GE AKTA Purifier FPLC System (GE Healthcare Systems, Chicago, USA). The sample was then run over a Superdex® 75 10/300 GL (Cytiva Life Sciences, Marlborough, USA) column with PBS buffer at a flow rate of 0.3 ml/min and collected again in separate fractions with the help of a fraction collector (Frac-950). Separate fractions were flash-frozen in liquid nitrogen and later subjected to further analysis via SDS-PAGE and blotting.

2.5.12 Thioflavin T (ThT) aggregation assay

Samples (100 µl) were incubated at 37 °C in black µClear 96-microwell plates (655906, Greiner Bio-One, Kremsmünster, Austria) that were sealed to prevent evaporation. The ThT fluorescence intensity of each sample was recorded every 10 min using the Infinite M200 PRO plate reader (Tecan, Männedorf, Switzerland) with 440/490 nm excitation/emission filters set. For all measurements, a concentration of 10 µM ThT and 5 µM Aβ was used. To ensure a monomeric state, Aβ solutions were placed in an ultrasonication bath for 5 min, centrifuged for 20 min at 16.000 x g and added shortly before starting the measurement.

2.5.13 Presto Blue assay

Cell viability was investigated by using the resazurin-based Presto Blue assay (Invitrogen, Carlsbad, USA). Upon addition to the cells, the resazurin is reduced by metabolically active cells to resorufin, which exhibits a measurable bright fluorescence that is proportional to the number of living cells. For the cell viability measurements, Presto Blue was directly added to cells after treatment in a 1:10 ratio of reagent and medium. After a short incubation of 30 min at 37°C, the fluorescence was measured in a microplate reader (Infinite M200 PRO, Tecan, Männedorf, Switzerland).

2.5.14 Caspase 3/7 assay

To study the effect of differently modified Aβ on neuronal apoptosis, the Caspase-Glo® 3/7 assay (Promega, Madison, USA) was used following the manufacturer's instructions. In this assay, Caspase-Glo® 3/7 substrate is first mixed with Caspase-Glo® and then added directly to the cells after treatment in a 1:1 ratio of cell solution and reagent. In the case of a 24-well plate, 200 µl solution was added to 200 µl cell suspension. This leads to cell lysis and subsequently to the cleavage of the substrate by the liberated caspase, releasing free amino luciferin. This in turn is used by the luciferase in the reagent to generate a luminescent signal proportional to the caspase-3/7 activity. A sample (100 µl) of each well was transferred into a white 96-well microplate (CELLSTAR®, Greiner Bio-One, Kremsmünster, Austria), and luminescence was measured in a microplate reader (Infinite M200 PRO, Tecan, Männedorf, Switzerland).

2.6 Microscopical investigation of cellular Aβ binding and uptake

2.6.1 Immunocytochemistry (ICC)

For immunocytochemical detection of protein localization and expression, cells grown on coverslips were fixed for 15 min in 4 % paraformaldehyde (PFA) before permeabilization with 0.1 % Triton-X100 (in PBS) for 10 min. After blocking with 3 % BSA in PBST, 100 µl of primary antibody in 1 % BSA was added to each coverslip and incubated at room temperature for 1 h. To remove unbound antibodies, the coverslips were subsequently washed with 0.5 % BSA in PBST three times. Afterwards, respective secondary antibodies in a 1 % BSA solution were added, and coverslips were incubated for another hour at 23 °C in the dark, followed by three washing steps. Finally, the coverslips were mounted on a microscopy slide using VECTASHIELD® Antifade Mounting Medium with DAPI (H-1200-10) and observed on the Zeiss AxioVert 200 M Apoptome (Carl Zeiss, Oberkochen, Germany).

2.6.2 Cellular binding assay

To assess the binding of differently modified and aggregated Aβ species to full-length TREM2 in a cellular system, HEK 293 Flp-In myc-TREM2-FLAG_T2A_DAP12 and HEK 293 Flip-In cells were incubated with increasing concentrations of Aβ. The cells were therefore seeded on PDL-coated µ-Slide 18-well chambers (Ibidi, Gräfelfing, Germany). To minimize uptake and investigate binding, cells were placed on ice and the medium was changed to Opti-MEM supplemented with 1 µM, 500 nM, 250 nM, 125 nM, 62.5 nM, or 0 nM Aβ. Cells were kept on ice for 2 h and then washed three times with fresh medium. Then cells were fixed and subjected to the ICC protocol (see section 2.6.1), with the exception that no permeabilization step was performed and PBST was replaced by normal PBS.

2.6.3 Uptake of Aβ and fluorescent beads by microglia

Uptake of oligomer-enriched Aβ variants or 1.0 µm latex beads was investigated by seeding primary microglia from C57BL6 and Trem2^{T66M} transgenic mice (provided by Hannah Scheiblich, AG Heneka) on poly-D-lysine (PDL)-coated coverslips in 24-well plates. Fluorescent 1 µm beads were blocked with 35 mg/ml IgG-free BSA in PBS solution. Cells were

incubated with 100 beads per cell or Aβ oligomers at a concentration of 1 µM in DMEM GlutaMAX^{TM} for 2 h before they were fixed, permeabilized, and stained. Coverslips were mounted on glass slides and observed using a VISISCOPE CSU-W1 confocal microscope. As a control, cells were also treated with 10 mM Cytochalasin D (CytoD) for 20 min to block actin polymerization and thereby phagocytosis, endocytosis, and pinocytosis (Ting-Beall, Lee et al. 1995, Lin, Singla et al. 2018) before changing to the assay conditions described before.

2.6.4 Aβ chase in primary microglia

To assess binding and uptake of differently modified Aβ variants in the presence or absence of TREM2/sTREM2 individually, a chase experiment was performed. Therefore, WT or Trem2^{T66M} primary microglia were either treated as described in section 2.6.3 or with a 500 nM solution of Aβ oligomerized (Method-1) in the presence or absence of recombinant sTREM2/hIgG1-Fc and incubated on ice for 2 h, followed by fixation and staining. Additionally, to assess the uptake of bound Aβ, primary microglia were first incubated with Aβ on ice for 2 h and then washed and further incubated at 37 °C and 5 % CO_2 for another 2 h. The cells were then fixed, permeabilized, and stained as described before (see section 2.6.1).

2.7 Statistical analysis

Statistical analysis was performed using GraphPad Prism 8 (GraphPad Software, Inc., La Jolla, US). For statistical analysis, three or more independent samples/experiments were analysed. P values below 0.05 were considered significant (*$p<0.05$; **$p<0.01$; ***$p<0.001$). The statistical values are reported as mean ± standard deviation (SEM) unless stated otherwise.

Statistical details of each experiment (test used, value of n, and significance) can be found in the figure legends.

3 RESULTS

3.1 Generation and characterisation of Aβ and sTREM2 for interaction studies

This study aimed to investigate the interaction between TREM2 and Aβ and its possible implications for AD. Furthermore, the characterisation and use of differentially modified Aβ variants either by phosphorylation state or by the state of aggregation should give a more conclusive idea about the preferred interaction. Therefore, the first part of this work focused on developing an in vitro system to investigate the interaction of Aβ with TREM2 by expression and isolation of the ligand-binding domain of TREM2 fused to the Fc-region of the human IgG1 heavy chain.

3.1.1 Transient expression of soluble TREM2

For expression of the recombinant soluble TREM2-Fc, the sequence encoding for the ectodomain of TREM2 (NM_018965.3) comprising amino acids 1-157 and containing also the natural signal peptide of TREM2, which is naturally cleaved after successful expression, as well as disease-associated variants, were sub-cloned from previously established vectors (Ibach, Mathews et al. 2021) into the pFUSE-hIgG1-Fc1 vector (Invivogen, San Diego, USA). In order to verify the successful cloning, the constructs were transiently expressed in HEK293 cells, and the presence and size of recombinant protein in the cell culture supernatant (**Figure 9** A), as well as cell lysates (**Figure 9** B), were determined after 48 h via SDS-gel electrophoresis and sub-sequential Western blot analysis. Detection with an antibody against TREM2 (4B2A3) confirmed the presence of the construct at its theoretical size of around 50 kDa, especially in the supernatant and, to a lesser extent, in the cell lysate. However, the sTREM2-T66M-Fc variant was predominantly detected in the cell lysate and only slightly in the supernatant.
Furthermore, a comparison of the expression of the recombinant sTREM2-Fc fusion protein, with an expected molecular weight (MW) of around 50 kDa, to the expression of sTREM2

without a tag and, thereby, an expected MW of around 28 kDa, showed a migration pattern at the expected sizes.

The untagged variant, however, presented in the supernatant more as a smear in its migration, ranging in size from 28 kDa to roughly 40 kDa, while the fusion protein rather migrated at the

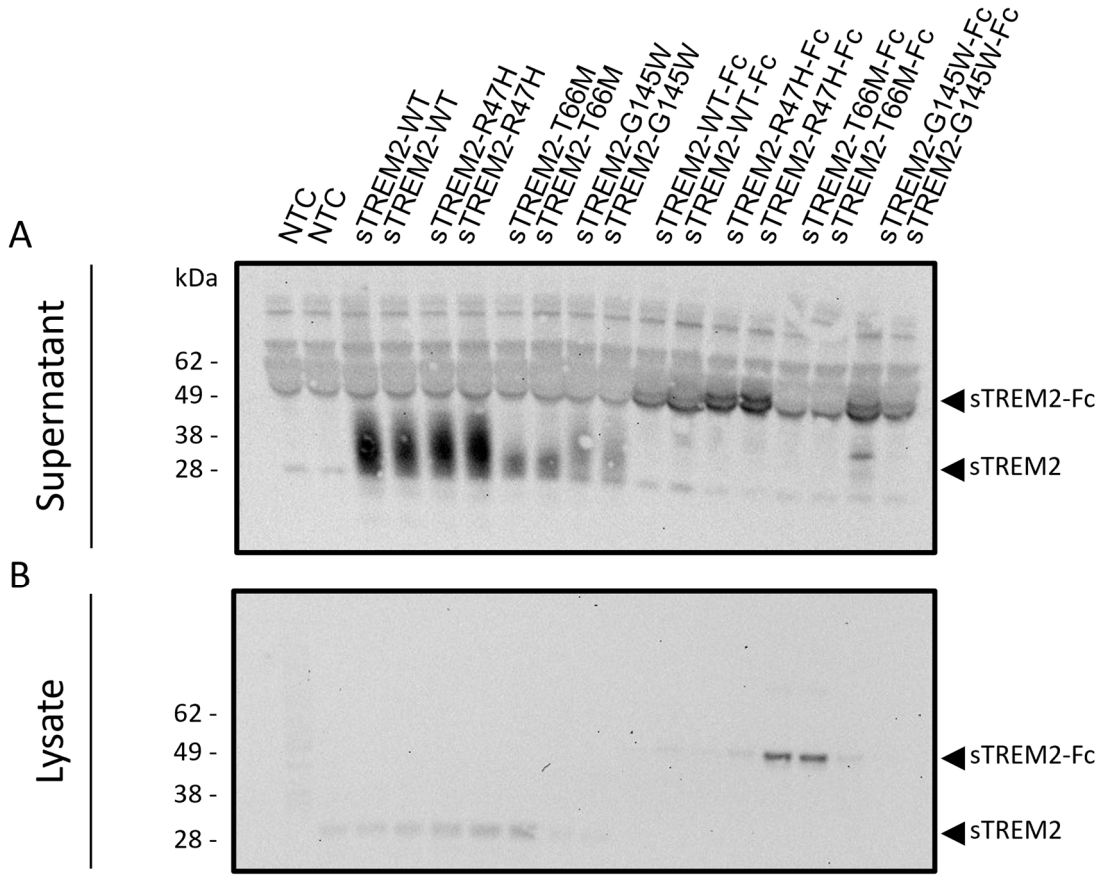

Figure 9 Transient expression of soluble TREM2 variants.

HEK293 cells were transiently transfected with the indicated constructs, either containing the human TREM2 sequence with a stop codon at aa position 158 or the ectodomain of TREM2 fused to the Fc domain of the human heavy chain. 48 h after transfection, samples of TCA-precipitated supernatant (A), as well as cell lysates (B), were separated via SDS-gel electrophoresis and further analysed via Western blotting. Detection with the TREM2-specific antibody 4B2A3 confirmed the presence of sTREM2 and sTREM2-Fc fusion proteins at their expected molecular weights of around 28 kDa and 50 kDa, respectively, in the cell lysates. While in the supernatant, the untagged protein migrated as a diffuse smear ranging in size from 28 kDa to 40 kDa, the fusion protein showed a more defined band at around 55 kDa. Furthermore, expression levels varied between disease-associated variants, with sTREM2-T66M/sTREM2-T66M-Fc predominantly detected in the cell lysate compared to the other variants, which were predominately expressed in the supernatant. sTREM2-T66M/sTREM2-T66M-Fc showed only a slight signal in the supernatant (n=1).

expected 50 kDa and showed a single defined band. In the lysates, the general expression of both proteins is very low, and as described before are hardly detectable; instead, untagged sTREM2 migrates as a single band at around 28 kDa, while the fusion protein is observed at around 49 kDa.

3.1.2 Stable expression of sTREM2

Following the successful confirmation of expression of the generated sTREM2-Fc constructs, cells were further expanded, and stable cell lines were generated by selection with 400 µg/ml Zeocin over the course of two weeks. This concentration of Zeocin was found to efficiently kill all non-transfected cells within this time frame. After two weeks, the selection reagent was changed to 200 µg/ml and expression was again checked via Western blotting from the supernatant with an antibody against the Fc-domain of the human heavy chain (**Figure 10** A). The expression pattern also resembled the previously shown expression pattern from transient transfection, with the T66M variant again showing low levels in the supernatant. Levels of other variants in the supernatants were similar, with those of the WT being slightly higher. Additionally, the detection of hIgG1-Fc revealed the presence of minor amounts of Fc not fused to sTREM2.

As it had been described that TREM2 undergoes strong glycosylation, resulting in a variety of different glycosylated variants of the soluble form of TREM2, represented by the smear-like migration pattern as also seen in **Figure 9** (Ibach, Mathews et al. 2021), it was tested if sTREM2, when expressed recombinantly with a tag, also undergoes glycosylation. Therefore, the TCA-precipitated supernatant of the generated stable cell lines was treated with PNGase F, a glycosidase able to cleave almost all asparagine-linked oligosaccharides. Western blot of PNGase F treated and untreated samples revealed that hIgG1-Fc on its own is already glycosylated, as represented by the shift in migration after treatment. Treatment of the recombinant sTREM2-Fc resulted in an even stronger change in migration and was consistent throughout all variants.

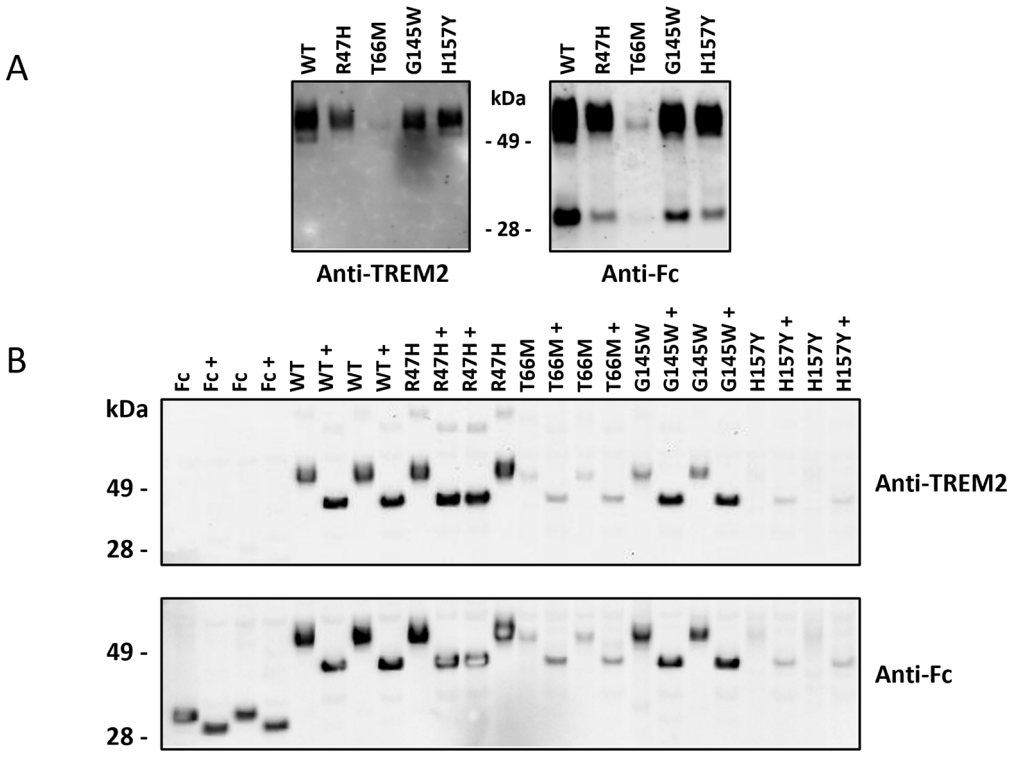

Figure 10 Characterisation of stable cell lines via Western blot.

Detection of the mutant variants in the supernatant of stable cell lines by antibodies against TREM2 (4B2A3) as well as against hIgG1-Fc. Expression is almost consistent throughout all variants except for sTREM2-T66M-Fc, which shows lower expression (n=3). B) Treatment of TCA-precipitated supernatant from stable cell lines with PNGase F (+) reveals a change in the migration pattern, confirming glycosylation of recombinant proteins (n=2).

Previous studies showed that the mutation of TREM2 from threonine to methionine at position aa 66 leads to the retention of TREM2 in the endoplasmic reticulum (Kleinberger, Brendel et al. 2017, Ibach, Mathews et al. 2021). In line with that, it is shown in **Figure 9** A, B and **Figure 10** A that sTREM2-T66M-Fc is predominantly found in the cell lysate but much less in the supernatant. Thus, localization of sTREM2-Fc within the cell was further investigated by immunocytochemical staining with antibodies against "trans-Golgi network protein 2" (TGN46) and calnexin as markers for the trans-Golgi network and the endoplasmic reticulum, respectively (**Figure 11**). Comparison of this staining with an additional staining against TREM2 confirmed that, except for the T66M variant, all variants show strong co-localization with the trans-Golgi marker, which is often observed for extracellular proteins before secretion (Huang, Ma et al. 2019). Staining of sTREM2-T66M-Fc confirmed that indeed, the soluble form of this TREM2 variant shows localization mainly in the endoplasmic reticulum.

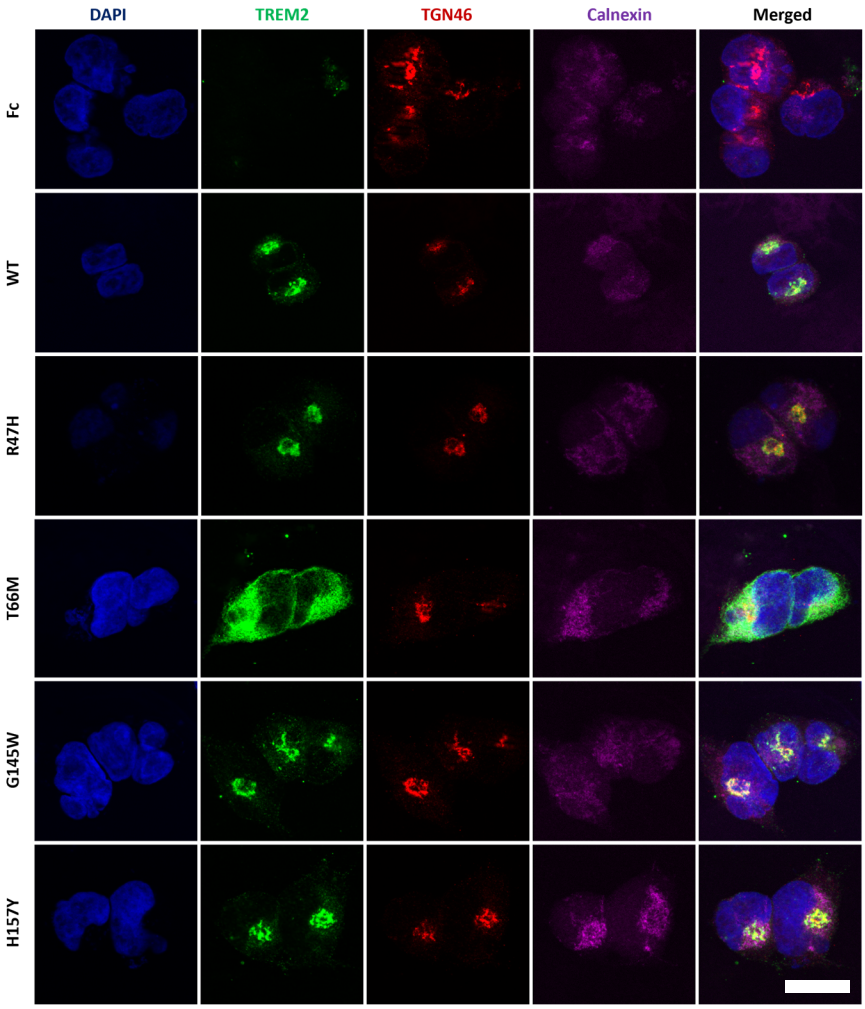

Figure 11 Expression and localization of sTREM2-Fc.

Immunostaining of generated stable cell lines. Nuclei are stained by DAPI (blue), sTREM2-Fc by antibody against TREM2 (AF1828, green), the trans-Golgi network by anti-TGN46 (red), and the endoplasmic reticulum (ER) by anti-Calnexin (purple). TREM2 staining reveals its predominant localization in the trans-Golgi network, except for the T66M variant. This variant shows less focused expression and strong co-localization with the ER marker, confirming its retention in the ER (n=3). Scale bar = 25 µm

3.1.3 Purification of sTREM2

For functional binding studies, the expressed recombinant protein should be further purified to avoid interference from other secreted proteins in the supernatant. This was done by taking advantage of the fact that hIgG1-Fc is fused to the ectodomain of TREM2. By using immobilized protein-G, a protein commonly expressed on the cell membrane of *Streptococcal* bacteria with high affinity for human immunoglobulins, the recombinant protein was captured directly from the supernatant and further purified as described schematically by **Figure 12** A (see methods section 2.4.11).

Therefore, 400 ml of supernatant collected from the generated stable cell lines expressing the different sTREM2-Fc variants or cell lysate in the case of T66M variant was collected and loaded separately on HiTrap™ Protein G HP 1 ml columns (Cytiva Life Sciences, Marlborough, USA) and was then sequentially washed and eluted using a fast liquid protein chromatography (FPLC) system (**Figure 12** B). The protein purification process was monitored via the inbuilt UV-spectrophotometer showing the absorbance at 280 nm. As seen in the UV spectrum, large quantities of unbound proteins are washed out in the beginning, while the amount of desired recombinant protein that comes off during elution is rather low but comparable throughout the variants except for R47H, which, like in **Figure 10** A, seems slightly lower. Again, the supernatant from the T66M variant (**Figure 12** B, T66M Extra) shows almost no protein being present after elution.

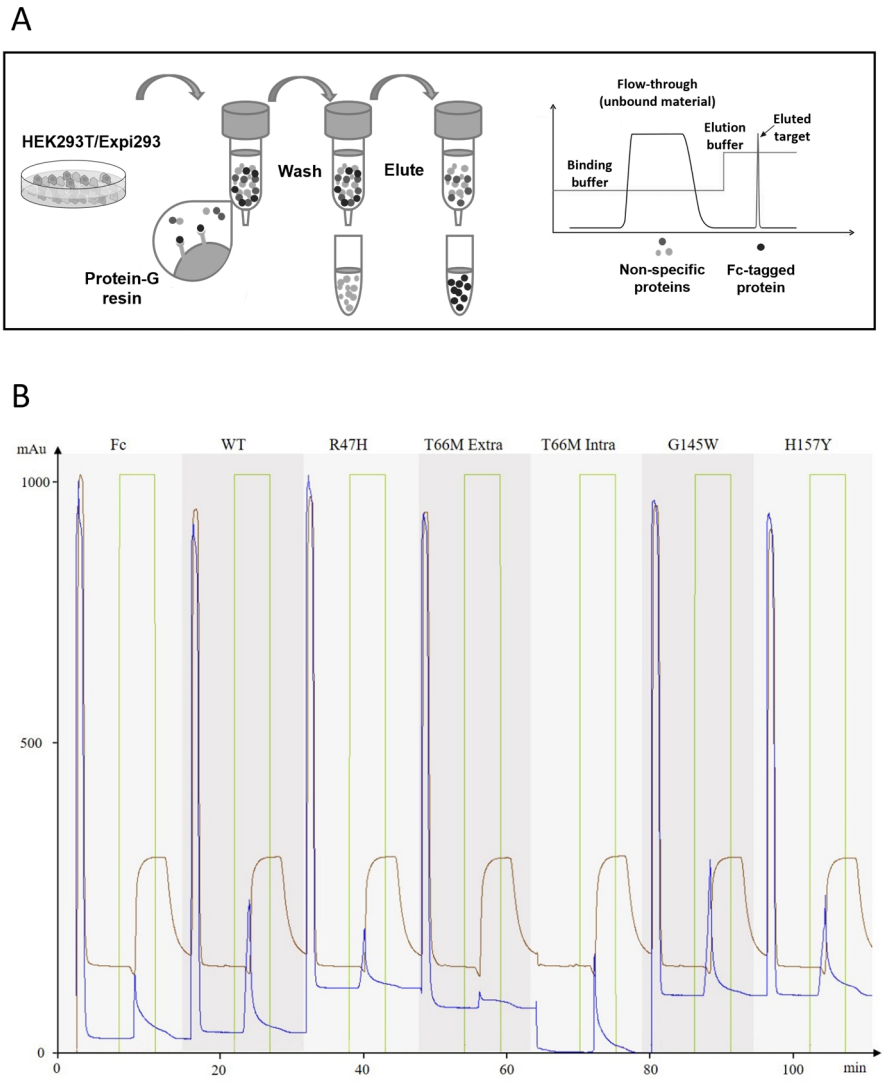

Figure 12 Purification of wild-type and mutant forms of sTREM2-Fc.

A) Schematic overview of the purification process. Taking advantage of the high affinity of the bacterial cell membrane-derived protein-G to the human Ig-domain, proteins recombinantly fused to such can be captured from cell culture supernatant using protein-G immobilized on beads in a batch or column format. Following extensive washing, the pure protein can be easily eluted again, making use of the instability of this binding at pH levels below 3. B) Expressed hIgG1-Fc, sTREM2-Fc, and all its mutant forms were sequentially purified from 400 ml of supernatant or cell lysate (T66M intra) via affinity purification using a protein G sepharose column. The absorbance at 280nm (blue line) was monitored via the inbuilt UV spectrophotometer of the FPLC to compare the UV profiles during elution (green line) of the different variants and to determine the fractions to be pooled. Brown lines represent conductivity of the sample (n=1).

While the general process of purifying sTREM2-Fc from the supernatant was working, the amount of protein that could be successfully purified was still too small and not sufficient to proceed with binding studies. Therefore, the idea was to procure a monoclonal cell line via limited dilution cloning. Hereby, the existing stable cell line expressing wild-type sTREM2 was diluted in a 96-well plate to a single cell per well in selection medium. After isolating single cell clones, the clones were expanded and screened via Western blotting for the highest-expressing clone. The idea was that a stable cell line consisting of only high-expressing cells with varying expression levels of the transgene would increase the amount of recombinant protein in the supernatant.

Comparison of 1 ml of TCA-precipitated supernatant from this single cell clone to the original pool of cells and the supernatant of transiently transfected cells, however, showed that the amount of purified protein did not increase, and the amount of protein gained from transient transfection was almost 10-fold higher (**Figure 13**).

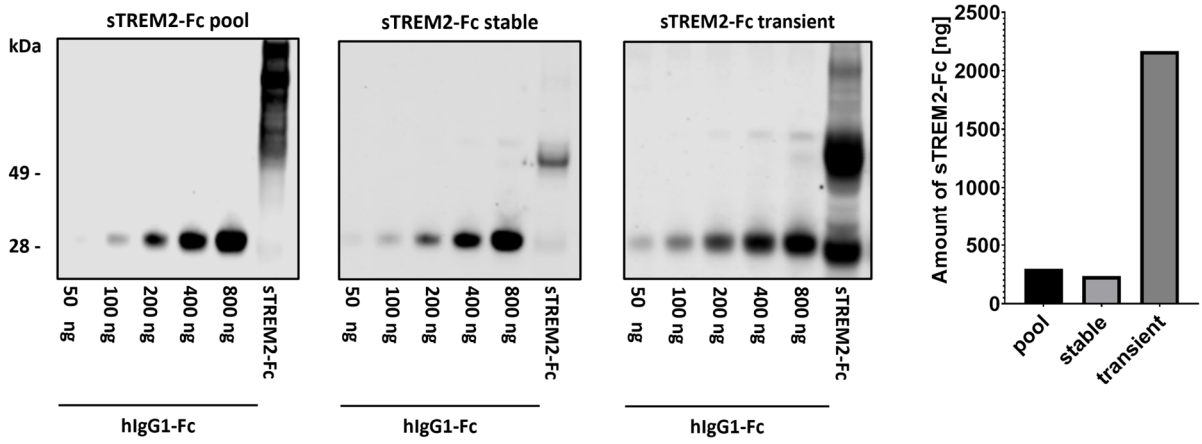

***Figure 13 Comparison of sTREM2 expression in stable and transient cell lines**.*

Western blot analysis of 1 ml of TCA-precipitated supernatant from stably expressing sTREM2-WT-Fc cell lines as well as HEK293 cells transiently transfected with the sTREM2-WT-Fc construct. The reactivity of Fc-specific antibody was compared to pure recombinant hIgG1-Fc loaded in known amounts to determine the amount of recombinant sTREM2-Fc in the sample. Pooled as well as monoclonal cell lines show comparable amounts of protein but of different quality, as apparent from the appearance of additional bands migrating at a higher molecular weight. Transiently transfected cells produced an almost 10-fold excess of protein compared to the stable cell line (n=2).

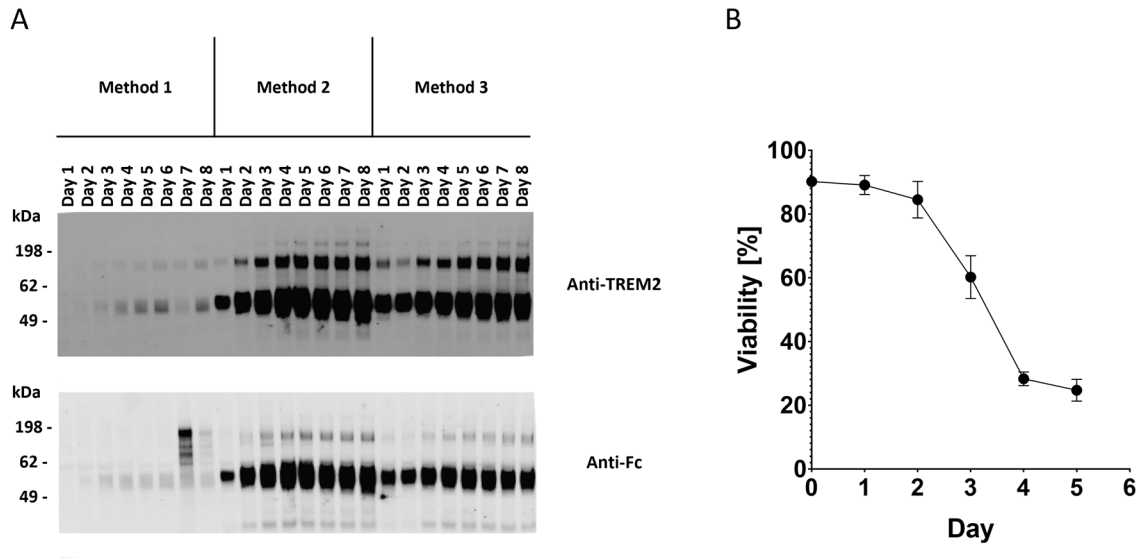

Figure 14 Transient transfection of sTREM2-Fc via polyethyleneimine (PEI).

A) To maximize the yield of sTREM2-Fc expression, three different transfection protocols were compared by subjecting a direct sample of 20 µl from the supernatant after transfection to SDS-PAGE and subsequent Western blot analysis (see section 2.4.11). Samples were taken over a period of 8 days to identify the optimal time point for collection. Secreted protein was detected using the human TREM2-specific antibody AF1828 (top) and the antibody against human IgG1-Fc (bottom). B) Cell viability of the culture prepared according to Method 2 over a period of 5 days. Viability was analysed via trypan blue staining and counting of viable cells via an automated cell counter. After 5 days, viability reached 20 % and no further increase in expressed protein was observed in the Western blot (n=3).

As transient transfection proved to be a much more effective way of expressing recombinant proteins, an alternative method was desired to replace the highly expensive transfection via Lipofectamine 2000. This led to the investigation of polyethyleneimine (PEI) as a transfection reagent. PEI is a stable cationic polymer that allows DNA to enter the cell by first condensing it into positively charged particles, which can then easily bind to the anionic cell surface for endocytosis (Boussif, Lezoualc'h et al. 1995, Sonawane, Szoka et al. 2003). As it is much more cost-efficient, it allows the transfection of large quantities of cells at a time. As a similar procedure had been described for the purification of multispecific multivalent antibodies (Fang, Sehlin et al. 2017), it was aimed to adapt this method for the expression of sTREM2-Fc. For optimization, three varying protocols were tested to transfect Expi293^{TM} cells in suspension (see section 2.4.11), and a sample of the supernatant was collected after a period of 8 days. All

samples were subsequently compared via Western blotting for their expression of the recombinant protein using anti-TREM2 (AF1828) and Fc-specific antibodies (**Figure 14** A). In the first method, cells were transfected at a high concentration (20 million viable cells (mvc)/ml) and diluted to the final volume after 3 h and additionally supplemented with valproic acid (VPA) after 24 h. VPA, a known inhibitor of histone deacetylases (HDACs), has been shown to increase protein expression in transient expression systems by inducing growth arrest and a subsequently longer protein production phase (Wulhfard, Baldi et al. 2010). Nevertheless, this method showed a dramatic decrease in cell viability (not shown) and comparably low protein expression. For the second and third method, cells were transfected at a cell density of 3 mvc/ml in half of the final volume and diluted to the final volume after 24 h. However, while cells in the second method were given VPA as an enhancer of expression, cells in the third method were kept untreated. Both methods yielded a good amount of protein, but in this case, the addition of VPA could indeed increase the protein expression even further. After 5 days, cultured cells reached a cell viability of only 20 % (**Figure 14** B), and no further increase in protein levels was observed in the Western blot (**Figure 14** A), which was thereby determined as the ideal time point of collection. Following the established method, it was possible to produce a sufficient amount of each sTREM2-Fc variant at high purity, as confirmed by Western blot with TREM2 and Fc-specific antibodies (**Figure 15** A) as well as silver staining (**Figure 15** B). In the silver staining, all variants presented as a small smear as well as two additional high molecular weight bands, which were barely observable in the Western blot.

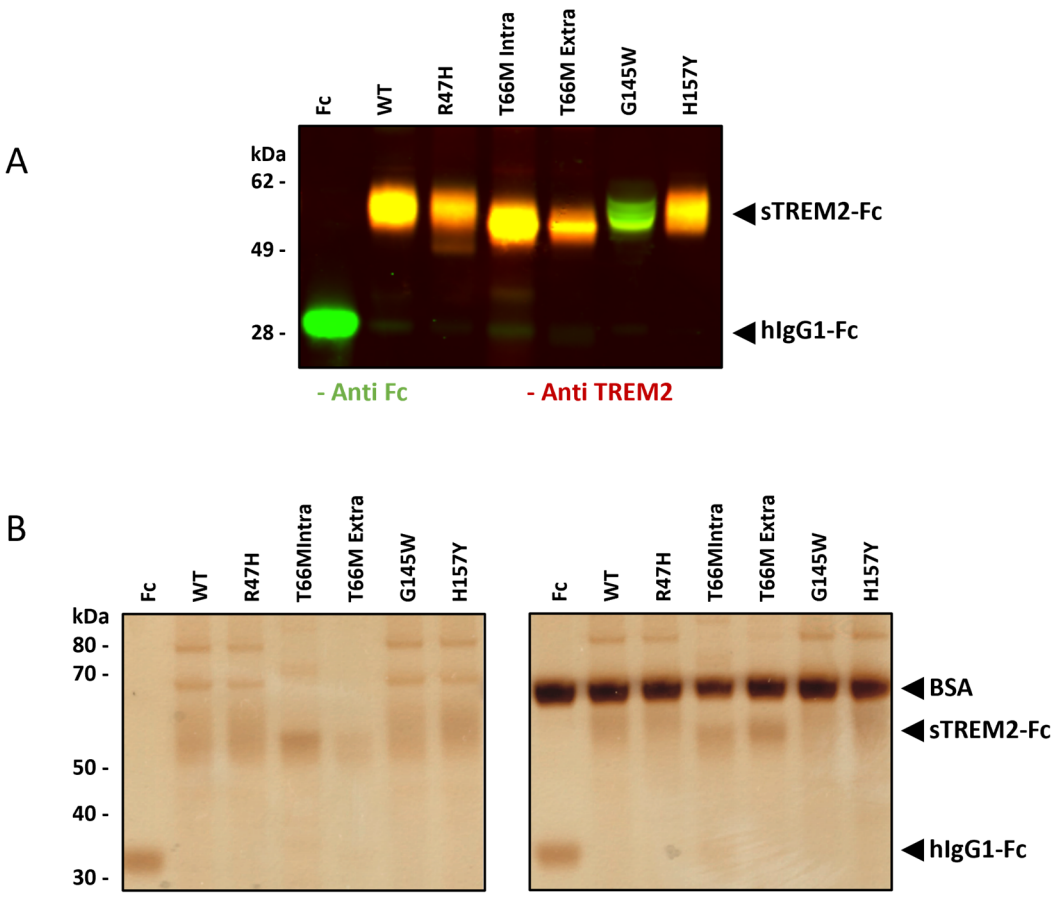

Figure 15 Purity of recombinant sTREM2-Fc.

A) ´The purity of isolated proteins was analysed by subjecting a sample of each variant to Western blot analysis and silver staining B). Depending on the storage temperature, purified sTREM2-Fc variants were supplemented with (right) and without (left) 1 % BSA and 0.01 % sodium azide (n=1).

While the prepared proteins were usually flash frozen in small aliquots and only thawed when needed, sometimes it was necessary to store proteins for a short period at 4 °C, in which case the recombinant proteins were supplemented with 1 % BSA as well as 0.01 % sodium azide (**Figure 16** B right). This ensured the integrity of the proteins as determined via SDS-PAGE and subsequent Coomassie blue staining of samples stored over a period of 3 weeks at 4 °C with and without supplementation with 1 % BSA (**Figure 16**).

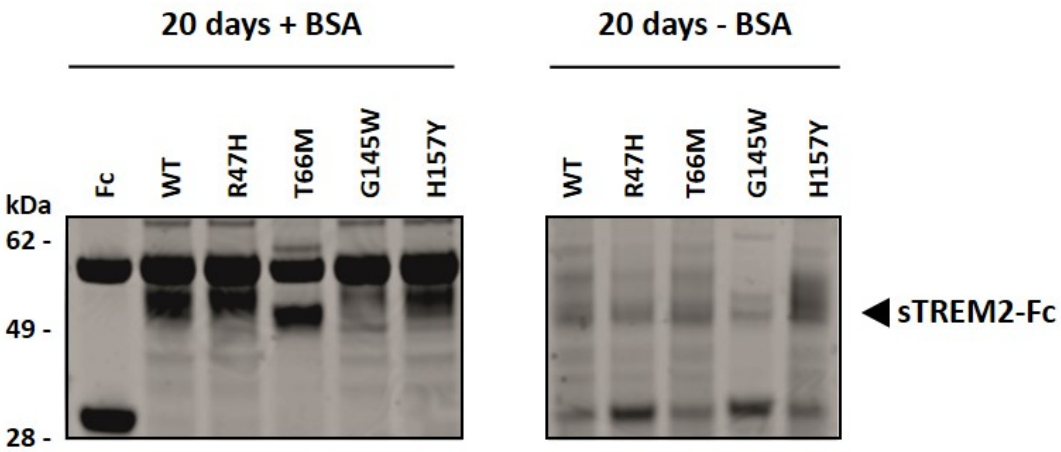

Figure 16 Stability of purified recombinant proteins*. The integrity of proteins was checked by SDS-PAGE and subsequent Coomassie blue staining after storage of the proteins with or without supplementation of BSA and sodium azide for 3 weeks at 4 °C. The addition of BSA and sodium azide protected proteins from degradation, and no change in samples compared to freshly purified proteins (see Figure 15) was observed. While degradation of protein was evident in samples without BSA, as seen by decreased signal intensity, smearing of bands, and an increase in the signal of the Fc band (n=1).*

3.1.4 Purification of sTREM2-TEV-Fc and cleavage

As a hIgG1-Fc-tag functions very well in helping to improve the stability and solubility of its recombinant fusion protein as well as simplifying its purification, it seemed to be the ideal choice and was used throughout this study. However, such a tag might interfere with the biochemical and biophysical properties of the target protein.

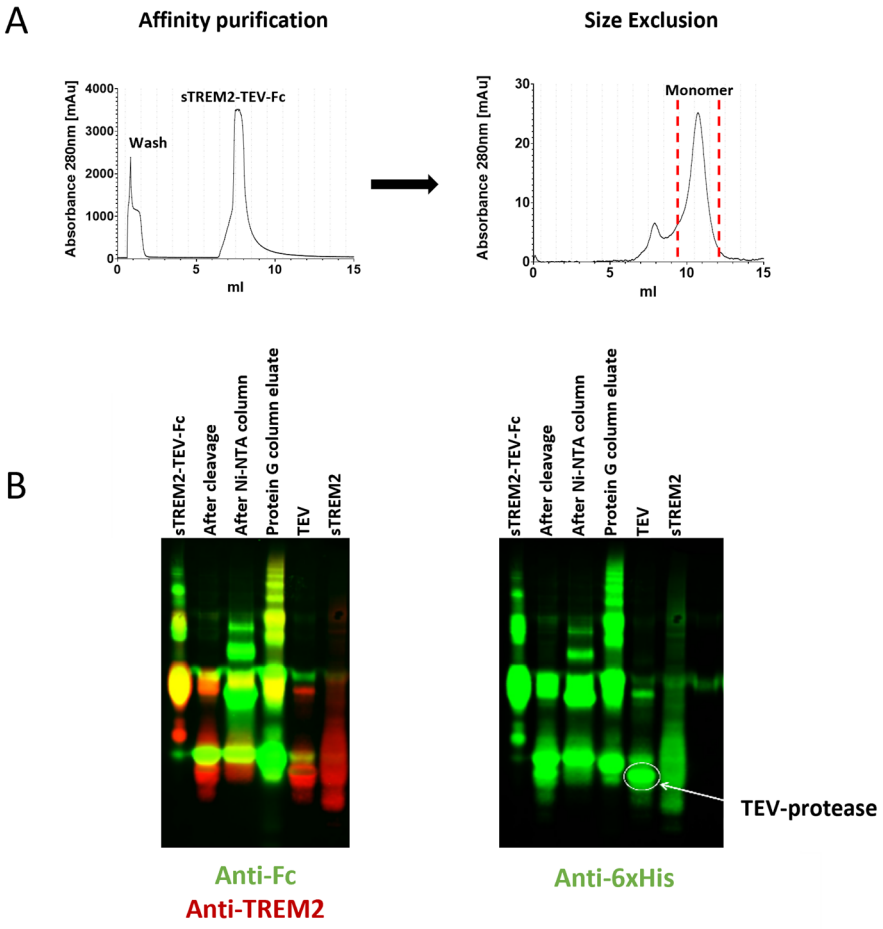

Figure 17 Purification of sTREM2-TEV-Fc via affinity and size exclusion chromatography.

Recombinant sTREM2-TEV-Fc was purified after transient expression in Expi293™ cells via sequential protein G affinity and size exclusion chromatography to isolate solely monomeric protein (A). The purified protein was further cleaved via TEV protease, and His- tagged TEV protease and Fc were removed by immobilized metal affinity chromatography (IMAC) and protein G affinity chromatography respectively. Successful isolation was additionally confirmed by subjecting a sample of each purification step to Western blotting (B). Antibodies specific for TREM2 as well as human Fc confirmed the highly pure sTREM2 without any remaining TEV protease (anti-6xHis antibody).

Therefore, the previously used construct was modified via side-directed mutagenesis following the Gibson method (Gibson, Young et al. 2009). This way, a cleavage site (ENLYFQ) specifically detected by the Tobacco Etch Virus (TEV) protease was introduced between the sTREM2 domain and the Fc-tag (Parks, Leuther et al. 1994). As a result, allowing the highly specific cleavage of the Fc-domain from the desired protein after its purification. The first part of this multi-step purification procedure was done as already described for sTREM2-Fc (**Figure 17** A).

As the TEV protease, however, requires recombinant protein in a pure and monomeric state to exclude unwanted inhibitory effects on the enzyme and guarantee its access to the cleavage site, the recombinantly expressed sTREM2-TEV-Fc was further subjected to size exclusion chromatography (SEC) following the protein-G affinity purification (**Figure 17** A). This procedure ensured that only fractions containing the monomeric protein were used for further purification (fractions between dotted lines). After digestion of the protein via the 6X His-tagged TEV protease, the protease was simply removed by a nickel-nitrilotriacetic acid (Ni-NTA) column, and the flow-through was subjected to another round of protein-G affinity chromatography, separating the untagged sTREM2 (flow-through) from the hIgG1-Fc or uncleaved protein (eluate). Successful purification was then assessed by the analysis of a sample of each purification step via Western blotting. Using antibodies against TREM2, Fc, and 6xHis confirmed the presence of sTREM2 in the final fraction with minimal impurities of TEV protease or Fc (**Figure 17** B).

3.1.5 Characterisation of modified Aβ species

As recent investigations (Zhong, Chen et al. 2017, Zhao, Wu et al. 2018) suggested a preferential interaction of TREM2 with the oligomeric species of Aβ rather than its monomeric or fibrillary form, it was vital to find a reproducible way to prepare Aβ in its oligomeric form and further characterise it to identify the existing oligomeric species in size and quantity. Furthermore, it was of great interest as to how the phosphorylation of Aβ at either serine 8 (pS8) or serine 26 (pS26) might affect the binding of Aβ to TREM2 in comparison to its non-phosphorylated counterpart. The disease-associated and most commonly investigated variant of Aβ is Aβ 1-42, which was also supposed to be the central part of this investigation. At the beginning of this work, however, it was not possible to synthesize Aβ 1-42 phosphorylated at serine 26, for unknown reasons. As a result, experiments were commonly performed with Aβ 3-42, another common AD-associated variant of which all modified species were available (Aβ 3-42, Aβ 3-42 pS8 and Aβ 3-42 pS26). Additionally, experiments were also performed with Aβ 1-42 and Aβ 1-42 pS8 and compared to their 3-42 counterparts to investigate if phosphorylation-induced effects are conserved throughout different length variants. Recent work on the effect of phosphorylation of Aβ on its aggregation behaviour (Kumar, Rezaei-Ghaleh et al. 2011, Kumar, Wirths et al. 2016) already suggested that the phosphorylation of Aβ might speed up the whole aggregation process and thereby result in oligomer-enriched preparations of different compositions, again supporting the importance of characterising used oligomer preparations. Also, during thioflavin T aggregation assays, phosphorylation of Aβ at serine 26 presented an accelerated assembly process (**Figure 18** B), while phosphorylation at serine 8 rather increased the time needed until a stable endpoint of the aggregation was reached (**Figure 18** A and B). Also, while the total change in fold fluorescence fluctuated between experiments, it was always observed that the pS8 variants had much higher endpoints than the non-phosphorylated peptides (**Supplementary 1**). Phosphorylation on S26, on the other hand, showed much less change in fluorescence during aggregation. Throughout the study, two different protocols for the preparation of oligomer-enriched Aβ fractions have been applied to assess potential effects that might arise from different size distributions of oligomers between preparations. While aggregation of the different phosphorylated peptides for 3 h at 37 °C led to fractions with enrichment of especially high molecular weight oligomeric Aβ (**Figure 19** Method 1), the sequential incubation at 23 °C for 16 h and at 4 °C for 24 h showed an oligomer distribution of rather low to high molecular weight (**Figure 19** Method 2). Comparison of the different variants revealed that phosphorylated species presented with higher amounts of

oligomers especially when phosphorylated at S26. Furthermore, bands at the top of the native gel indicate very large assemblies, possibly fibrils, which form during the sample preparation and are not removed from the oligomer preparations using the given method (**Figure 19**). Since modified and unmodified species show differential behaviour regarding their aggregation, it was also expected that the composition of oligomeric preparations might differ depending on Aβ species used. Therefore, the different oligomer-enriched preparations were further characterised via size exclusion chromatography (SEC) under non-denaturing conditions. Absorbance spectra at 280 nm revealed two major peaks, one eluting relatively early at around 8 ml, representing high molecular weight species, and a second broader one at around 17 ml representing smaller species. The former was especially dominant in Aβ 3-42 pS26, while for all other species, the later peak was prevalent. Interestingly, the pS8 species presented itself with a much broader peak than its unmodified counterpart (**Figure 20**).

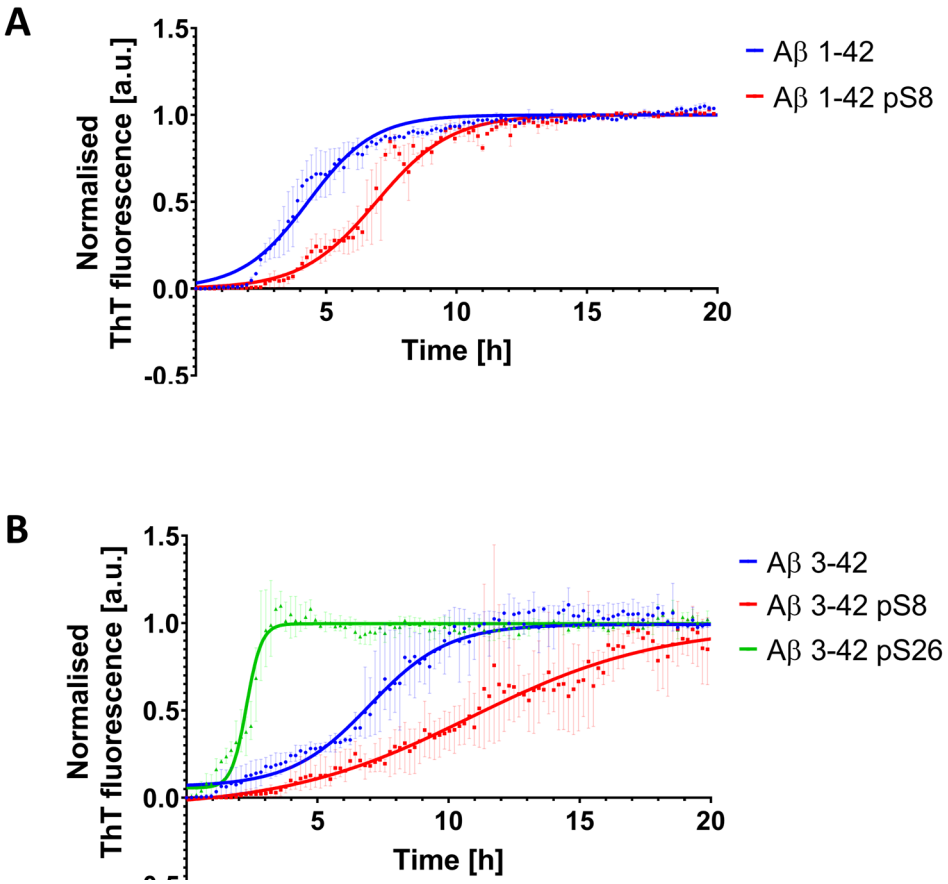

Figure 18 Differential aggregation behaviour of post-translationally modified Aβ species.

Monitoring the relative ThT fluorescence of 5 µM Aβ over a time course of 20 h shows that phosphorylation at serine 26 of Aβ 3-42 drastically shortens the time till a stable plateau is reached compared to non-modified Aβ. In contrast, phosphorylation of Aβ at serine 8 both in the 1-42 (n=2 ±SEM) as well as the 3-42 (n=3 ±SEM) background elongated the time till the plateau was reached. Curve of each variant was normalised to highest ThT reactivity respectively.

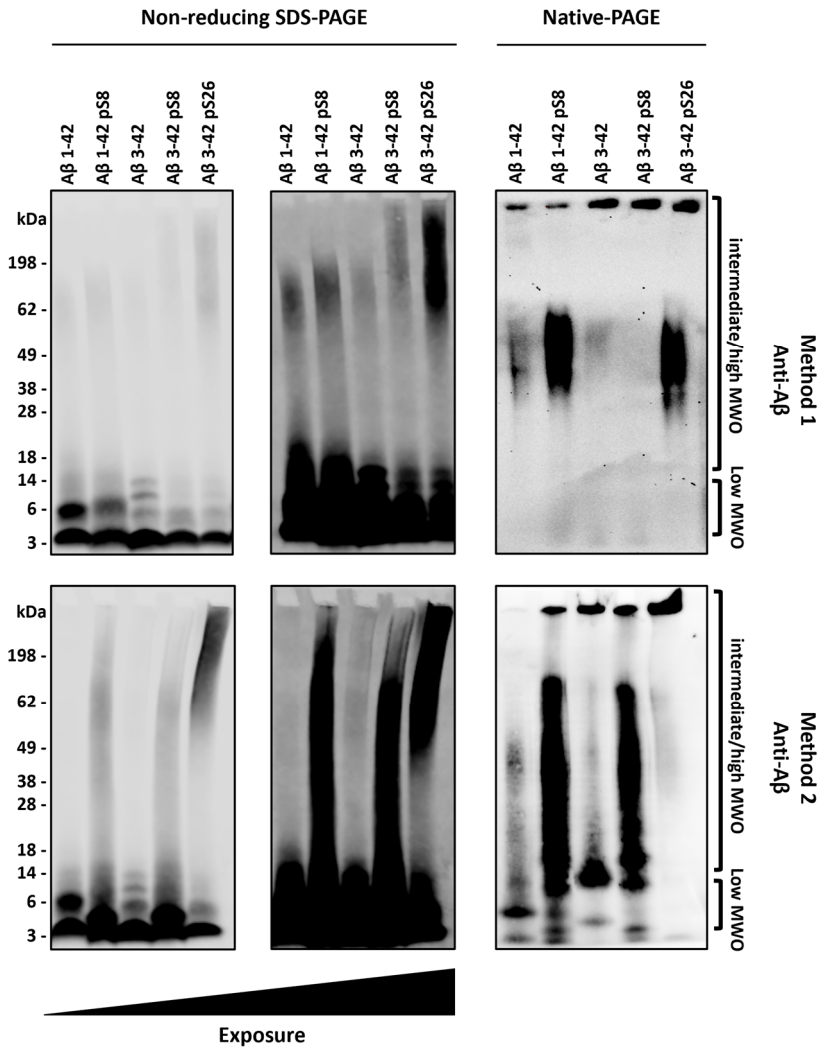

***Figure 19 Preparation of oligomer-enriched species**.*

Separation of the oligomer-enriched Aβ used throughout this study was done under non-reducing conditions using SDS-PAGE and Native-PAGE. Therefore, peptides were either aggregated beforehand for 3 h at 37 °C (Method 1) or sequentially incubated for 16 h at 23 °C and 24 h at 4 °C (Method 2). Western blot signals confirm a mixture of SDS-stable monomers and oligomers of varying sizes (low/intermediate/high molecular weight oligomers (MWO)). Method 1 procures especially high molecular weight assemblies, while Method 2 shows a higher appearance of oligomers of low or intermediate size. Indicated molecular weights as determined by a molecular weight marker during SDS-PAGE do not correlate with native gels.

The distribution throughout the different fractions after size exclusion was further analysed by Western blotting (**Figure 21** A). Hereby, the detection of Aβ in the separate fractions confirmed the distribution as seen in SEC. So, only small amounts of Aβ were detectable in earlier fractions of Aβ 3-42 (Fractions 8-10), and almost all Aβ was detected in the later eluates (Fractions 12-16). In contrast, the pS8 variants were detected throughout the fractions 8-16 in almost similar amounts, in line with the broad peaks observed in SEC. Furthermore, the amount of Aβ in the later eluates was comparable to the pS26 variant, as also seen by their similar broadened peak in the elution profile. Nevertheless, the pS26 variant, unlike other variants, presented large amounts of Aβ being eluted in the earlier fractions (Fractions 8-10). Thus, calculating the size that each eluted fraction represents with the help of a molecular weight standard and categorizing it into low (<12 kDa), intermediate (12-60 kDa) and high molecular weight (>60 kDa) assemblies revealed that the oligomer preparations of unmodified Aβ consist mainly of low, the one of pS8 of low to intermediate, and the one of pS26 of high molecular weight assemblies (**Figure 21** B).

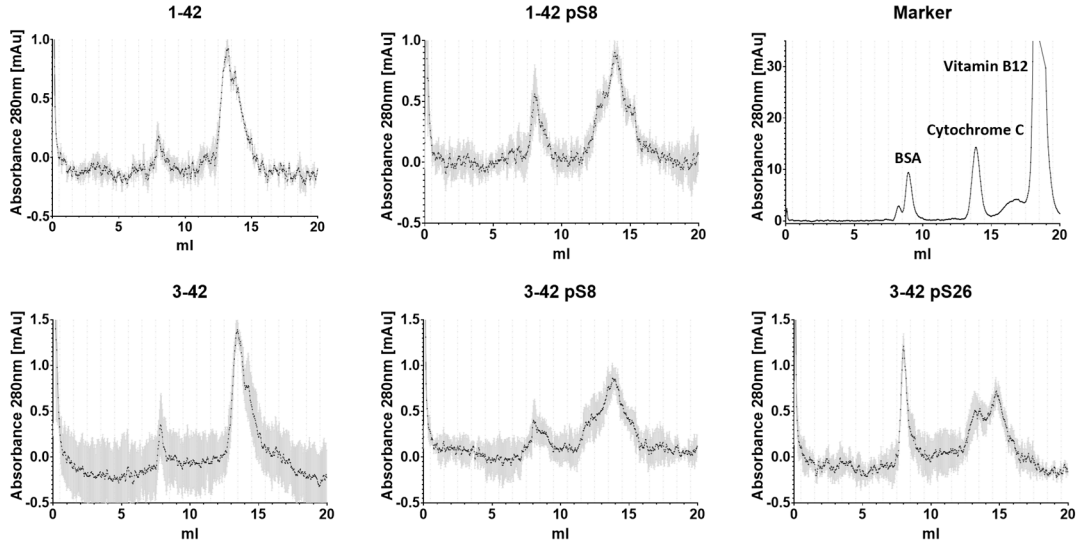

***Figure 20 Characterization of oligomer-enriched Aβ preparations via SEC**.*

Oligomer-enriched Aβ preparations (Method 2) of phosphorylated and non-phosphorylated Aβ 1-42 as well as 3-42 were separated via size exclusion chromatography (SEC Superdex 75 10/300 GL) and monitored via absorbance measurement at 280 nM (n = 3; ±SEM). Comparison to the marker containing bovine serum albumin (66.5 kDa), cytochrome C (12 kDa) and vitamin B12 (1.3 kDa) reveals that non-phosphorylated Aβ as well as Aβ phosphorylated at serine 8 mainly peaks in the range between 4 and 12 kDa, suggesting predominantly low molecular weight oligomers, while phosphorylation at serine 26 shows a higher signal in earlier fractions, representing high molecular weight assemblies at around 60 kDa.

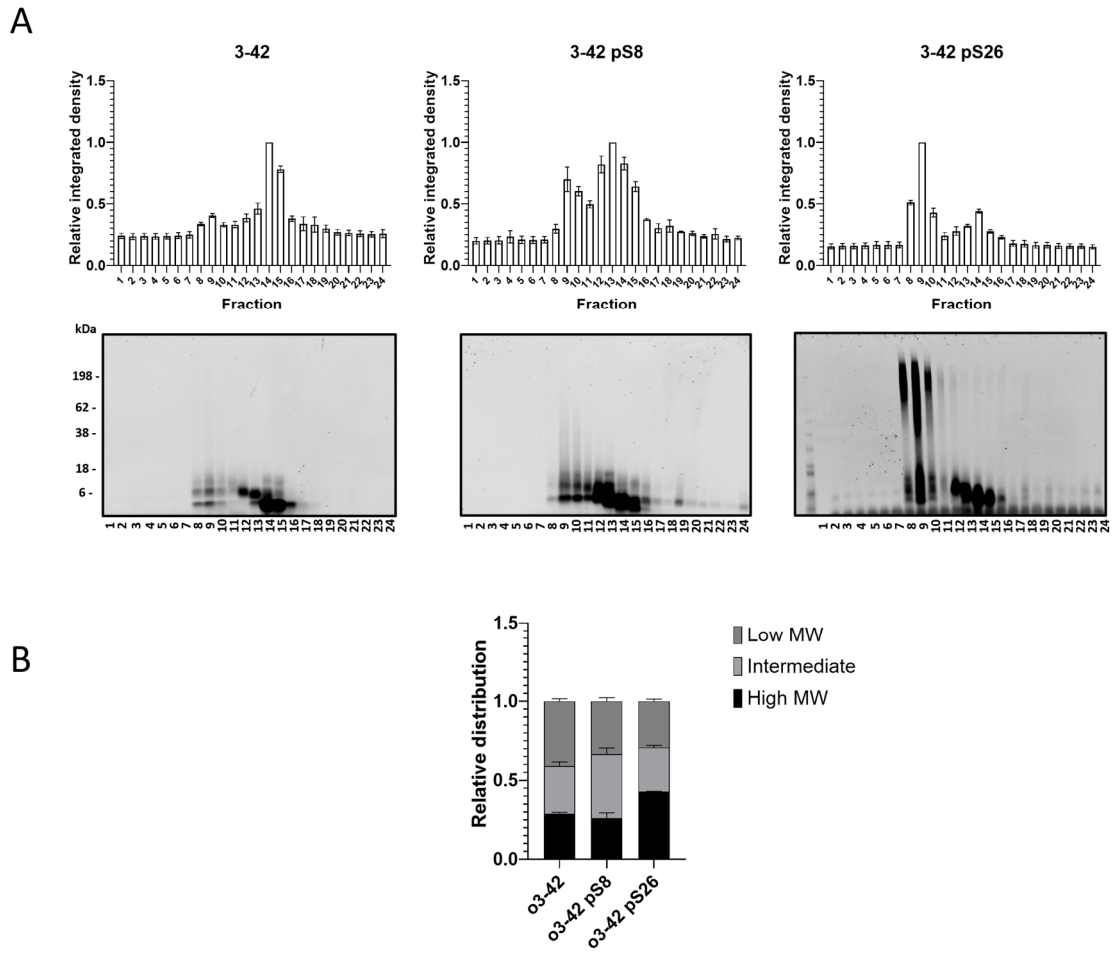

Figure 21 Characterisation of oligomer-enriched Aβ after SEC via Western blotting.

*A) 20µl of SEC fractionated Aβ samples (24 fractions 1ml each) directly loaded on SDS-PAGE gel were visualized via blotting using the generic anti-Aβ antibody (4G8) and the integrated density of each lane was quantified in Image Studio software (LI-COR, Germany). B) Using the molecular weight standard as a reference fraction, preparations were differentiated into low (≤12 kDa), intermediate (12-60 kDa), and high (>60 kDa) SDS stable molecular weight assemblies. Graphs show the relative composition of each oligomer preparation from three independent experiments. The results indicate that oligomer preparations of unmodified Aβ consist mainly of low molecular weight assemblies; preparations of pS8 of low to intermediate; and preparations of pS26 of high molecular weight assemblies. (n=3 ±SEM). Significant changes to the unmodified peptide were determined for each fraction individually *p<0.05; **p<0.01; ***p<0.001*

3.2 Interaction studies

3.2.1 Interaction of differentially aggregated forms of Aβ with sTREM2

To test if the aggregation state of Aβ affects binding to TREM2 as it had been proposed before (Zhong, Chen et al. 2017, Zhao, Wu et al. 2018), different binding studies were performed using the before-mentioned monomeric and oligomer-enriched fractions of Aβ as well as the generated sTREM2-Fc. In all experiments, recombinant hIgG1-Fc (Fc) was used as a control for the specificity of the binding.

In a dot-blot assay investigating the binding capacity of different Aβ variants of different aggregation states to the immobilized sTREM2 (**Figure 22** A), it was seen that interaction was mainly occurring when the oligomeric form of the Aβ variants was applied (**Figure 22** B). This increase in binding to oligomers compared to monomers was significantly increased and only seen for sTREM2-Fc but not for Fc alone. Furthermore, increased binding of oligomeric Aβ 1-42 compared to monomeric 1-42 was also detectable in an enzyme-linked immunosorbent (ELISA)-like solid phase binding assay in which sTREM2 (**Figure 22** D) or Aβ (**Figure 22** C) was immobilized and checked for its binding capacity to one another.

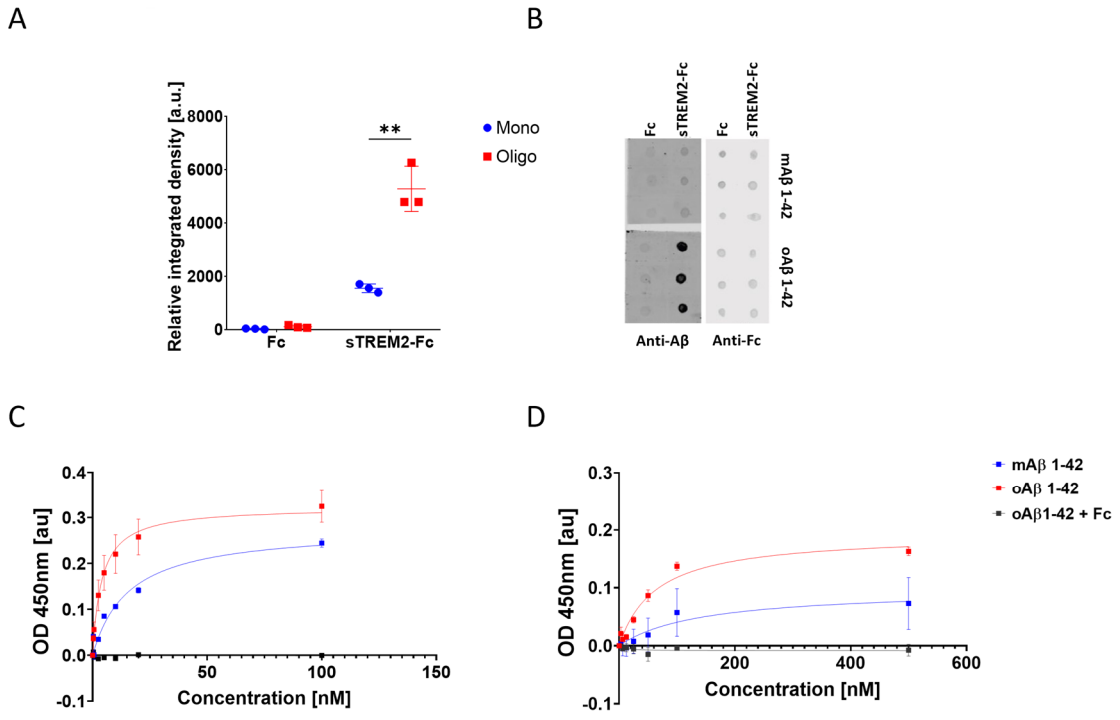

Figure 22 Binding of monomeric and oligomeric Aβ 1-42 to sTREM2-Fc.

Dot-Blot analysis for the binding of monomeric (mAβ) and oligomeric Aβ (oAβ) to immobilized sTREM2-Fc spotted in triplicates onto a nitrocellulose membrane. The integrated density of each spot was normalized to the respective anti-Fc signal and blotted in a graph (A). Each dot represents the mean signal of one experiment (n = 3 independent experiments, unpaired t-test). An exemplary dot blot for sTREM2-Fc, presenting binding to oAβ 1-42 but not to mAβ1-42 is shown in (B).

*Solid phase binding assay showing binding between Aβ and sTREM2-Fc by immobilizing increasing concentrations of either in duplicates on a 96-well ELISA plate and incubating it with a solution of the respective other in the mobile phase (C and D). The saturation binding curve of sTREM2 was calculated using GraphPad Prism, revealing stronger binding of oligomeric Aβ compared to monomeric Aβ. C) Binding of sTREM"-Fc to immobilized Aβ and D) Binding of Aβ to immobilized sTREM2-Fc (n = 3 independent experiments). *p<0.05; **p<0.01*

3.2.2 Differential interaction of modified Aβ species with sTREM2

After identification of the preferential binding of sTREM2-Fc to oligomeric Aβ, as well as the suitability of sTREM2-Fc for binding studies, additional binding studies were performed in order to identify possible effects of Aβ phosphorylation on the interaction with TREM2.
As a result of the findings up to this point, further studies proceeded predominantly with investigating binding to oligomeric Aβ species rather than monomeric as long as it was feasible, as especially in binding studies with cells, the toxic effect of the oligomeric species occasionally restricted their use.
At first, the previously shown dot-blot experiment was therefore extended, now also including monomeric Aβ (mAβ) and oligomeric Aβ (oAβ) from either Aβ 1-42 (**Figure 23** A) or 3-42 (**Figure 23** C), as well as their via phosphorylation at serine 8 (pS8, red) or serine 26 (pS26, blue) modified variants. The results showed that in the Aβ 1-42 (**Figure 23** A) as well as in the Aβ 3-42 (**Figure 23** C) background, a slight but not significant increase in binding to Aβ phosphorylated at pS8 was observable. Phosphorylation of Aβ 3-42 at serine 26, on the other hand, showed a significant increase in binding. Similarly, immobilizing sTREM2-Fc at increasing concentration in a solid phase binding assay also revealed a higher affinity of phosphorylated Aβ in both Aβ 1-42 (**Figure 23** B) as well as 3-42 (**Figure 23** D) backgrounds for sTREM2. This was also reflected by the theoretical dissociation constant (K_D) at equilibrium, which was found to be in the nanomolar range, similar to other studies (Zhong, Chen et al. 2017), and was lowest for pS26, followed by pS8, and lastly by non-phosphorylated Aβ.

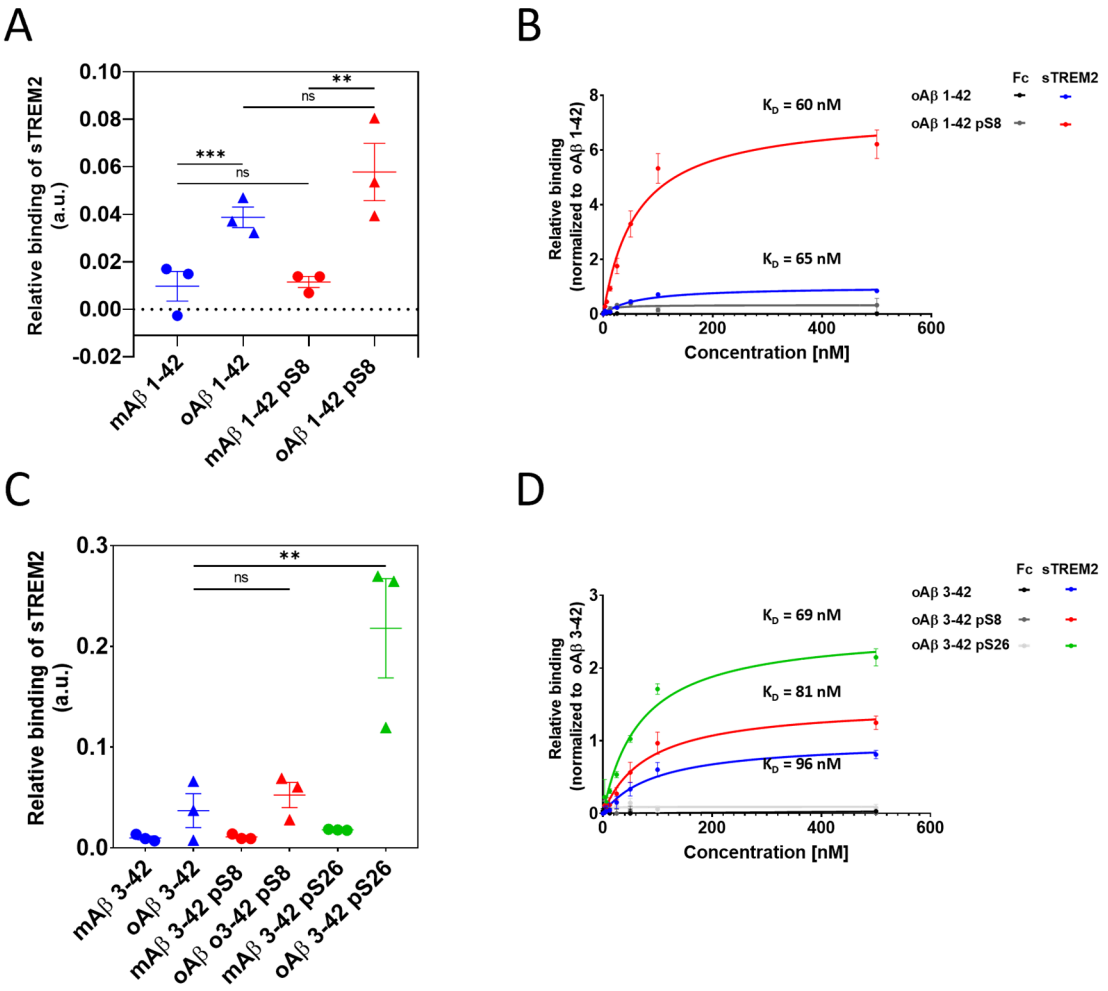

Figure 23 Differential binding of Aβ variants to sTREM2-Fc as determined by Dot-blot and solid phase assay.

(A) Dot-Blot analysis for the binding of different phosphorylation-state Aβ variants at different aggregation state in the 1-42 (A) and 3-42 (C) backgrounds as well as different aggregation states (circle = monomeric Aβ (mAβ); triangle = oligomeric Aβ (oAβ)) to sTREM2-Fc spotted in triplicates onto a nitrocellulose membrane. The integrated density of each spot was normalised to the respective anti-Fc signal and blotted in a graph (A). Each data point represents one experiment (n = 3 independent experiments, unpaired t-test).

*Solid phase binding assay comparing binding between phosphorylated and non-phosphorylated oAβ 1-42 (B) or oAβ 3-42 (D) and sTREM2-Fc by immobilizing sTREM2-Fc or just hIgG1-Fc as control (black and grey curves) in increasing concentrations as duplicates on a 96-well ELISA plate and incubating it with a 100 nM oligomer-enriched solution of Aβ in the mobile phase (n = 3 independent experiments). The binding of unmodified Aβ is indicated in blue, pS8 in red, and pS26 in green. Both Dot-Blot as well as solid-phase assays show a preferential interaction of phosphorylated Aβ with sTREM2-Fc but not with the control. As also represented by their theoretical K_D values as calculated at equilibrium. *p<0.05; **p<0.01; ***p<0.001*

As the previous results already hinted towards the differential binding of phosphorylated and non-phosphorylated Aβ to sTREM2-Fc, this was further investigated by using an immunoprecipitation assay. To do so, magnetic protein G-coupled beads were incubated together with Fc-tagged sTREM2 to create a bait that can be easily added to the different oligomer-enriched solutions of the different variants to fish for interaction partners. In a separate analysis via Western blot, the fraction bound to the beads as well as the unbound fraction could then be compared to the initial input (**Figure 24**).

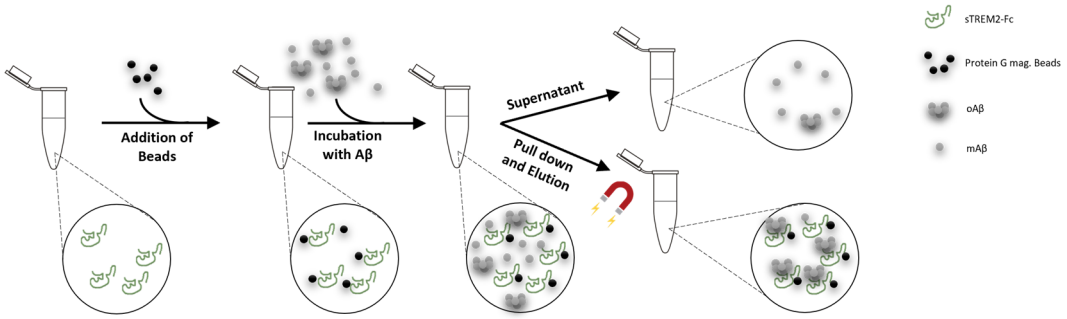

Figure 24 Schematic overview of immunoprecipitation assay.

As the Fc-tag of soluble TREM2 easily binds to protein G, incubation of the recombinant protein with magnetic protein G-coupled beads results in an ideal bait that can be readily added to other solutions for the detection of interaction partners. Thereby, incubating a solution of Aβ enriched in oligomers of different sizes with such a bait will be able to further tell which size of oligomers preferentially bind to sTREM2-Fc and are thereby found after magnetic pull down of the beads in the eluate or which show only weak interaction and thereby remain in the original solution.

The resulting Western blot confirmed once again the preferential interaction of sTREM2-Fc with aggregated species of Aβ, as those were commonly found in the eluate of the beads (bait), while the remaining solution mainly contained the monomeric fraction (**Figure 25** A). Furthermore, the relative amount of Aβ that can be pulled down by sTREM2-Fc from the oligomer-enriched fractions of the phosphorylated and non-phosphorylated peptides was calculated (**Figure 25**) by comparing the integrated density of the Western blot signal in the eluate to the input signal (**Figure 25** B). Hereby, monomers and oligomers were quantified separately.

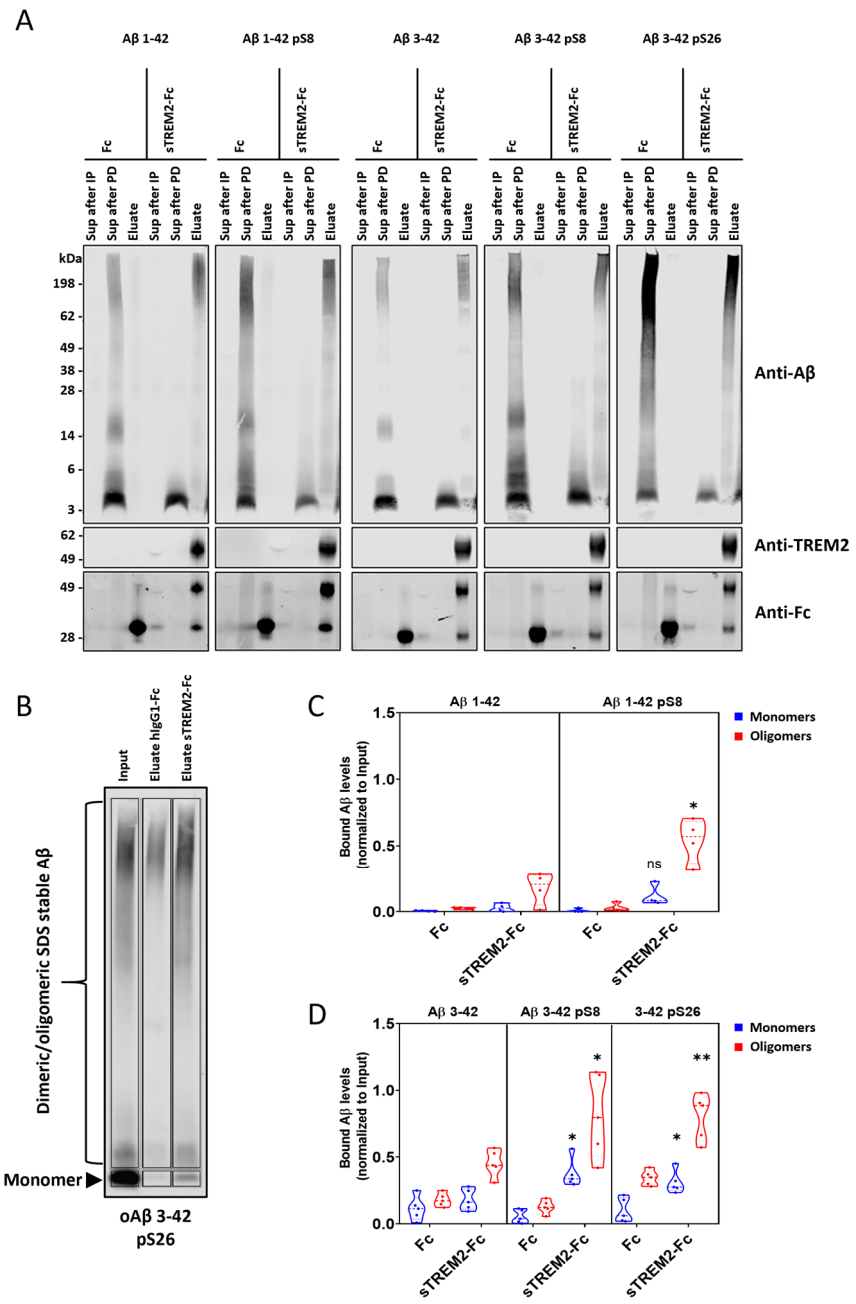

Figure 25 Differential binding of Aβ variants as determined by immunoprecipitation assay.

*A) Representative Western blot of samples from pull-down (PD) experiments for oAβ with sTREM2-Fc or with Fc alone as a control. Efficient pre-coupling of sTREM2-Fc or Fc alone to protein-G magnetic beads is confirmed by the depletion of these proteins from the buffer solution in the supernatant after pre-incubation of beads ("Sup after IP" lanes). A preferential pull-down of oAβ by sTREM2 is indicated by robust signals for aggregated forms of Aβ in the "Eluate" fractions detected in the upper regions of the gels, while large portions of mAβ remain in the supernatant after the pull-down ("Sup after PD"). Differential binding was visualized by a violin plot of IntDen of signals for the monomer band or oligomeric forms, as shown exemplary in (B) of Aβ 1-42 (C) and 3-42 (D) variants. Values were normalised to the respective input. Each dot represents an independent experiment. All data represent the mean ± SEM (n = 4 for Aβ 1–42 or n = 5 for Aβ 3–42 variants, unpaired t-test with Welch correction, *p<0.05; **p<0.01; ***p<0.001). Data adapted from already published results (Joshi, Riffel et al. 2021, Joshi 2022).*

As seen before, phosphorylation of the peptides in the Aβ 1-42 (**Figure 25** C) and 3-42 (**Figure 25** D) backgrounds led to stronger binding to sTREM2 and therefore to a significantly more efficient pull-down.

Finally, the differential interaction of modified Aβ species with TREM2 was further investigated in a cell-based system using the full-length receptor to expand previous studies and test if the differential interaction of Aβ species is also observed with membrane-bound full-length TREM2.

Therefore, the previously in the lab generated and characterised monoclonal cell line (Ibach, Mathews et al. 2021) with a stable bicistronic expression of TREM2 and DAP12, as well as HEK293 as the respective control, were incubated with increasing concentrations of monomeric Aβ 1-42 as well as its modified variants pS8 and pS26 for 2 h on ice to assess binding. Immunocytochemical staining of Aβ after fixation of cells confirmed the increase in cell-associated Aβ in a concentration-dependent fashion (**Figure 26**), especially in TREM2-expressing cells compared to non-expressing control cells. Furthermore, Aβ binding was especially observed in areas of the membrane with high expression of TREM2 as observed by co-staining against TREM2 (**Supplementary 2**).

Analysis of the integrated density of Aβ staining per cell followed by non-linear regression analysis (Gompertz growth) supported the observed increase in binding in TREM2-expressing cells over the control (**Figure 26** A). Additionally, as indicated by the inflexion point of the curves, binding of Aβ 1-42 pS8 and pS26 variants to the cells occurs already at lower concentrations in comparison to the non-phosphorylated Aβ 1-42 (**Figure 26** B), in accordance with previous in-vitro studies.

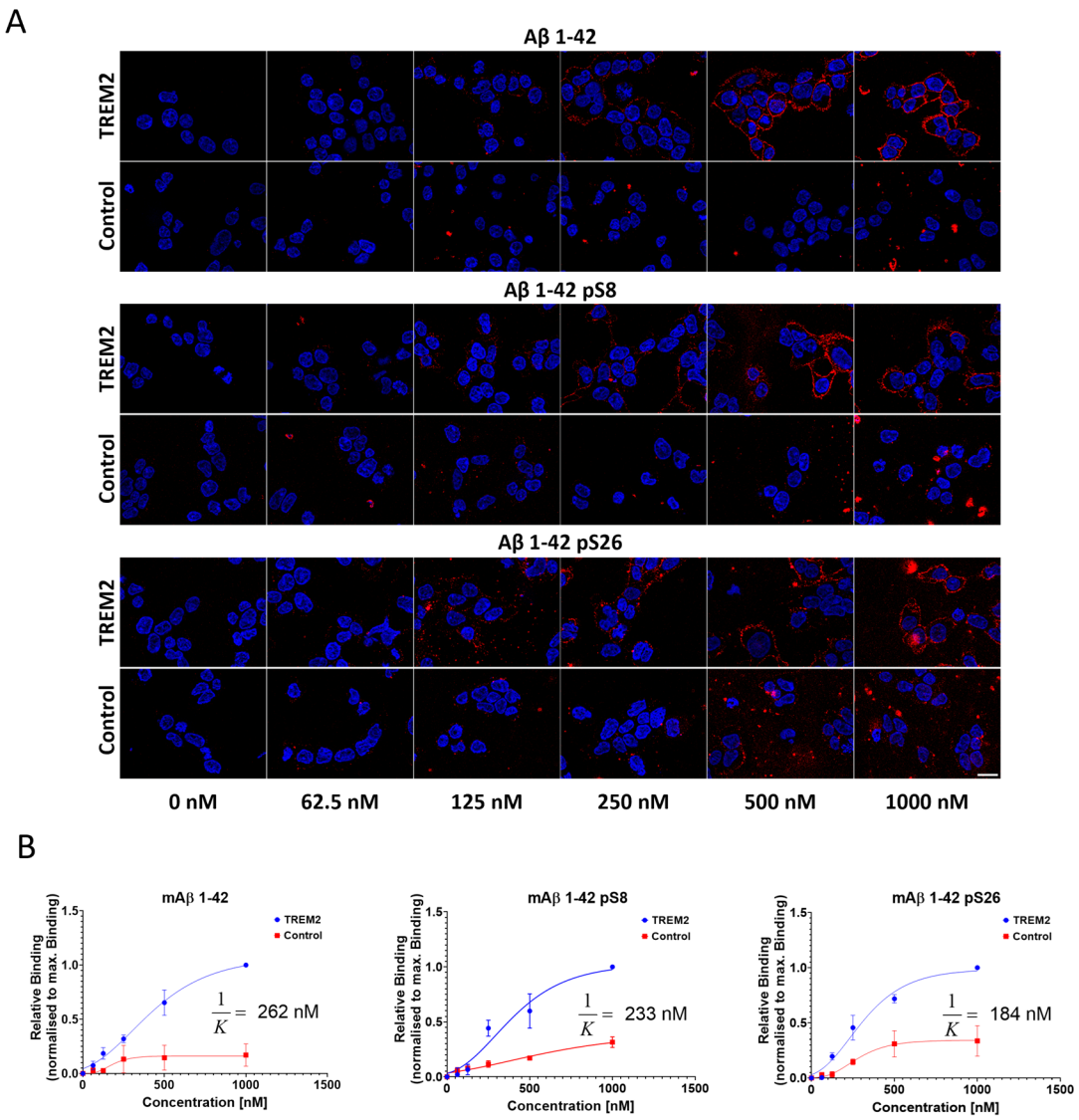

Figure 26 Binding of differentially modified Aβ in a TREM2 expressing cell system.

A) Binding of the three different monomeric variants Aβ 1-42, Aβ 1-42 pS8, and Aβ 1-42 pS26 was compared by incubation of HEK293 cells (Control) or HEK293 cells with bicistronic expression of TREM2 and DAP12 (Ibach, Mathews et al. 2021)(TREM2) for 2 h on ice. Immunocytochemical analysis after fixation by staining nuclei with DAPI (blue) and Aβ with the generic anti-Aβ antibody 82E1 (red) revealed a concentration-dependent increase in the binding of Aβ to cells, especially in the TREM2 expressing system. B) Quantification of anti-Aβ IntDen from 50 cells per experiment at a given concentration plotted as mean ± SEM (n = 3) followed by non-linear regression analysis (Gompertz-growth function). Lower inflexion points of phosphorylated Aβ compared to non-phosphorylated Aβ indicate stronger Aβ association with cells at already lower concentrations. Inflexion points are indicated in the respective graphs by 1/K values.

Similar behaviour was investigated in a more biologically relevant system, as the overexpression of TREM2 in HEK cells poses as a rather artificial system. Therefore, primary microglia from wild-type (WT) C57BL/6 mice expressing endogenous TREM2 were prepared and exposed to oAβ 1-42 as well as its phosphorylated variants pS8 and pS26 in a similar fashion as before. The cells were incubated on ice in the presence of the different variants for 2 h and subsequently investigated via immunocytochemical staining. Additionally, the effect of human sTREM2-Fc or Fc alone, present during the oligomerization of Aβ, was to be investigated. Co-staining with phalloidin and the generic Aβ antibody 82E1 revealed binding of Aβ 1-42 and Aβ 1-42 pS8 as small puncta on the cell surface, while pS26 presented rather large spherical signals much brighter than the other two variants. Nevertheless, comparison with the staining of Lamp1, a lysosomal marker, confirmed only binding to the cell surface but no uptake yet (**Figure 27** A). Quantification of the Aβ signal per cell showed a similar tendency as in the previous experiment, with a small increase in binding of phosphorylated Aβ over non-phosphorylated Aβ for pS26, while pS8 shows not much change, even a slight decrease in binding occasionally (**Figure 27** B). Comparable results were also seen before using Aβ 3-42 variants in the same experimental setup (already published data;(Joshi, Riffel et al. 2021, Joshi, Riffel et al. 2021)). Interestingly, the addition of sTREM2-Fc but not Fc during the aggregation of Aβ from monomers to oligomers increased the binding of Aβ 1-42 as well as Aβ 1-42 pS26 to the cell surface, as seen by the increase in small puncta at the cell surface (**Figure 27** A). An effect of sTREM2 on the binding of pS8 to the microglial surface was also observed, although this difference was not statistically significant.

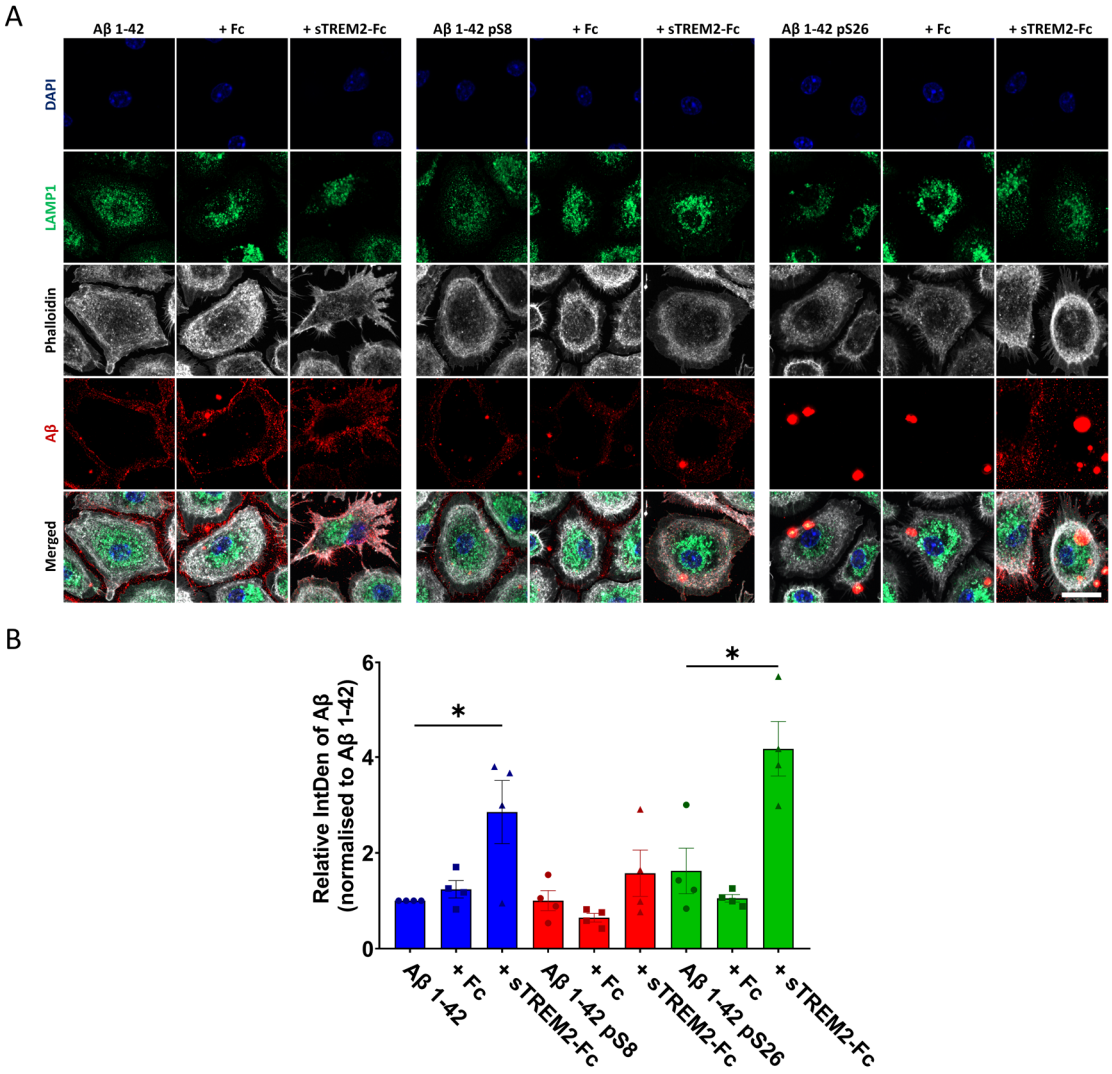

Figure 27 Binding of differentially modified Aβ to primary microglia.

*A) Representative immunocytochemical staining images of primary microglia from wild-type (WT) mice and a plot showing the normalised IntDen of Aβ 1-42 signal per cell after incubation of cells on ice for 2 h with 0.5 µM oAβ prepared by aggregation of Aβ variants (23 µM) at 37 °C for 3 h in the presence or absence of sTREM2-Fc/Fc (1 µM) B) Following fixation, cell nuclei were stained by DAPI (blue) and actin fibres by phalloidin (white), while Aβ was stained via the generic antibody 82E1 (red). The Lamp1 antibody was employed as a lysosomal marker (green) (scale bar = 25 µm). Each dot represents the average value of normalised integrated density calculated by manually drawing a border around randomly selected Aβ positive cells (30 cells/group/experiment), and hence a total of 120 cells/group (n = 4, unpaired t-test with Welch correction). Only a slight increase in the binding of modified Aβ variants was observed compared to non-modified Aβ. Pre-incubation of Aβ during oligomerization with sTREM2-Fc but not Fc, on the other hand, significantly increased the amount of Aβ detected at the cell surface. Data represent the mean ± SEM. *, $p < 0.05$*

3.3 Functional aspects resulting from the differential binding of sTREM2 to modified Aβ species

3.3.1 TREM2 modulates cellular uptake of differentially modified Aβ species

TREM2 is predominantly found on the cell surface of microglia throughout the brain and has been proposed to take part in a variety of different pathways regulating microglial survival, inflammatory response, lipid metabolism, differentiation, as well as phagocytosis (Atagi, Liu et al. 2015, Jay, Miller et al. 2015, Zhong, Chen et al. 2017). As phagocytosis of Aβ from plaques by microglia has been proposed to be inhibited by the interaction with oAβ (Pan, Zhu et al. 2011), the idea was to investigate if the observed differential interaction of TREM2 and modified oAβ species might also change phagocytic uptake by microglia. Therefore, primary mouse microglia expressing endogenous TREM2 (WT) and mice with the TREM2^{T66M} knock-in (KI) mutation were incubated in the presence of oAβ 1-42, 1-42 pS8, or 3-42 and its phosphorylation-state variants pS8 or pS26 (see section 2.5.1 2nd way). As shown before, the T66M mutation of TREM2 leads to its retention in the ER, which in this case was supposed to result in a functional knockout of TREM2 functions like regulation of phagocytosis. Following fixation, internalized Aβ was detected via immunocytochemical staining with the generic anti-Aβ antibody 4G8. Lamp1 was detected with an anti-Lamp1 antibody as a lysosomal marker (**Figure 28** A and **Supplementary 3**). Staining as well as quantification of internalized Aβ per cell revealed increased uptake of oAβ 3-42 pS26 but decreased uptake of pS8 in both Aβ 1-42 as well as 3-42 background as compared to unmodified Aβ (**Figure 28** B). This was also observed in microglia from mice with the knock-in mutation T66M (**Figure 28** A and **Supplementary 3**), but overall internalization of all Aβ variants was strongly decreased in those cells, similar to WT cells pre-treated with cytochalasin D (CytoD) as an inhibitor of endocytosis, phagocytosis, and micropinocytosis (Ting-Beall, Lee et al. 1995, Lin, Singla et al. 2018). Furthermore, the validity of using the TREM2^{T66M} KI mutation as a functional knockout of TREM2 in binding and uptake studies was confirmed by the decreased uptake of fluorescent beads seen in those microglia compared to their WT counterpart (**Supplementary 4**).

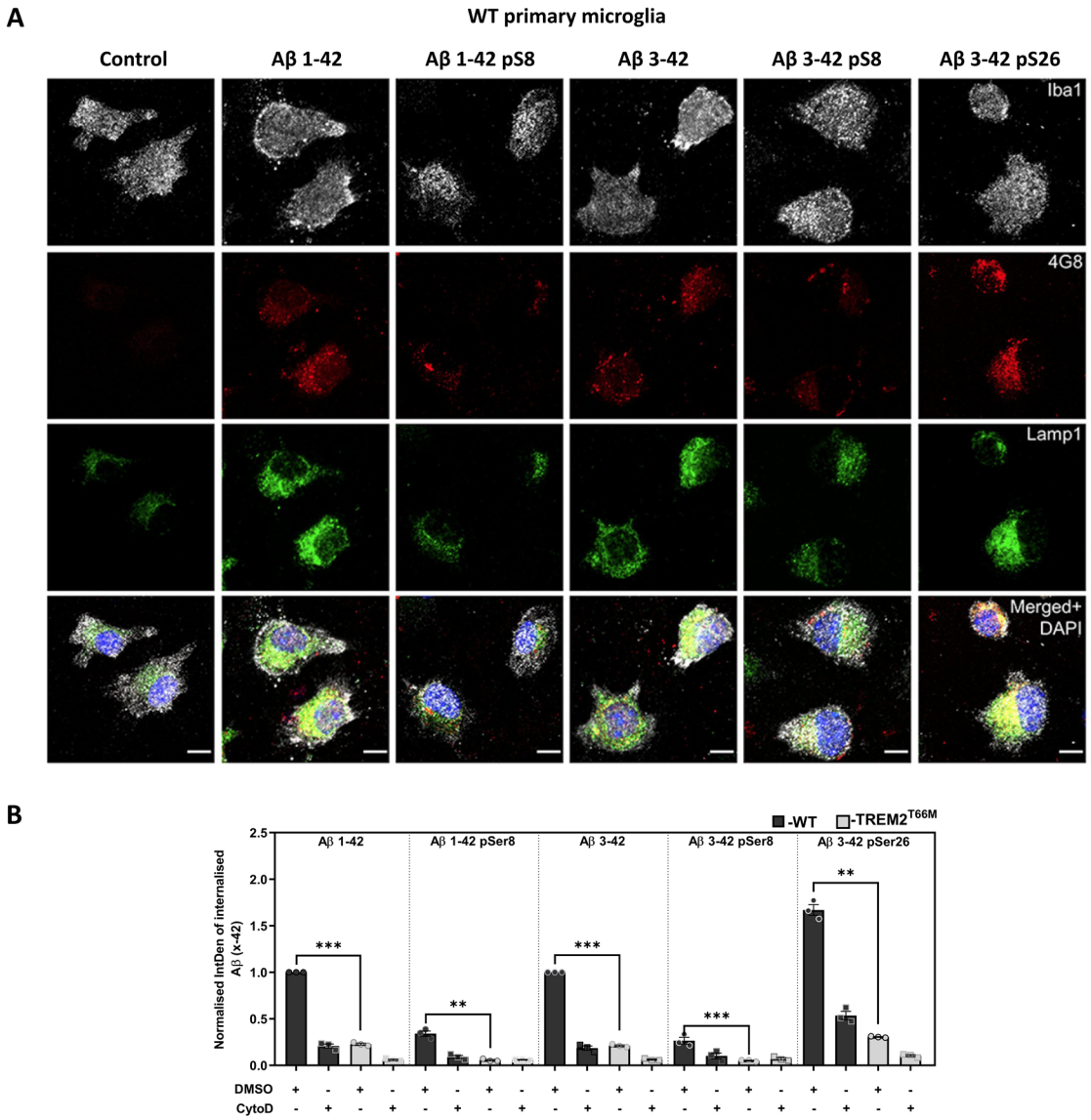

Figure 28 Differential uptake of Aβ variants by primary microglia.

A) Exemplary immunocytochemical staining of primary microglia from WT mice after treatment with 1 µM oligomeric Aβ for 2 hours at 37 °C. Microglial cells were stained using the Iba1 antibody (white), while Aβ was stained via the generic antibody 4G8 (red). The Lamp1 antibody was employed as a lysosomal marker. Scale bar = 10µm

*The difference in the internalisation of different Aβ variants by primary microglia from WT and TREM2^{T66M} mice after treatment with 1 µM oligomer rich Aβ for 2 hours at 37 °C was determined via immunocytochemical staining. Each dot represents the average value of normalized integrated density, calculated by manually drawing a border around randomly selected Aβ positive cells, 10 cells/image, 50 cells/coverslip (100 cells/experiment and hence total of 300 cells/group (n = 3, unpaired t-test with Welch correction).Data represent the mean ± SD. **, $p < 0.01$; ***, $p < 0.001$*

Data adapted from already published results (Joshi, Riffel et al. 2021, Joshi 2022).

An important hallmark of Alzheimer's disease is the progressive loss of neurons and the concomitant loss of cognitive functions, especially memory. The exact reasons for the demise of neurons are still under debate, but a large amount of evidence over the years suggests the involvement of Aβ accumulation and resulting neurotoxicity (Pike, Walencewicz et al. 1991, Yan, Chen et al. 1996, Mucke, Masliah et al. 2000). While most of those studies investigated the accumulation of extracellular Aβ, more and more studies today also describe an intracellular accumulation of Aβ, which might even precede extracellular plaque formation (Masters, Multhaup et al. 1985, Wirths, Multhaup et al. 2001). Nevertheless, the origin and role of this intracellular Aβ is still under debate. So, as TREM2 plays a supposedly critical role in the uptake of Aβ in microglia (Jiang, Tan et al. 2014, Kleinberger, Yamanishi et al. 2014), the idea was that the presence of the soluble form of TREM2 might also increase Aβ uptake in different cells. This was recently observed and described by Belsare, Wu et al. (2022), who showed that incubation of Aβ oligomers and fibrils with sTREM before addition to neuronal cells increased the amount of Aβ being internalized.

Primary neurons (21 days in vitro cultured (DIV21)) were therefore exposed to oAβ prepared via oligomerization at 37 °C for 3 h in the presence or absence of sTREM2-Fc or Fc. Internalization of Aβ was afterwards determined via immunocytochemical staining with an anti-Aβ antibody (82E1) (**Figure 29**). No internalized Aβ in the cell soma was detectable in all cases. However, Aβ was strongly accumulated at the processes of the neurons and staining revealed partial colocalization of phalloidin puncta and Aβ. These puncta have recently been described to mark presynaptic vesicles, possibly indicating the preferential localization of Aβ at synapses (Yu, Jans et al. 2018). The amount and distribution of Aβ showed no obvious alterations between Aβ (**Figure 29** A) and Aβ pre-treated with sTREM2-Fc (**Figure 29** C) or Fc (**Figure 29** B) at the given possible resolution of the microscope (Zeiss Apoptome). Upon sTREM2-Fc/Fc treatment, the overall number of cells (not counted) and number of processes per cell appeared lower, suggesting a possible neurotoxic effect of sTREM2-Fc/Fc directly or an effect caused indirectly by the preincubation of Aβ with such.

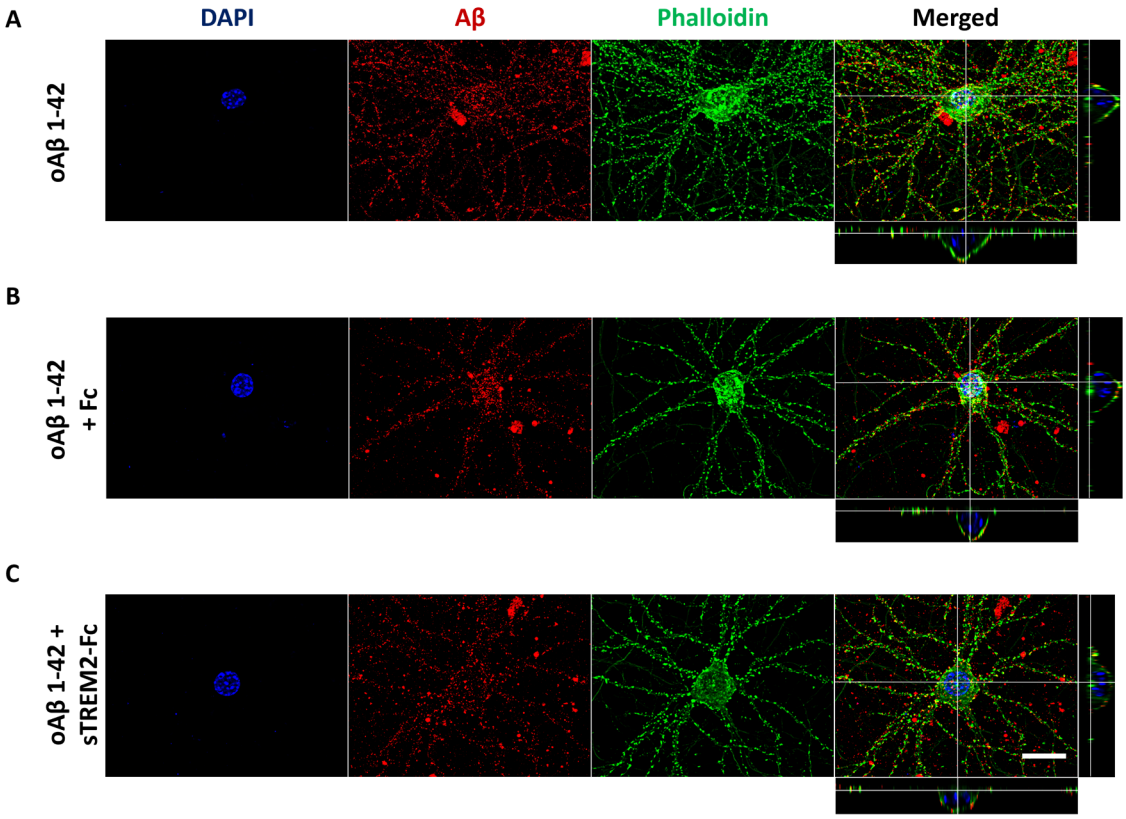

Figure 29 Binding and uptake of Aβ by neurons in presence or absence of sTREM2.

Primary mouse cortical neurons cultured for 3 weeks (DIV21) were incubated for 4 h at 37 °C with 0.5 µM oAβ prepared by aggregation of Aβ 1-42 (23 µM) at 37 °C for 3 h in the absence (A) or presence of sTREM2-Fc/Fc (B/C) (1 µM). Following fixation, cell nuclei were stained by DAPI (blue) and actin filaments by phalloidin (green), while Aβ was stained via the generic antibody 82E1 (red). (Scale bar = 25 µm) Maximum intensity projection as well as an orthogonal view of the cell reveal no detectable Aβ within the cell soma but abundant signals of Aβ bound to the surface of the soma and neurites of the neurons.

3.3.2 Inhibitory effect of sTREM2 on Aβ aggregation

Since the development of the amyloid cascade hypothesis, amyloid β aggregation has been at the centre of research efforts to find ways to slow down or even prevent the disease progression of AD. Recently, the Food and Drug Administration (FDA) approved an anti-Aβ antibody targeting oligomeric species of Aβ for the treatment of AD (Budd Haeberlein, Aisen et al. 2022). But efforts are also made to identify natural compounds interfering with Aβ assembly (Pagano, Tomaselli et al. 2020) as well as endogenous mechanisms that regulate Aβ aggregation in vivo.

Indeed, after determining oligomeric Aβ as a potential ligand for TREM2, two independent studies presented consistent results showing an effect of the soluble TREM2 domain not just in binding but also in the inhibition of Aβ aggregation in vitro (Vilalta, Zhou et al. 2021, Belsare, Wu et al. 2022). While the effect of adding sTREM2 in sub-stoichiometric amounts during aggregation to inhibit further Aβ aggregation was quite well shown, nothing was reported on how modifications of Aβ by phosphorylation might modulate this effect. That even small variations can change the behaviour of peptides can already be seen quite evidently by the differential aggregation behaviour of Aβ 1-42 compared to 1-40 (Meisl, Yang et al. 2014). Since phosphorylation of Aβ already showed differential binding to sTREM2-Fc, it was tested whether TREM2 also affects the aggregation of these modified Aβ species (**Figure 30**).

Indeed, sTREM2 decreased the aggregation of all tested Aβ variants, similar to what was reported for Aβ 1-42 (Vilalta, Zhou et al. 2021, Belsare, Wu et al. 2022). This was further confirmed by Western blot analysis showing the reduction of fibrillary material in the top wells of the gel accompanied by an increase in low molecular weight reactivity after aggregation of Aβ for 15 h in the presence of increasing concentrations of sTREM2 (**Figure 30** F). Evidently, already the truncation of the first two amino acids had a severe effect on the onset and overall aggregation, as seen by the ThT curves in the absence of sTREM2 (**Figure 30** A compared to C and B compared to D). This effect seemed to dominate any effect caused by the phosphorylation. So, for example, higher concentrations of sTREM2 in the Aβ 1-42 background (**Figure 30** B compared to A) and lower concentrations in the Aβ 3-42 background (**Figure 30** D compared to C) were necessary to inhibit aggregation of pS8 variants when compared to their respective non-modified peptides. Thus, for Aβ 1-42 a change in overall fluorescence (reflecting the fibril formation) after 15 h is only observed in the control and in the presence of 100 nM sTREM2, while for Aβ 1-42 pS8 an increase in fluorescence is still observed after addition of 250 nM sTREM2. In the case of Aβ 3-42 even the addition of 1000 nM sTREM2

still showed a change in fluorescence after 15 h, while for Aβ 3-42 pS8 the addition of 500 nM and 1000 nM sTREM2 already inhibited aggregation and showed no change in fluorescence anymore. Unfortunately, it was not possible to compare kinetic features like half-time and aggregation rate between the different reactions after addition of sTREM2 since almost all curves did not present in a sigmoidal shape at the given aggregation duration. However, onset of aggregation (lag-phase) was further prolonged by the addition of sTREM2 in a concentration dependent manner in the Aβ 1-42 background but not in the 3-42 background.

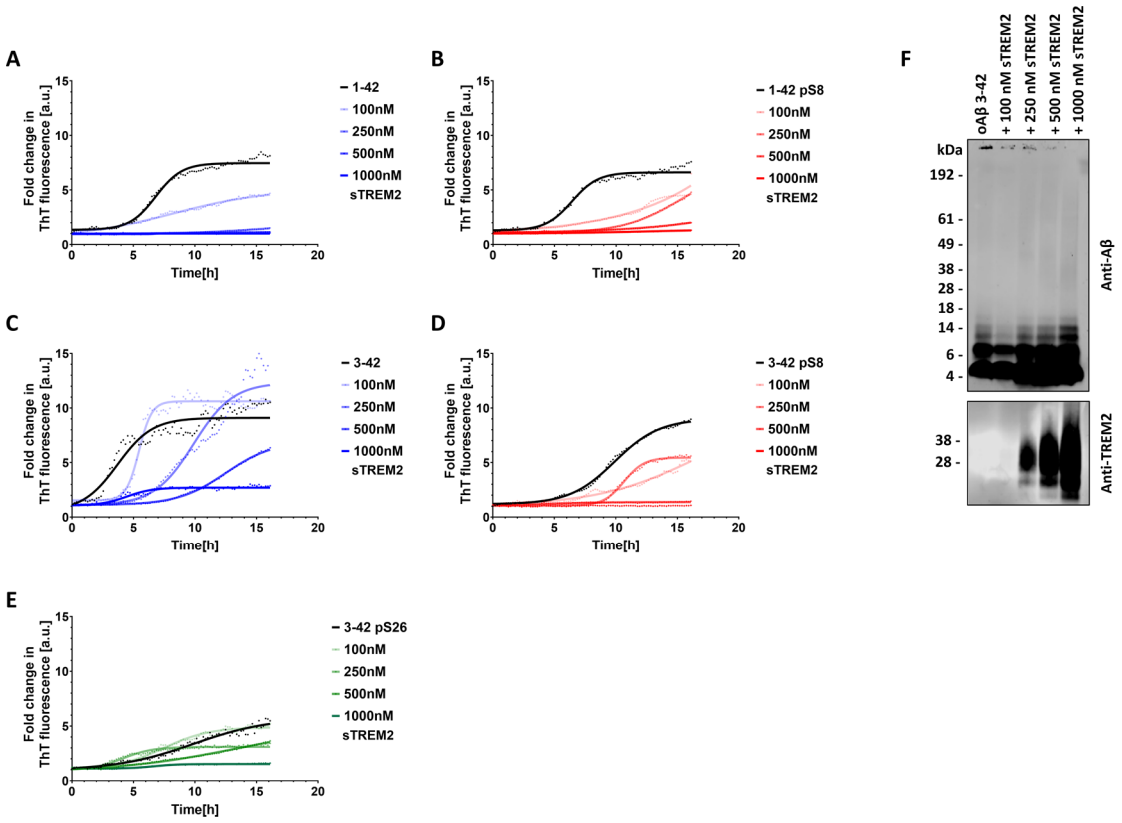

Figure 30 Inhibition of Aβ aggregation by sTREM2.

A-E) Thioflavin T reactivity of different Aβ variants in the presence of sTREM2 in different concentrations was monitored over 15 h in a 96-well plate. Data points represent the fold change in fluorescence compared to the initial signal and derive from the mean of three independent experiments. Additionally, a non-linear curve fit was performed (sigmoidal dose-response curve with variable Hill slope). Variants showed a concentration-dependent delay and decrease in aggregation. The dose-dependent effect on aggregation was further confirmed by Western blot analysis of samples at the endpoint of aggregation with the generic anti-Aβ antibody (4G8) as well as an antibody against human TREM2 (AF1828), exemplary Western blot of Aβ 3-42 samples (F). For a comprehensive comparison of Western blots, see ***Supplementary 5****.*

3.3.3 Effects of Aβ on cellular viability

In the literature, oligomers or higher assemblies of Aβ are often considered to be much more toxic than monomers (Walsh, Klyubin et al. 2002), giving rise to the assumption that an inhibitor of Aβ aggregation might protect cells from Aβ-induced toxicity. Indeed, it has been recently reported that sTREM2 might ameliorate the toxic effect induced by Aβ oligomers (Vilalta, Zhou et al. 2021).

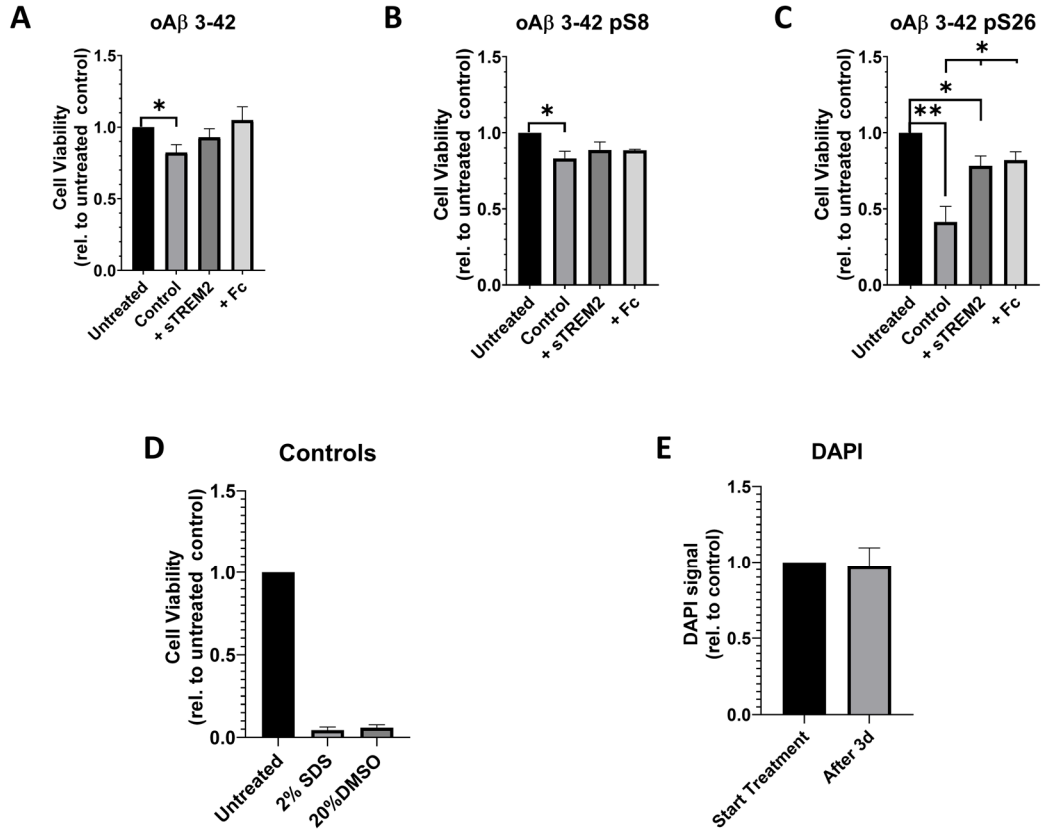

Figure 31 Effect of soluble TREM2 on Aβ cytotoxicity in a resazurin based assay.

A-C) The cytotoxic effect of 10 µM oAβ after pre-incubation with soluble TREM2-Fc or the respective control for 30 min at 37°C on SH-SY5Y cells (differentiated for 5 days) was measured (after 24 h) using the Presto Blue proliferation assay (Thermo Fisher Scientific). The cytotoxic effect as seen by cell viability after treatment with oAβ 3-42 (~80 % viability), 3-42 pS8 (~80% viability), and 3-42 pS26 (~40% viability) was mostly reversed by addition of soluble TREM2-Fc but also by addition of hIgG1-Fc. C) The addition of 2 % sodium dodecyl sulphate (SDS) or 20 % dimethyl sulfoxide (DMSO) as positive control showed almost complete loss of cell viability. E) Comparison of DAPI fluorescence as measured by the fluoresce plate reader from a sample at the start and the end of treatment showed no significant changes in cell number over the course of the treatment.

To test this hypothesis, cells of the human neuroblastoma cell line SH-SY5Y were first differentiated for 3 days and then exposed to a high concentration (10 µM) of the different oAβ species that had been kept in the presence or absence of sTREM2-Fc/Fc for 30 min at 37 °C before the addition of Aβ to the cells (**Figure 31**). A significant toxic effect of peptides was observed after 24 h via the resazurin-based cell viability assay Presto Blue™ for all species but especially for pS26. This effect was partly reversed in all cases where oAβ was exposed beforehand to either sTREM2-Fc or Fc alone (**Figure 31** A, B, and C). The addition of sodium dodecyl sulphate as well as dimethyl sulfoxide was further employed as a positive control, strongly decreasing cell viability to confirm the functioning measurement of cell viability (**Figure 31** D). To ensure that there was no ongoing proliferation of cells, which would have affected Presto Blue measurements, separate wells of cells were fixed and subsequently stained with DAPI at the start and end of the assay. As the fluorescent DAPI signal did not differ between those two time points, it was concluded that the cell number of differentiated SH-SY5Y cells also did not change (**Figure 31** E).

To test viability in a more biologically relevant system, primary cortical mouse neurons (DIV21) were exposed for 5 h to oAβ prepared via oligomerization at 37 °C for 3 h in the presence or absence of sTREM2-Fc or Fc. Subsequent immunocytochemical staining using antibodies against cleaved caspase 3 as a marker for apoptosis as well as against receptor-interacting serine/threonine-protein kinase 1 (RIP1), a protein also involved in apoptosis and necrosis, revealed that the addition of sTREM2-Fc during aggregation of Aβ had rather adverse effects since higher cleaved caspase signal intensity was observed similar to cells treated with staurosporine, a known inducer of apoptosis (**Figure 32** A). This was furthermore seen by antibody staining against RIP1, which, like cleaved caspase 3, exhibited higher expression in the presence of sTREM2-Fc.

To quantify levels of apoptotic signal and compare them to other modified Aβ species, caspase levels of cells in culture were measured by the Caspase-Glo® 3/7 Assay System (Promega, Madison, USA) (**Figure 32** B). This assay confirmed the observed effects of sTREM2-Fc on neuronal cell viability since the addition of sTREM2-Fc or even Fc alone already increased the measured caspase signal, thereby showing no beneficial or neuroprotective effect. Furthermore, it was seen that Aβ 1-42 pS8 as well as pS26, but not the non-phosphorylated Aβ, significantly increased caspase levels, suggesting a higher toxicity of those variants, which is in line with

reports on higher toxicity of phosphorylated variants in the 1-40 background (Kumar, Rezaei-Ghaleh et al. 2011, Kumar, Wirths et al. 2016).

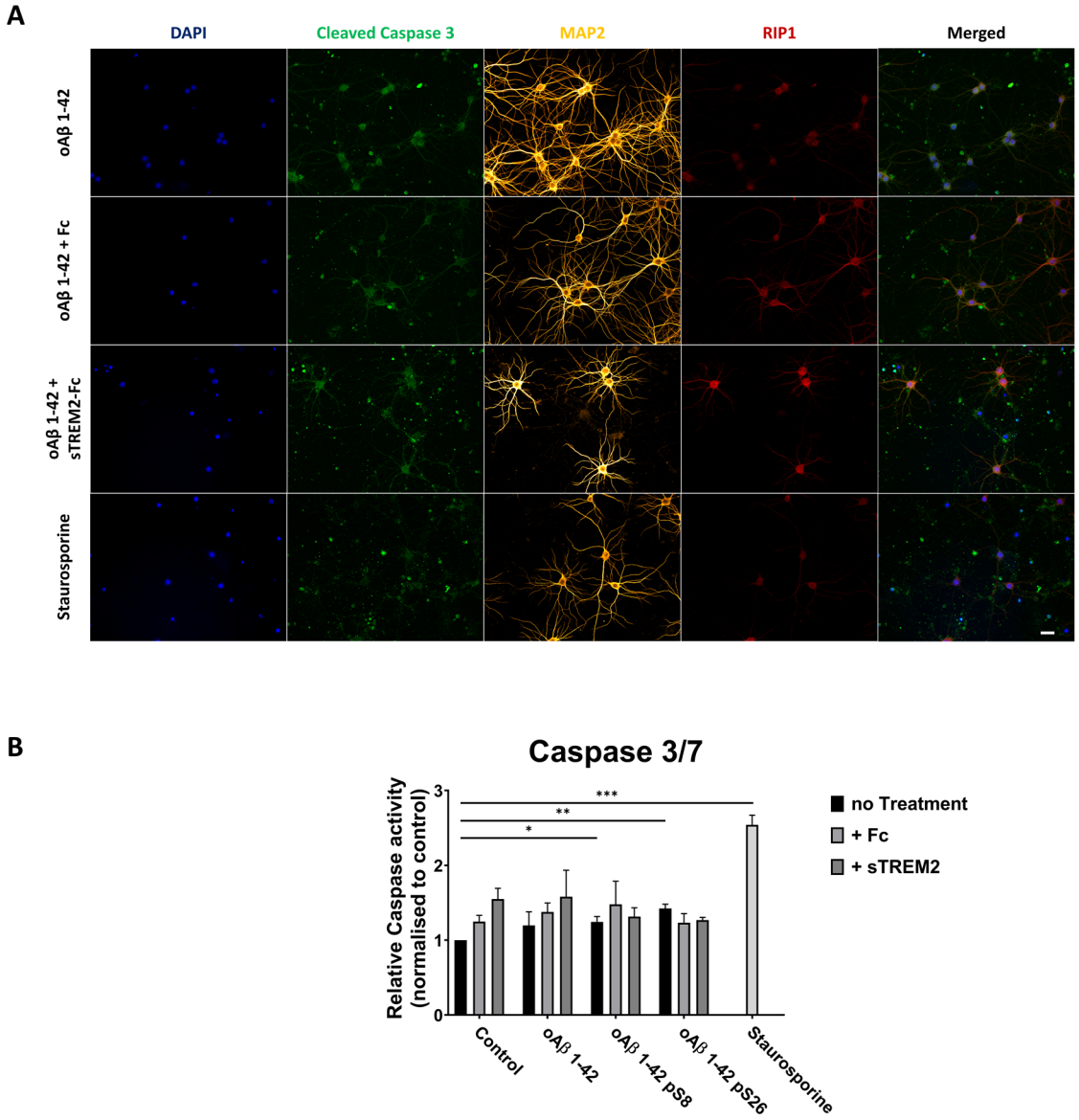

Figure 32 Influence of Aβ aggregated in presence of sTREM2-Fc on neuronal viability.

A) Representative images showing primary mouse cortical neurons cultured for 3 weeks (DIV21) that were incubated for 5 h at 37 °C with 0.5 µM oAβ prepared by aggregation of Aβ 1-42 (23 µM) at 37 °C for 3 h in the presence or absence of sTREM2-Fc/Fc (1 µM). Following fixation, cell nuclei were stained by DAPI (blue) and neuronal cells by antibody against the microtubule-associated protein 2 (MAP2, yellow). Antibody against cleaved caspase 3 (green) and against receptor-interacting serine/threonine-protein kinase 1 (RIP1, red) was used as a marker of autophagy and necrosis (scale bar = 25 µm). B) Cells after 5 h of treatment were lysed, and caspase 3/7 activity was determined (n = 3, unpaired t-test with Welch correction). Data represent the mean ± SEM. Staining and caspase assays show that the addition of sTREM2-Fc, Fc, and staurosporine, a protein kinase inhibitor and inducer of apoptosis, all decrease cellular viability and lead to an increase in apoptosis.

3.3.4 Effect of differentially modified Aβ on TREM2 signalling

TREM2 regulates microglial survival, inflammatory response, lipid metabolism, differentiation, as well as phagocytosis (Atagi, Liu et al. 2015, Jay, Miller et al. 2015, Zhong, Chen et al. 2017) by controlling several signalling pathways downstream of TREM2. This occurs via interaction with its co-receptor the intracellular adaptor protein DNAX-activation protein 12 (DAP12 or TYROBP) (Takahashi, 2005). Ligand binding to TREM2 causes phosphorylation of tyrosine within the immunoreceptor tyrosine-based activation motif (ITAM) of the DAP12 protein (**Figure 7**), subsequently creating the binding site for many proteins containing a SRC homology (SH2) domain, like the spleen tyrosine kinase (Syk). Syk in turn, is involved in the activation of a variety of downstream signalling pathways after its phosphorylation. Thereby, leading to a cascade of signalling events and thus also to the phosphorylation of extracellular signal-regulated kinases (ERK) or the mammalian target of rapamycin (mTOR) (Turnbull, Gilfillan et al. 2006, Ulland, Song et al. 2017). Recently, it was shown that oAβ as well could evoke the phosphorylation of Syk (Zhao, Wu et al. 2018, Zhong, Wang et al. 2018).

In order to test activation in an endogenously TREM2-expressing system, primary microglia from WT and TREM2^{T66M} knock-in mice were treated with differentially modified oAβ 3-42 species for 1 h (**Figure 33**). Phosphorylation states of Syk, Erk, and mTOR in prepared cell lysates were then assessed by Western blotting (**Figure 33** A), determining signal intensity via antibodies specific for phosphorylated Syk (pSyk, **Figure 33** B), phosphorylated ERK (pERK) and total ERK (tERK, **Figure 33** C) as well as phosphorylated mTOR (pmTOR) and mTOR (mTOR, **Figure 33** D). No change in any of those pathways was observed after incubation with unmodified or modified oAβ species. Incubation with sTREM2-Fc and anti-TREM2 antibody, on the other hand, showed increased signal in all pathways in both microglia from WT as well as from TREM2^{T66M} knock-in mice.

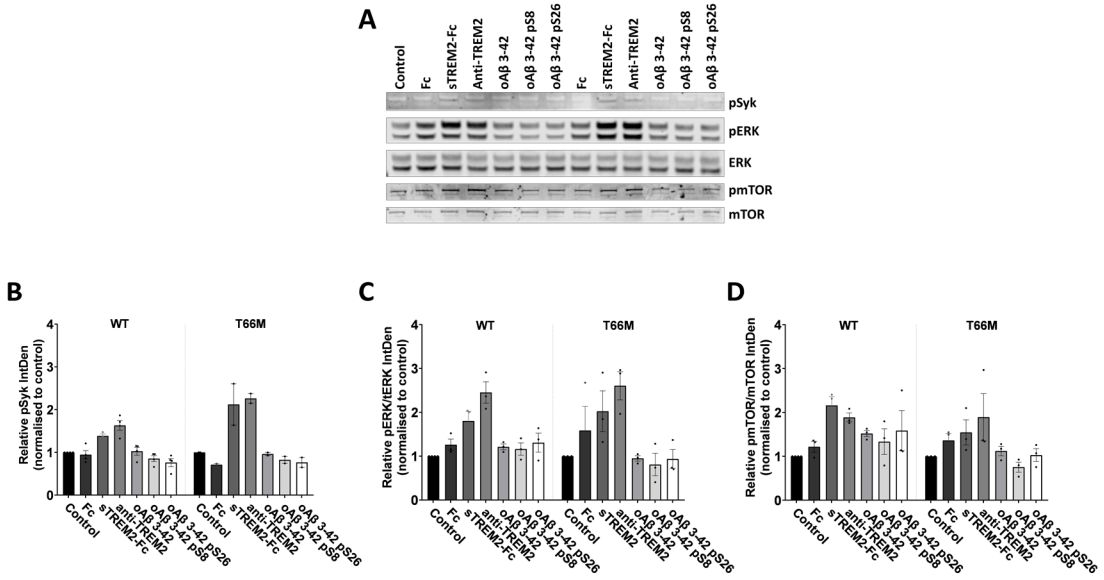

Figure 33 TREM2 downstream signalling activation in primary mouse microglia.

Primary microglia from WT and TREM2^{T66M} mice were exposed for 1 h to differentially modified Aβ 3-42, sTREM2-Fc/Fc, or an anti-TREM2 antibody (4B2A3) as a control. Following exposure, cell lysates were prepared and subsequently analysed via Western blotting, looking for activation of signalling pathways downstream of TREM2. Therefore, antibodies detecting pSyk (B), pERK/tERK (C), and pmTOR/mTOR (D) were employed (A, exemplary western blot bands), and their respective signals were quantified and normalised to the signal from untreated control (B-D). (n = 3 or n = 2 for pSyk (T66M) , unpaired t-test with Welch correction). Data represent the mean ± SEM. No changes in pSyk, pERK/tERK, or pmTOR/mTOR were observed upon Aβ treatment. Treatment with sTREM2-Fc or anti-TREM2, on the other hand, led to increased signalling activation in WT as well as T66M microglia.

3.4 Effect of single point mutations within sTREM2 on Aβ interaction

The great interest in TREM2 as a key microglial receptor in Alzheimer's disease arose roughly a decade ago when independent studies identified a very rare allelic variant of this receptor to be associated with a 3-to-4.5-fold increased AD risk (Guerreiro, 2013; Johnsson, 2013), thereby making it, together with the ApoE4 allele, one of the strongest known risk factors involved in sporadic AD. By now, GWAS have identified a handful of additional point mutations that have all been found to be connected to AD, or frontotemporal lobe dementia. The common denominator, if exists, on the other hand, has not been determined yet. So, it was tested whether, as it has been described before for the mutation of arginine to histidine at amino acid 47 (R47H), where the mutation interferes with the ligand binding surface and thereby decreases binding to its ligands, other point mutations similarly modulate binding to Aβ. Thus, the effect of point mutations, more precisely mutations of threonine to methionine (T66M), glycine to tryptophan (G145W), histidine to tyrosine (H157Y), or the before-mentioned R47H, on binding to Aβ was examined. First, the binding of the different mutant isoforms was investigated by a solid-phase binding assay, immobilizing oligomeric Aβ 1-42 onto the surface of a 96-well ELISA plate and presenting it with different concentrations of sTREM2-Fc in the mobile phase. From the binding curves, as received by blotting bound sTREM2-Fc signal against the used concentration (**Figure 34** A), it was observed that all mutant variants show a slightly decreased affinity to oAβ as compared to the WT. Determining the dissociation constant at equilibrium (**Figure 34** B) showed, in accordance with the literature, that the lowest affinity to Aβ is observed for the R47H variant (Belsare, Wu et al. 2022). Other variants, except T66M, only slightly and not significantly decreased binding affinities compared to the WT. This was further confirmed by dot-blot analysis spotting oligomer-enriched or monomeric Aβ 1-42 onto a nitrocellulose membrane and separately incubating the membranes with the mutant sTREM-Fc variants in the supernatant (**Figure 34** C). Also in this experiment, sTREM2-R47H-Fc bound in a lower amount to the spotted Aβ, suggesting a decreased affinity of this variant even towards monomeric Aβ. Interestingly, sTREM2-T66M-Fc also showed a strongly decreased binding, even less than the R47H variant.

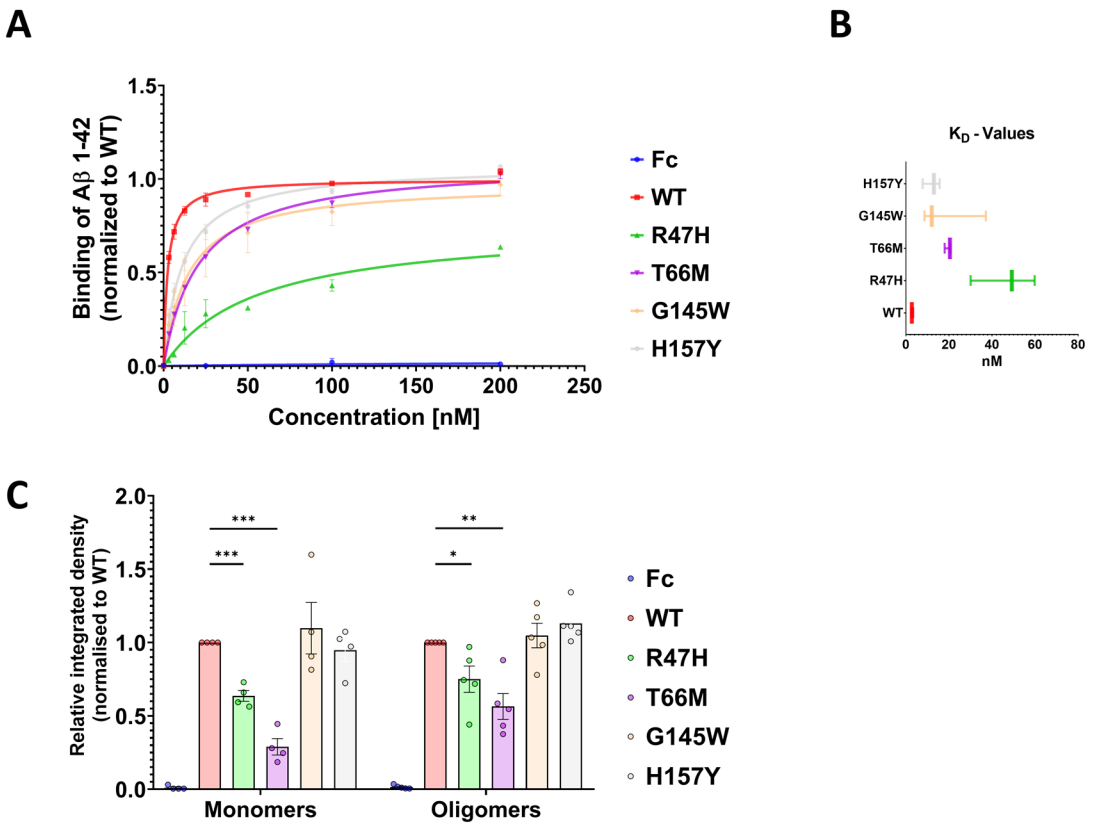

Figure 34 Differential binding of mutant sTREM2-Fc to Aβ 1-42.

Solid-phase binding assay showing binding between oAβ 1-42 and sTREM2-Fc and its different mutant forms. Aβ was immobilized in duplicates on a 96-well ELISA plate and incubated with different concentrations of sTREM-Fc in the mobile phase (A) (n = 3). B) Calculated K_D values plotted against each other reveal that all mutant variants decrease binding compared to sTREM2-WT-Fc, but especially sTREM2-T66M-Fc and sTREM2-R47H-Fc express decreased binding. C) Dot-Blot analysis for the binding of sTREM2-Fc and mutants to oligomer-enriched or monomeric Aβ 1-42 spotted in triplicates onto a nitrocellulose membrane. The integrated density of each spot was normalised to the respective anti-Fc signal and plotted in a graph. Each data point represents the mean signal of one experiment ± SEM (n = 4, unpaired t-test with Welch correction).

3.5 Sub-cloning of phosphomimicking variants for future experiments with in vivo models

While most of this work focused on determining the TREM2 and Aβ interaction and function in vitro, evidence on how the investigated interactions might be reflected in an in vivo model was still missing. In order to get more information from the in vivo system, ways were searched that could elucidate interactions in a more biologically relevant system. Partly, this was done by combining phosphorylation state-specific antibodies to detect phosphorylated Aβ, as well as antibodies against TREM2 to simultaneously detect both proteins within in vivo samples (Joshi, Riffel et al. 2021, Joshi, Riffel et al. 2021, Kumar, Kapadia et al. 2021). But in order to prepare for future experiments with in-vivo models that express the respective phosphorylation site variants of Aβ, constructs were cloned that can express phosphomimicking variants of Aβ in the in-vivo system via lentiviral transduction. Phosphomimetics make use of the fact that certain mutations, in this case, from serine to aspartate, resemble the biophysical properties of phosphorylated serine (Chen and Cole 2015). This would create quite a flexible system, allowing to investigate the different variants individually, but furthermore, transduction of mice expressing endogenous TREM2 as well as TREM2-deficient mice would also allow to confirm results from previous in vitro binding studies.

Therefore, as a first step, the sequence of the human amyloid β precursor protein (APP751) containing a Swedish mutation (K670M/N671L) as well as mutations within the Aβ-sequence for either serine-8 or 26 to aspartate or alanine was sub-cloned into a lentiviral expression vector, and the successful cloning was afterwards confirmed by transient transfection and expression analysis via Western blotting using antibodies specific for APP containing the Swedish mutations as well as against the c-terminal fragments of APP (**Figure 35** A). Expression is only seen in HEK cells transfected with the APP-containing vector but not in the non-transfected control or cells transfected with the empty vector. Thereby, the basis for the production of lentiviral particles and further transduction was confirmed and is planned to be employed in further experiments. In the meantime, experiments were performed to support the idea that phosphorylated variants and phospho-mimicking variants share biophysical properties. Therefore, similar to before, ThT-reactivity of the different variants was monitored over a time period of 20 h (**Figure 35** B, C), showing indeed that aggregation of Aβ 1-42 pS8 and S8D occurs almost at the same time but with slightly stronger aggregation of the phosphorylated variants (**Figure 35** B). Also, Aβ 1-42 pS26 and S26D share common behaviour, as both variants aggregate very quickly but with a barely noticeable increase in

fluorescence (**Figure 35** C). In the end, both results support the suitability of these phosphomimicking variants for investigations in in vivo models.

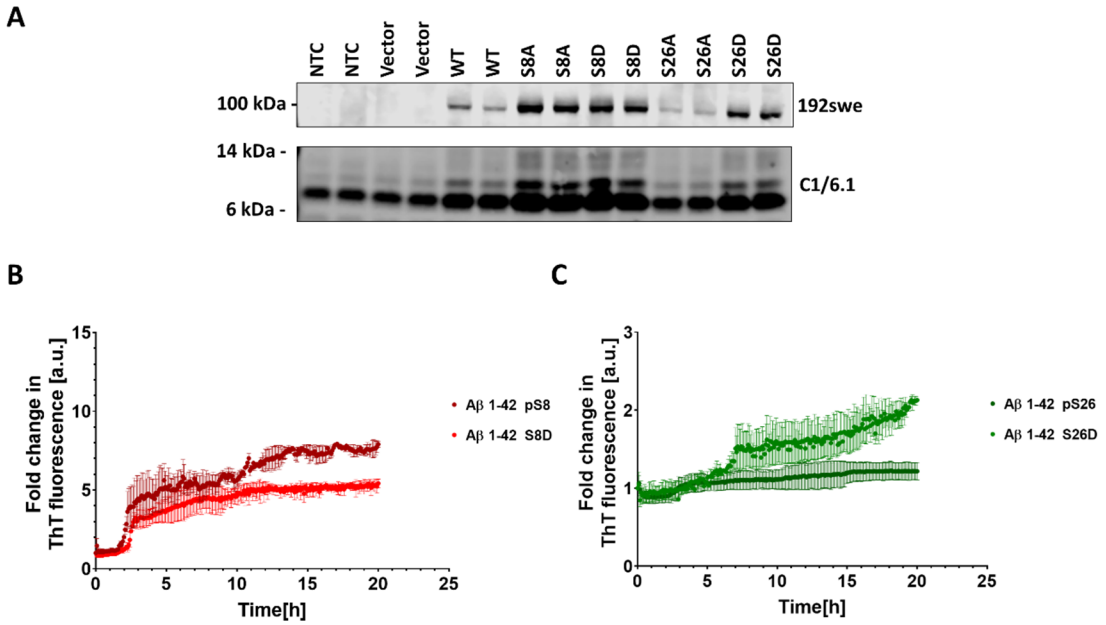

Figure 35 Replacing phosphorylated Aβ by phosphomimicking mutations for the use in an in-vivo system.

A) Human amyloid β precursor protein (APP751) containing a Swedish mutation (K670M/N671L) as well as a mutation within the Aβ-sequence for either serine-8 or 26 to aspartate or alanine was sub-cloned in a lentiviral expression vector, and successful cloning was confirmed by transient transfection and expression analysis via Western blotting. B) Thioflavin T reactivity of synthesized Aβ 1-42 pS8 compared to S8D (B) or pS26 compared to S26D (C) was monitored over 20 h in a 96-well plate. Data points represent the fold change in fluorescence compared to the initial signal and derive from the mean of two independent experiments. Antibodies against the Swedish mutation, as well as APP c-terminal fragments, confirmed successful cloning and expression of the construct in HEK293 cells. Phosphomimicking Aβ variant S8D shows comparable aggregation behaviour as phosphorylated species, while S26D shows slightly divergent aggregation from its phosphorylated counterpart.

4 DISCUSSION

4.1 Generation, characterisation and purification of a Fc-tagged soluble domain of TREM2

The purpose of this study was to generate a model system for studying the interaction between differentially modified Aβ species and TREM2. As the investigation of a complex system, presenting not only TREM2 but also other putative receptors for Aβ interaction complicates the identification of ongoing interactions, only the ligand binding domain was first to be isolated in vitro. Since its discovery and the description of its involvement in Alzheimer's disease (AD) (Guerreiro, Wojtas et al. 2013, Jonsson, Stefansson et al. 2013), TREM2 has been the focus of many studies, which also led to the investigation of Aβ as a putative ligand for TREM2 (Zhong, Chen et al. 2017, Zhao, Wu et al. 2018). Such studies have already suggested that the isolation of certain parts of TREM2 can be beneficial to investigate their interaction in ligand-binding studies (Zhong, Chen et al. 2017, Kober, Stuchell-Brereton et al. 2020, Vilalta, Zhou et al. 2021, Belsare, Wu et al. 2022). Thereby, not only Aβ but also other molecules like ApoE, DNA, and low- and high-density lipoproteins (Atagi, Liu et al. 2015, Bailey, DeVaux et al. 2015, Wang, Cella et al. 2015, Song, Hooli et al. 2017) were identified via such an approach, and their interaction with TREM2 was subsequently verified. As it had been shown that TREM2 undergoes proteolytic cleavage (Wunderlich, Glebov et al. 2013, Thornton, Sevalle et al. 2017), releasing a soluble form of TREM2 (sTREM2) containing the ligand binding domain and spanning the amino acids (aa) 1-157 into the extracellular space, it was decided to use such a soluble form of TREM2 for the here shown interaction studies. This way, not only would the results elucidate the binding of the functionally relevant soluble form of TREM2, but they could also give information on the binding of the full-length receptor via its binding domain.

Whereas studies already showed binding of the extracellular domain aa 1-172 and identified possible regions within the sequence where binding might happen, not so many studies have been focused on revealing the function of sTREM2 (Zhong, Chen et al. 2017, Zhao, Wu et al. 2018)

Despite being able to recombinantly express this soluble TREM2 in HEK293 cells, as seen in **Figure 9**, it proved to be quite difficult to use this extracellular secreted form of TREM2 for

binding studies, as collection and concentration of the supernatant also led to the co-purification of other proteins or even denaturation of the desired protein, which both might potentially interfere with functional binding.

As it has been shown that the Fc-tag improves the stability and half-life of its binding partner and also serves as a tag for easy purification (Roopenian and Akilesh 2007), this approach was also applied for sTREM2. The expression of fusion proteins, including the disease-associated mutant forms of sTREM2, proved to be quite consistent throughout this study (**Figure 10**), with only minor variations. The only exception to that appeared to be sTREM2-Fc with a point mutation at aa 66 from threonine to methionine (sTREM2-T66M-Fc). From other studies on the full-length receptor and studies on the FTD-like syndrome as well as Nasu-Hakola disease (Paloneva, Manninen et al. 2002, Kleinberger, Yamanishi et al. 2014, Kleinberger, Brendel et al. 2017), both can be caused by the T66M mutation, it is known that this variant leads to a retention of TREM2 in the endoplasmic reticulum (ER) and thus to impaired transport to the cell surface. Consequently, presenting with non-functional TREM2 signalling and, in return, also with low amounts of sTREM2, which would usually be cleaved from the full-length membrane-bound receptor after its activation. Interestingly, this interaction seemed to also occur for the soluble form of TREM2 containing the T66M mutation, as seen by Western blot (**Figure 9** and **Figure 10**) and immunohistochemical staining (**Figure 11**), suggesting a similar underlying mechanism as for the full-length receptor. Hereby, the proposed effect of T66M on the native folding of TREM2 (Kleinberger, Yamanishi et al. 2014) might also occur in soluble TREM2. Thus, the unfolded protein does not pass the sensitive control mechanism (Malhotra and Kaufman 2007), which prevents the T66M variant from forward transport in the secretory pathway. In the end, underlining the importance of the soluble domain and especially aa 66 for the overall stability and function of TREM2. However, as weak signals indicated small amounts of sTREM-T66M also being secreted into the supernatant (**Figure 9**, **Figure 10**, **Figure 12**), this control mechanism might be overcome by overexpression of the proteins, thus allowing the secretion of probably misfolded or immature proteins (Hammond and Helenius 1994). As such, the different mobility of the sTREM2-T66M variants observed in the Western blot might be an additional indication of immature glycosylation.

As Western blot results before and after treatment with PNGase indicated, not only Fc but also sTREM2 undergo glycosylation (**Figure 9** and **Figure 10** B). This is not surprising, as both Fc (Beck, Wagner-Rousset et al. 2008) and the full-length TREM2 (Ma, Allen et al. 2016) have been described before to exhibit complex glycosylation. Unfortunately, here shown experiments did not give insight into how exactly the glycosylation of sTREM2-Fc matches

that of sTREM2 or the full-length receptor. Nevertheless, the distinct migration patterns of sTREM2 and sTREM2-Fc in the Western blot (**Figure 9**) already suggested possible differences. Therefore, future experiments elucidating the influence of the expression system and cells on TREM2 glycosylation might be pivotal, as the differential glycosylation might also affect correct functioning and binding, which is also seen for mutant variants exhibiting abnormal glycosylation compared to WT (Park, Ji et al. 2016) as well as the here described binding of sTREM2-T66M-Fc with Aβ (**Figure 34**).

Comparing expression levels, glycosylation, and mobility in gels were thus important steps for ensuring comparability of the generated system to the in vivo expressed sTREM2 and to exclude any possible effects introduced by the tag before proceeding to the generation of cell lines stably expressing the constructs.

The second big advantage of the Fc-tag, besides stability, is its easy purification, and concentration of the target protein. Thereby, subjecting the supernatant of HEK293 cells stably expressing the different recombinant proteins allowed for successful isolation and purification as confirmed by UV spectra (**Figure 12**). Hereby, a comparison of the different mutant variants in terms of their expression and the amount of protein that was successfully purified revealed only minor differences, except for the already mentioned retained T66M variant. The proposed advantage of the generation of a single-cell clone only consisting of high-expressing cells over a stable pool of cells in order to boost protein production (Elgundi, Sifniotis et al. 2017, Zitzmann, Schreiber et al. 2018) showed no success in this study (**Figure 13**). Suggesting that even if higher-expressing cells are present, the cells might shut down production of the recombinant protein once a certain concentration is reached within the supernatant. Thus, higher concentrations of sTREM2-Fc in the supernatant might interfere with cellular viability, in which case a more frequent replacement with fresh medium might also have been feasible for a continuous collection of recombinant protein. Nevertheless, comparing the amount of sTREM2-Fc that was isolated from stable cells and transiently transfected cells showed an almost 10-fold higher amount for the latter, which is also why no further attempts on improving stable cell lines were undertaken (**Figure 13**). The problem for transient transfection, on the other hand, was its heterogeneity as well as the high cost of the so-far used transfection reagent Lipofectamine 2000, which, in the case of an upscaling of the whole process to satisfy the needs of recombinant proteins, would have resulted in unacceptable costs. To ameliorate this problem, a more cost-efficient transfection reagent in the form of polyethyleneimine (PEI) was considered and optimized (Boussif, Lezoualc'h et al. 1995, Longo, Kavran et al. 2013). Furthermore, it was thought that the transfection of cells in suspension could further improve

the transfection efficiency over adhered cells (Fang, Sehlin et al. 2017).
Using PEI as a method of transfection allowed, in contrast to the generation and optimization of stable cell lines, the production of large amounts of recombinant protein without having to find a stable cell line for each mutant variant of sTREM2-Fc with sufficient expression. Furthermore, with a transient expression system, milligram amounts of protein can be purified in principle within a week without further medium changes (Raymond, Tom et al. 2011).

Unlike Lipofectamine 2000, PEI is much more variable in transfection efficiency and yield, especially depending on the cell amount to be transfected (Lehner, Wang et al. 2013). This made it important to first find an appropriate protocol of transfection for maximizing yield while at the same time keeping the amount of reagent used to a minimum. This included the fact that for every new batch of PEI prepared, a trial transfection was performed first in order to identify the ideal DNA: PEI ratio. Initial analysis of 3 different methods revealed that independent of the method, the protein being expressed increased roughly up until day 5 post-transfection, while cell viability dropped within those 5 days down to 20 % (**Figure 14**). And while mostly in line with the literature, the decrease in cell viability upon expression of sTREM2-Fc occurred often faster than described for other proteins expressed via PEI (Fang, Sehlin et al. 2017), which might indicate a possible negative effect induced by the expressed sTREM2-Fc on cellular viability. In addition to the toxic effect that is, of course, caused by the transfection of large amounts of DNA itself (Fang, Sehlin et al. 2017).
For further optimization, previous studies on recombinant protein expression have also suggested the addition of supplements like cell cycle inhibitors after the transfection to further increase protein yields (Backliwal, Hildinger et al. 2008). And indeed, also in this study, it was confirmed that by inducing cell cycle arrest via valproic acid, protein expression was further spurred (**Figure 14**).
On the other hand, studies had also reported that the transfection medium might interfere with the transfection itself, which supposedly can be bypassed by transfecting cells at an extremely high density (Backliwal, Hildinger et al. 2008). This was, however, not confirmed in this study, as transfection at a high density of cells led to very low cell viability and, respectively, low expression as seen by the Western blot signal (**Figure 14**).

Finally, the appropriate quality and stability of purified products were confirmed via Western blot as well as silver staining (**Figure 15**). Half-life experiments, on the other hand, suggested that while the Fc-tag supposedly stabilizes its fusion partner (Beck and Reichert 2011), the addition of bovine serum albumin and sodium azide is still advantageous for the storage of the purified proteins to prevent degradation (**Figure 16**). This could indicate other co-purified

agents/proteases that might degrade the target protein but are inhibited by the presence of BSA. Thus, it would also explain why the purified sTREM2 presented with weak additional bands in the silver staining but not in the Western blot (**Figure 15**). However, BSA might have also decreased the adsorption of the purified protein to the vial and thereby affected the recovered amount of protein. Since peptides are usually stored under non-sterile conditions, degradation of the proteins might also have been a result of microbial growth and subsequent release of proteases.

4.2 Tobacco etch virus (TEV) cleavage of the Fc-tag

Even though the Fc-fusion tag is a useful tool for the expression and purification of sTREM2, it still presents unwanted properties that have the potential to interfere with certain experimental setups. So do Fc-fusion proteins, for example, form stable dimers upon their expression (Beck and Reichert 2011), which can even assemble into higher-order structures and complexes under the right conditions (Czajkowsky, Hu et al. 2012). And while such behaviour is considered advantageous when using the Fc-fusion protein as therapeutic agent, it might mask, change, or even lead to effects that might be simply a result of this complex and thereby not resemble the in-vivo situation. Thus, Fc-tags are commonly used to increase the avidity of expressed fusion proteins to their target, as the complexed fusion protein can effectively bind more target protein while at the same time increasing the plasma half-life of the construct (Czajkowsky, Hu et al. 2012). And while in binding studies this does not affect discriminating binding partners, it might lead to an overestimation of the binding strength and capacity. In aggregation studies, it might be even more difficult since the assembly of the Fc-domain into complex structures might also be reflected in the analysis. Furthermore, when investigating cellular responses, one has to consider that a variety of cells express receptors susceptible to binding to the Fc-domain, leading to responses independent of the fusion partner (Liu 2018). While most of those unwanted effects can be controlled by setting up appropriate controls, it is still not entirely possible to exclude misinterpretation of the results within certain experiments. This was addressed by the extension of the existing vector for expression of sTREM2-Fc by introducing a TEV-cleavage site between the sTREM2 domain and the Fc-tag (Parks, Leuther et al. 1994). Based on a highly pure monomeric preparation as procured by SEC (**Figure 17** A), it was possible to successfully cleave Fc from sTREM2 (**Figure 17** B), thereby providing sufficient yields of homogenous protein and consequently an important tool to study the specific effects of sTREM2.

4.3 Characterisation of modified Aβ species

The influence of post-translational modifications on protein function is a major key to proteomic diversity in every organism. So, it is not surprising that Aβ can also undergo several different posttranslational modifications (PTM) resulting in changes in its biochemical and biophysical properties. Especially the variety of different n-terminal truncated forms of Aβ has picked up researchers' interest as being some of the most common PTMs (Moore, Chakrabarty et al. 2012). Indeed, truncation of the n-terminal Aβ sequence has been shown to enhance aggregation of the different peptides and promote cell toxicity (Jawhar, Wirths et al. 2011). Pyroglutamate-modified Aβ (AβpE3), another truncated form of Aβ, has been described by Saido, Iwatsubo et al. (1995), who identified that after cleavage of the first two amino acids, glutamate at position 3 undergoes dehydration, resulting in the formation of pyroglutamate. Similar to other truncated forms and in line with the assumptions about the importance of PTMs for the structure of proteins, pyroglutamate Aβ exhibited greater stability, hydrophobicity, and insolubility (Kuo, Webster et al. 1998). So, when studies in our lab identified that Aβ can also undergo posttranslational modification via phosphorylation at serine 8 (pS8) and serine 26 (pS26), it was of great interest to see how those modifications manifest in the behaviour of Aβ. Studies mainly focusing on the Aβ 1-40 background could indeed describe a variety of different observations regarding the phosphorylated variants. For example, it was shown that phosphorylation differentially affects the aggregation of Aβ 1-40 in comparison to their unphosphorylated counterpart. Phosphorylation at serine 26 resulted in the formation of low and intermediate molecular weight, highly toxic soluble oligomers that, even at extended time periods, did not proceed to higher molecular assemblies or fibrils (Kumar, Wirths et al. 2016). Phosphorylation at serine 8, on the other hand, showed a rather adverse effect by exhibiting a higher propensity to aggregate together with increased toxicity (Kumar, Rezaei-Ghaleh et al. 2011). Furthermore, phosphorylation of Aβ at serine 8 protected the peptide from degradation via the cell surface and secreted proteases like the insulin degradation enzyme (IDE) (Kumar, Singh et al. 2012).

As it has not been described so far if those changes are also conserved among the different length variants of Aβ, it was of utmost importance to also monitor the aggregation of Aβ phosphorylation-state variants in a 1-42 and 3-42 background and whether this affects the generation of oligomer preparations for their use in the following binding studies.

Indeed, it was confirmed that also in those models, phosphorylation at serine 26 could drastically shorten the aggregation time of the peptide, while phosphorylation at serine 8,

especially in the Aβ 3-42 background, increased the time till a stable end state of aggregation was reached (**Figure 18**). Nevertheless, this stable end state of aggregation varied in overall ThT fluorescence between the variants (**Supplementary 1**), with Aβ pS26 showing the lowest and Aβ pS8 the highest fluorescence. Thus, suggesting that pS8 forms more fibrils or fibrils with an increased association of the ThT dye. In conclusion, the effect of phosphorylation at serine 8 on aggregation is comparable to what is described for Aβ 1-40 (Kumar, Rezaei-Ghaleh et al. 2011), but only when looking at the overall change in fluorescence and not in terms of the onset of the aggregation process. This seems to be further enhanced in an n-terminally truncated Aβ variant. The effect of pS26 on aggregation, on the other hand, appeared to be conserved throughout the different length variants. Thereby implicating that in the case of pS8, the attachment of two additional aa at the c-terminus as well as the truncation at the n-terminus delay the onset of aggregation compared the other variants which was not described in the Aβ 1-40 background. It is known that n-terminally truncated peptides may aggregate more easily, as seen in the non-phosphorylated peptides, but the exact reasons are not fully understood yet. For example, it has been proposed that this occurs due to the reduction of electrostatic repulsion between molecules (Schilling, Lauber et al. 2006), an effect that very well could be reversed by the addition of a negatively charged phosphate group. Unfortunately, this would not explain why a similar behaviour isn't observed for pS26, except if one considers structural differences of the formed assemblies that arise from the different position of the phosphate group. Thus, the effect of pS26 on increasing electrostatic repulsion and thereby slowing down the aggregation of Aβ 3-42 might be less effective than it is for pS8.

As the described differential Aβ aggregation will consequently result in a rather heterogeneous mixture of different molecular weight assemblies within an oligomer preparation, it is of importance when investigating the interaction between such a mixture and other interaction partners like soluble TREM2 to characterise the present states of Aβ during the interaction. Separation of such preparations via native- and SDS-PAGE (**Figure 19**), as well as size exclusion chromatography (**Figure 20**) and Western blotting (**Figure 21**), revealed that oligomer preparations from unmodified Aβ present themselves mostly as low molecular weight assemblies, while Aβ phosphorylated at serine 8 showed a much higher tendency to form intermediate-sized assemblies. Phosphorylation at serine 26, on the other hand, which showed the fastest aggregation compared to the other variants, also showed a higher presence of high molecular weight assemblies (**Figure 21** B). Resulting from those observations was that when comparing the different unphosphorylated and phosphorylated variants in interaction studies, it should be considered that any seen effect might not just solely arise as a result of

phosphorylation itself but also might be a representation of the different aggregation propensities. This is especially important when talking about the interaction of the different oligomer preparations, as they will have a different size distribution of Aβ assemblies. Future binding studies could therefore focus on the isolation of Aβ oligomers of only one defined size. Nevertheless, this could probably be quite challenging, as it is to be assumed that, especially for the fast-aggregating variants, Aβ will quickly resume aggregation during the course of isolation and the following binding studies. Still, the different aggregate states might reflect the distinct effects caused by site-specific phosphorylation on self-assembly and aggregate characteristics.

4.4 Differential interaction of Aβ variants and TREM2

Since TREM2 had been reported to facilitate phagocytosis of Aβ (Wang, Ulland et al. 2016) in the brain, it was not surprising when studies identified Aβ as a ligand for its binding domain, as their association often precedes an internalization event. The region between aa 31-91 has been described as being especially involved in the interaction with Aβ (Zhong, Wang et al. 2018). Further studies therefore focused on the interaction between the ligand binding site and different species of Aβ. The obtained data indicate that especially oligomeric Aβ exhibits a high affinity for sTREM2, while only a very low affinity for monomeric and fibrillary Aβ was observed (Lessard, Malnik et al. 2018, Zhao, Wu et al. 2018, Zhong, Wang et al. 2018, Kober, Stuchell-Brereton et al. 2020, Vilalta, Zhou et al. 2021).

In the present study, the interaction of the generated sTREM2-Fc also showed a preferential interaction with oligomer-enriched Aβ preparations in comparison to a monomeric Aβ, as seen by dot-blot analysis (**Figure 22** A, B), a solid-phase binding assay, and pull-down experiments (**Figure 22** C). Together, these results confirmed previous observations made with the extracellular domain of TREM2 (aa 1-172), and additionally, these effects also apply to the more physiologically relevant sTREM2 of 157 aa, a variant generated in vivo via shedding of the full-length receptor. At the same time, they also verified the rationale for using the generated Fc-fusion protein for binding studies. Furthermore, the Fc-tag did not show any direct effect on binding, as the tag alone was not capable of binding to Aβ in any experiment. Nevertheless, one should exercise caution, as the Fc-tag very well induces dimerization of the fusion protein and thereby might not reflect accurately the sTREM2 binding as accessibility of the binding site might be different between monomer and dimer.

After establishing an adequate system to study binding to Aβ, follow-up experiments were

focused on repeating previous binding assays with differentially modified Aβ species. Hereby, phosphorylation of Aβ at serine 8 or 26 was to be investigated and how it might influence the interaction of Aβ with sTREM2. As the inability of manufacturers to procure Aβ 1-42 pS26 only allowed to compare the binding of Aβ 1-42 pS8 to non-phosphorylated Aβ 1-42 (**Figure 23** A, B), the experimental setup was further extended, now also investigating binding of the n-terminal truncated variants of Aβ (Aβ 3-42, pS8, and pS26)(**Figure 23** C, D). Interestingly, it was observed in dot-blot (**Figure 23** A, C) and solid-phase assays (**Figure 23** B, D) alike that phosphorylation of Aβ in the Aβ 1-42 background and similar fashion in the Aβ 3-42 background increased its association with sTREM2-Fc. This was also reflected in a lower dissociation constant for the phosphorylated peptides, which indicated a stronger affinity to sTREM2-Fc and/or a slow dissociation of the Aβ/sTREM2-Fc complex.

As it is described that TREM2 strongly interacts with negatively charged ligands (Kober, Alexander-Brett et al. 2016, Walter 2016)**,** the increased binding to sTREM2 might be a result of the negative charge added by the phosphorylation. This notion is supported by the finding that other post-translational modifications like pyroglutamate or nitration did not exhibit any effects on binding (Joshi, Riffel et al. 2021). Furthermore, immunoprecipitation assays (**Figure 24**) also showed a preferential pull-down of phosphorylated Aβ, especially of higher oligomeric state via sTREM2-Fc (**Figure 25**). Thus, again indicating that larger assemblies of phosphorylated Aβ might present with an increased negative charge over smaller assemblies and enhanced interaction with the ligand-binding surface of sTREM2. Consequently, the increased binding of Aβ pS26 over pS8 would reflect the increased propensity of pS26 to form oligomers of high molecular weight. Following this thought, one would also expect that bigger fibrils of phosphorylated Aβ could increase binding even more. But since Aβ pS26 is unable to form fibrils, this was not further investigated and leaves room for further studies. Thus, it could potentially show that, unlike non-phosphorylated Aβ, fibrils consisting of phosphorylated Aβ might pose as an even better binding partner than oligomers, as long as the accessibility of the binding site is not sterically hindered. Experiments comparing staining of unmodified and pS8 Aβ plaques around TREM2 positive microglia and microglia without surface TREM2 in the mouse brain indeed indicated that such enhanced interaction of TREM2 with pS8 fibrils might restrict respective plaque formation (Joshi, Riffel et al. 2021), as the pS8 plaque size around TREM2 positive microglia was significantly reduced, which was not observed with TREM2 negative microglia or with unmodified Aβ.

Finally, the differential binding of TREM2 was not only observed in a reaction tube but also, to a lesser extent in the binding of Aβ 1-42, pS8, and pS26 to HEK293 cells stably

overexpressing the full-length TREM2 receptor (**Figure 26**) and also in primary microglia expressing endogenous TREM2 (**Figure 27**). And while the effective increase in binding of phosphorylated over non-phosphorylated Aβ was only seen by a slight increase in the slope of the saturation binding curve (**Figure 26**), one can assume from the previous results that the effect might be restricted to oligomers instead of monomers. Unfortunately, the higher concentrations of oligomers needed for a binding curve also resulted in high cellular toxicity and thereby interfered with the analysis. Primary microglia, on the other hand, were a much more resilient and reliable system that also showed consistently increased binding of Aβ pS26 in all length variants (**Figure 27**) (Joshi, Riffel et al. 2021, Joshi 2022), but interestingly not of pS8. This suggests a more complex interaction between phosphorylated Aβ and TREM2 in vivo that cannot be simply explained by the additional negative charge and might be potentially different for the full-length receptor compared to its soluble form. Especially since Aβ oligomers prepared in the presence of sTREM2 showed an even stronger interaction with microglia under the same conditions (**Figure 27**). Thus, other cell surface receptors might also be involved in the binding process, which was also recently proposed by Belsare, Wu et al. (2022). They claim that sTREM2 might bind to cells and Aβ via distinct binding sites in order to facilitate the cellular association and even uptake of Aβ into the cell.

4.5 Influence of sTREM2 on phagocytosis and uptake

Looking at the two leading and likely interconnected theories for the development and cause of the sporadic form of AD, namely the aggregation of amyloid β and its accumulation as part of the amyloid cascade hypothesis (Hardy and Allsop 1991, Karran, Mercken et al. 2011), and the neuroinflammation caused by the deposition of Aβ and tau and hyperactive microglia (Rogers, Luber-Narod et al. 1988, Kinney, Bemiller et al. 2018), one can identify some clear common denominators. Both theories highlight the importance of microglia as well as their ability to clear the accumulating Aβ deposits via phagocytosis (D'Andrea, Cole et al. 2004, Hickman, Allison et al. 2008). Since TREM2 has been identified to mediate phagocytosis in microglia upon activation and ligand binding (Wang, Cella et al. 2015, Zhong, Wang et al. 2018, Belsare, Wu et al. 2022), it was assumed that a stronger or more effective ligand interaction with TREM2 might ultimately also affect the resulting phagocytic activity. Consequently, the interaction with differentially modified Aβ variants could result in differential phagocytic activity of microglia. And while distinct phagocytic responses to Aβ were observed between variants, they appeared to be independent of the previously described increased binding of phosphorylated variants.

Especially since phosphorylation of serine 8 led to a rather decreased uptake of Aβ compared to the un-phosphorylated variant, while pS26 showed the expected increase in uptake (**Figure 28**). This, however, was also observed in microglia without functional TREM2 expression (**Supplementary 3**); therefore, it rather represents a TREM2-independent effect. So, for example, the different aggregation states of the preparations might have led to changes in the time-dependent uptake or degradation of the different Aβ variants. Co-staining with a lysosomal marker (LAMP1) further supported that pS8 and pS26 might undergo differential uptake, as pS26 was found to colocalize with LAMP1 staining inside the cells, which was commonly observed to a lesser extent for pS8.

On the other side, in line with literature claiming that TREM2 facilitates the uptake of Aβ (Frank, Burbach et al. 2008, Kleinberger, Yamanishi et al. 2014, Ulland, Song et al. 2017), it was seen that non-functional TREM2 expression decreased uptake of all Aβ variants drastically and to a similar extent as blocking phagocytosis via cytochalasin D (**Supplementary 3** and **Supplementary 4**). Besides the clearance of Aβ via microglia, reports have also stated the presence and accumulation of intraneuronal Aβ, which at times even precedes clinical symptoms (Masters, Multhaup et al. 1985, Wirths, Multhaup et al. 2001). Additionally, sTREM2 had been shown before to bind and co-localize with neurons (Hsieh, Koike et al. 2009, Song, Hooli et al. 2017). Therefore, recently, the idea arose that sTREM2 modulates the uptake of Aβ into neurons. But in line with what was reported by Belsare, Wu et al. (2022), also in this study, the presence of sTREM2 did not increase the uptake of Aβ by cultured neurons (**Figure 29**). In fact, no intraneuronal Aβ in the soma was observed under the chosen conditions. However, additional conditions, for example, an extended period of incubation, could be tested to further characterise the uptake of Aβ and the potential role of sTREM2 in this process. Interestingly, the experiment did indicate the accumulation of Aβ at the presynaptic site, but the effect of sTREM2 on the presynaptic accumulation of Aβ could not be investigated because of the limited resolution. Thus, it will be interesting to further characterise the accumulation and potential functional implications using high-resolution microscopy. Studies have already shown that Aβ induces the loss of synapses in neurons (Takahashi, Milner et al. 2002, Ripoli, Cocco et al. 2014, Yu, Jans et al. 2018). Therefore, future investigations might determine how different modified Aβ species affect synaptic function and how the presence of sTREM2 could help or interfere with that.

4.6 Inhibitory effect of sTREM2 on Aβ aggregation and resulting toxicity

Aggregation and toxicity exerted by Aβ are considered key events in the initiation and progression of AD. Thereby, studies have elicited that not only fibrils but rather soluble oligomers present as very toxic species in the brain (Lambert, Barlow et al. 1998, Haass and Selkoe 2007). It is indicated that levels of soluble oligomers correlate better with disease progression and pathogenesis as compared to insoluble fibrils that show very little toxic effect on neurons (Walsh, Klyubin et al. 2002, Walsh and Selkoe 2007). Thus, the aggregation process of Aβ from initial monomers over oligomers to insoluble fibrils has been the target of many studies as a potential intervention for disease progression (Pagano, Tomaselli et al. 2020). Furthermore, recently, sTREM2 had been suggested to inhibit fibril growth of Aβ (Vilalta, Zhou et al. 2021, Belsare, Wu et al. 2022), which was further supported by observations showing increased amounts of high molecular weight assemblies detectable in mouse brain lysates from mice expressing no or non-functional TREM2 (Joshi, Riffel et al. 2021). Thus, it was of interest to test the effect of sTREM2 on modified Aβ species, as they also show an increased affinity for sTREM2.

The aggregation studies using ThT indeed showed that, in line with the literature, sTREM2 was able to inhibit aggregation in a concentration-dependent manner (**Figure 30**). And while differences between the variants were observable, the hypothesis that phosphorylated variants are more affected in their aggregation by the inhibitory effect had to be rejected. Instead, it was seen that the truncation of Aβ as well as its phosphorylation on its own affected aggregation behaviour in such a way that hardly any conclusion to the effect of the differential interaction with sTREM2 could be drawn. Overall, the data indicated that the inhibitory effect of sTREM2 on aggregation is lower with Aβ variants that have increased aggregation propensity (i.e., truncated and phosphorylated Aβ). Conclusively, for every modified species, there might exist a critical sTREM2 concentration at which the inhibitory effect of sTREM2 overweighs the Aβ self-assembly. Thus, a more extensive analysis of the curves determining the underlying aggregation kinetics and half-times could give a better insight into the specific inhibition of the different modified variants. Unfortunately, the here chosen time span and sTREM2 concentrations led to ambiguous sigmoidal curves with a vague endpoint of aggregation, rendering them unusable for such analysis. Therefore, further experiments with lower sTREM2 concentrations and over a longer period are necessary in the future. On the other hand, the here shown results could implicate that inhibition of aggregation might not be conferred via binding

to Aβ monomers. Thus, sTREM2 might bind to regions of the growing Aβ assembly, which in certain modified species are less accessible, and modulate the secondary nucleation reaction and fragmentation.

As a conclusion, these results insinuate that sTREM2 affects the aggregation of different modified Aβ species. Thus, the level of TREM2 as well as the intrinsic aggregation characteristics of the individual Aβ species could contribute to the alterations in plaque composition that have been observed in transgenic mice and human AD brains with different TREM2 mutations (Joshi, Riffel et al. 2021, Joshi, Riffel et al. 2021). The interaction of TREM2 could also decrease the neurotoxicity of Aβ (variants).

This was proposed by Vilalta, Zhou et al. (2021), who found that the presence of sTREM2 in a glial-neuronal culture could partially prevent Aβ induced toxicity. They further proposed that sTREM2 binds to low molecular weight species and to a lesser extend to monomers of Aβ, preventing them from aggregating into higher and more toxic soluble assemblies. In line with other studies showing that sTREM2 mainly interacts with oligomers and shows only a negligible interaction with monomers (Lessard, Malnik et al. 2018, Zhao, Wu et al. 2018, Zhong, Wang et al. 2018). Studies by Belsare, Wu et al. (2022) could not confirm the neuroprotective effect of sTREM2. Though sTREM2 decreased the aggregation of Aβ 1-40 and 1-42, it did not prevent Aβ induced toxicity in neurons. Initial experiments during this study with the neuroblastoma cell line SH-SY5Y at first indicated a protective effect of sTREM2-Fc on Aβ induced toxicity (**Figure 31**), but unlike seen in Vilalta, Zhou et al. (2021), this effect seemed to be caused by the Fc-tag as it was not limited to sTREM2-Fc but also seen for the Fc-control (**Figure 31** A, B, and C). Recent investigations in our laboratory, however, did not show effects of Fc alone on Aβ aggregation, suggesting that the interaction of Fc molecules with neurons protects against Aβ induced toxicity. Indeed, Fc receptors can be expressed on neurons, and the binding of antibodies could exert beneficial effects (Mohamed, Mosier et al. 2002, Fuller, Stavenhagen et al. 2014). Experiments with primary neurons (**Figure 32**), surprisingly presented opposite results as observed for the SH-SY5Y cells. While increased toxicity indicated by cleaved caspase 3/7 activity and neuronal loss was observed for the phosphorylated Aβ 1-42 species, similar to what is described for the Aβ 1-40 species (Kumar, Rezaei-Ghaleh et al. 2011, Kumar, Wirths et al. 2016), already Fc and sTREM2-Fc alone were exhibiting detrimental effects on neuronal viability, which were not further elevated or rectified by the presence of Aβ (**Figure 32**). And while no ill effect of Fc or Fc-fusion proteins has been described in the literature and was also not observed in experiments with SH-SY5Y cells, it is, however, possible that the prolonged incubation of sTREM2-Fc/Fc for 3 h (primary neurons)

in contrast to the relatively short incubation for 30 min (SH-SY5Y) at 37°C might have led to the formation of higher assemblies of sTREM2-Fc/Fc, which affected the highly sensitive primary neurons negatively. As SH-SY5Y cells were derived from human brain tumour and the primary neurons from the mouse brain, it is important to consider that both might have presented with different cell surface receptors or that primary neurons did not express any Fc receptors. Thus, binding to Fc receptors as suggested for the SH-SY5Y cells might not have been possible on the primary cells. In conclusion, this study was not able to fully unravel the effect of sTREM2 on neuronal viability.

4.7 TREM2 signalling activation by oAβ

Since its discovery, TREM2 has been described as being involved in a variety of different pathways all involved in maintaining microglia functions, including homeostasis, survival, lipid metabolism, the inflammatory response, differentiation, as well as phagocytosis (Atagi, Liu et al. 2015, Jay, Miller et al. 2015, Zhong, Chen et al. 2017).

Ligand binding to TREM2 induces a cascade of following signalling events that eventually leads to the phosphorylation of certain key proteins, amongst them the spleen tyrosine kinase (Syk), extracellular signal-regulated kinases (ERK), or the mammalian target of rapamycin (mTOR) (Turnbull, Gilfillan et al. 2006, Ulland, Song et al. 2017). And while the ligands that have been shown to bind to the TREM2 receptor are vast, there is considerable ambiguity for most of them about their capability of activating TREM2 and inducing downstream signalling. Several investigations reported the binding of Aβ to TREM2, but only two recent studies reported activation of TREM2 downstream signalling via phosphorylation of Syk (Zhao, Wu et al. 2018, Zhong, Wang et al. 2018).

However, neither the present study nor other investigations in our laboratory could confirm the activation of TREM2 signalling by Aβ in TREM2-expressing HEK cells (data not shown and Ibach, 2021) or in primary mouse microglia (**Figure 33**). However, increased levels of pSyk, pERK, and pmTOR were observed after treatment with TREM2 activating antibody (4B2A3) (Ibach, Mathews et al. (2021) and **Figure 33**), or soluble TREM2 (**Figure 33**). It might not be surprising that different results were obtained for HEK293 cells (Ibach 2021) and the primary microglia (Zhong, Wang et al. (2018), as those could result from the difference in human and mouse TREM2 responses to Aβ. However, as the present results with our primary microglia (**Figure 33**) also did not show significant changes in expression levels of pSyk after activation

with oAβ, it is possible that the time point at which downstream activation can be observed not only varies between cell types but also between different primary cell preparations. Zhao, Wu et al. (2018), for example, observed the strongest increase in pSyk levels already after half an hour of treatment but were also still able to detect changes even 6 hours later. Therefore, further investigations with a longer time span might identify a time point at which activation is also observed in the here-used microglial preparations. The studies by Zhong, Wang et al. (2018) and Zhao, Wu et al. (2018) additionally used oligomer preparations predominantly consisting of high molecular weight oligomers, which could indicate, that the activation of TREM2 might require a certain size of the oligomeric structure, possibly to cluster sufficient receptor molecules to induce downstream signalling, as it has been described for antibodies targeting TREM2 (Schlepckow, Monroe et al. 2020). Thus, the oligomer preparations in the present study might not have fulfilled this criterion.

The observed downstream signalling induced by sTREM2-Fc and anti-TREM2 antibodies (**Figure 33**) suggests that other receptors, possibly Fc-receptors, might be involved in the activation independent of TREM2. While it has been reported that sTREM2 can trigger microglial activation (Zhong, Chen et al. 2017), and is also seen here (**Figure 33**), it is important to note that treatment with Fc alone also indicated a possible activation of downstream signalling via pSyk, pERK, and pmTOR. Additionally, the here used antibody (4B2A3) has been verified in its specificity for human TREM2 (Ibach, Mathews et al. 2021), leading to the conclusion that the observed effect might be a result of the antibody's Fc-domain but not TREM2-specific. This is further supported by the results from the treatment of primary microglia expressing the loss of function mutation T66M. Even so this variant presents with a lack of cell surface TREM2, resulting in a functional knock-out as seen by the decreased phagocytic activity (**Supplementary 3**) (Kleinberger, Yamanishi et al. 2014), it showed similar or even stronger activation of downstream signalling after treatment with sTREM2-Fc or 4B2A3. Consequently, suggesting that other signalling pathways independent of the TREM2 receptor might be involved in Syk, mTOR, and Erk phosphorylation. The increase in the phosphorylation of these proteins could furthermore indicate that, upon lack of surface TREM2, those other yet unknown receptors might show increased cell surface expression and/or increased binding to their ligands.

4.8 Influence of disease-associated mutations on sTREM2-Fc – oAβ interaction

Originally, interest in TREM2 as an important protein in Alzheimer's pathology was sparked by the identification of an allelic variant supposedly associated with a 3- to 4.5-fold increased AD risk (Guerreiro, Wojtas et al. 2013, Jonsson, Stefansson et al. 2013).

By now, genome-wide association studies (GWAS) have identified a handful of additional variants connected to AD, or frontotemporal lobe dementia (Benitez, Cooper et al. 2013, Jin, Benitez et al. 2014). The common denominator, if it exists, however, has not been determined yet. Thus, this study sought to shed light on some of the most common disease-associated variants and how they affect the binding of sTREM2 to Aβ. This, in turn, would not only elucidate the role of disease-associated variants for the soluble form of TREM2 but might also be transferable to the full-length receptor and explain why those variants are associated with a higher risk for AD.

Initial experiments using the mutant forms of sTREM2-Fc showed that by substitution of a single amino acid, binding to oAβ 1-42 can be hindered to a certain extent. In line with previous findings (Zhong, Chen et al. 2017), mutations in the ligand binding pocket of sTREM2-Fc (R47H and T66M) showed a slight decrease in binding affinity (K_D) as seen by solid-phase binding assays (**Figure 34** A, B) as well as dot-blot assays (**Figure 34** C). It had been described before that the mutation of arginine to histidine interferes with ligand binding by decreasing the overall positive charge of the ligand binding surface (Sudom, Talreja et al. 2018, Belsare, Wu et al. 2022) and might also underlie the decreased interaction with oAβ found in the present study. The T66M mutation, on the other hand, is known to cause a misfolding of the entire protein (Kleinberger, Yamanishi et al. 2014, Kober, Alexander-Brett et al. 2016), probably resulting in decreased accessibility of ligands to the ligand binding surface. Results here showed that this variant also presents with decreased binding affinity, as would be expected from a protein with a less accessible binding surface. Interestingly, while the T66M mutant variant showed a similar maximum binding capacity (B_{max}) as the WT, the R47H variant presented with only half the B_{max}. This could indicate that the R47H mutation reduces binding affinity so much that even higher concentrations are necessary to completely saturate all binding sites and reach a similar B_{max}. Differences in the K_D between the T66M and the R47H variants could indicate, that the observed binding of oAβ to T66M might not only reflect binding to the ligand binding surface but also an unspecific binding outside of the ligand binding surface. Thus, the misfolding of TREM2 T66M might result in increased exposure of hydrophobic amino acids

and maybe even aggregation, which, as proposed for proteins in their non-native state, might increase their non-specific interactions with other proteins (Roberts 2007, Frutiger, Tanno et al. 2021).

Variants outside of the ligand binding pocket, e.g., G145W and H157Y, presented only minor changes in their capability of binding to Aβ compared to the wild-type TREM2. Therefore, their effect on AD might not depend directly on changes in the affinity to ligands. So, it has been shown in the case of the H157Y variant that this mutation can lead to enhanced shedding and consequently decreased levels of the full-length cell surface receptor TREM2 (Schlepckow, Kleinberger et al. 2017, Thornton, Sevalle et al. 2017). Thus, also leading to impaired phagocytic activity which might explain why this variant is associated with an increased risk of developing AD (Fu, Chen et al. 2023). In contrast, high levels of sTREM2, which would result from increased shedding of TREM2, have been proposed to have rather beneficial effects, as sTREM2 has been shown to have neuroprotective properties, can inhibit aggregation in vitro, and also induces microglial activation and reduces plaque load in mice (Zhong, Xu et al. 2019, Vilalta, Zhou et al. 2021). As this, however, contradicts with the known AD risk observed for the H157Y mutation, one possible explanation would be that its effect on AD pathology might rather be due to amyloid-independent pathways. Another explanation would be that full-length TREM2 is more important in exerting a protective role than sTREM2. This is further supported by the findings, that an antibody binding at the ADAM cleavage side of TREM2 and thereby reducing shedding and increasing the amount of full-length receptor on the surface resulted in reduced plaque loads in an AD mouse model (Schlepckow, Monroe et al. 2020).

The G145W mutation, on the other hand, has been shown to induce conformational changes within the intrinsically disordered region (IDR), leading to its shortening, while simultaneously not affecting membrane localization or glycosylation (Karsak, Glebov et al. 2020). Thus, as the IDR also contains the cleavage site for ADAM proteases (Feuerbach, Schindler et al. 2017, Schlepckow, Kleinberger et al. 2017, Thornton, Sevalle et al. 2017), it was proposed that shortening of the IDR might result in decreased proteolytic cleavage of TREM2 (Ibach 2021). Additionally, it was also reported that G145W resulted in decreased responses to antibody stimulation, as observed by cell size (Glebov, Wunderlich et al. 2016). While cells expressing wild-type TREM2 did present with a distinct change in cell morphology and decrease in overall cell size upon treatment with a TREM2-specific antibody, cells expressing the mutant forms G145W or T66M did not.

4.9 Validity of replacing phosphorylated Aβ by phosphomimicking variants

Previous investigations confirmed the presence of phosphorylated Aβ species in vivo (Kumar, Rezaei-Ghaleh et al. 2011, Kumar, Wirths et al. 2016, Kumar, Lemere et al. 2020, Kumar, Kapadia et al. 2021). Nevertheless, the presence of differentially modified Aβ species in vivo is very heterogeneous, with only a fraction of Aβ being present in a phosphorylated state (Popov, Indeikina et al. 2014, Yin, Wang et al. 2019). Thus, complicating the detection and isolation of these phosphorylated species. Furthermore, when investigating specific effects of the different phosphorylation variants, their low abundance makes separating effects caused by the non-phosphorylated and phosphorylated variants quite challenging. This is thought to be overcome in the future by the use of phosphomimicking variants of Aβ (pseudo-phosphorylated Aβ). The utilization of phosphomimetics is not a new concept (Thorsness and Koshland 1987), and it makes use of the fact that substitution of serine, in this case from serine to aspartate, resemble the biophysical properties of phosphorylated serine (Chen and Cole 2015). Following this approach, APP with mutations at Ser8/Ser26 would be expressed in the in vivo system in an already phosphorylation-like state in the case of Aβ S8D and S26D or in the form of phosphorylation-resistant variants as in the case of S8A and S26A, where serine is replaced by alanine.

In this study, lentiviral expression vectors could be generated containing the respective APP sequence with a Swedish mutation and their expression was confirmed in HEK293 cells via Western blot (**Figure 35** A).

Observed changes in the expression levels between variants could indicate differences in their transfection efficiency, but could also reflect, the codon bias of the here-used human derived cells (Desai, Zhang et al. 2004). The constructs, on the other hand, were designed for optimal codon-usage in a mouse system; thus, the here-described differences might not affect viral transduction and consequent expression in mice. In the end, the generated constructs would not only allow investigations of the different phosphorylation-like variants individually but their application could be further expanded into any in-vivo system taking advantage of their individual genetic background, for example, transduction in TREM2 knock-in or knock-out mice.

Nevertheless, as the phosphorylated variants would be replaced by a pseudo-phosphorylated variant, it is crucial to verify that the pseudo-phosphorylation does not change any important biophysical properties of phosphorylated Aβ. Initial experiments on aggregation indeed showed

comparable aggregation behaviour of the phosphorylated and the respective phosphomimicking Aβ species (**Figure 35** B and C). Still, further experiments on comparing, for example, the degradation, transport, and stability of the mimicking variants to their respective phosphorylated counterparts are necessary to solidify the claim that they effectively mimic phosphorylated Aβ.

5 CONCLUSION AND FUTURE OUTLOOK

In conclusion, in this study, a cellular expression system was established that allows efficient purification of sTREM2, which can be adapted to investigate the interaction of sTREM2 and its ligands in vitro and in vivo. The obtained results aided in confirming recent findings on the preferred interaction of TREM2 with higher molecular weight assemblies of Aβ. But more interestingly, the data indicated that posttranslational modification of Aβ via phosphorylation might modulate its interaction, thereby presenting yet another possible function of Aβ modification that might be relevant in AD. However, while differentially modified Aβ species were shown to exhibit differential functional effects regarding their toxicity, uptake, and assembly depending on the presence and absence of sTREM2, these did not always correlate with the differential interaction observed in the binding studies. Therefore, future studies have to be employed to identify the functional relevance that arises from the differential interaction of TREM2 with modified Aβ species, as it might be also depending on other factors which are present in an in vivo situation. Thus, the here-generated lentiviral construct expressing APP and phosphomimicking variants could present an important tool to expand studies to in vivo systems. In the end, future investigations will have to determine the exact role of sTREM2 in AD and if raising sTREM2 levels is beneficial or not in the treatment of the disease. Nevertheless, the here provided results will help to understand how distinct modified Aβ species might be affected by increased sTREM2 levels differently. This, of course, could aid in the future to develop more specific therapeutic strategies to interfere with amyloid aggregation and deposition of such modified species. Thus, pharmacological targeting of sTREM2 could be established to complement the recently developed antibodies against oligomeric Aβ for the treatment of AD.

Supplementary 1

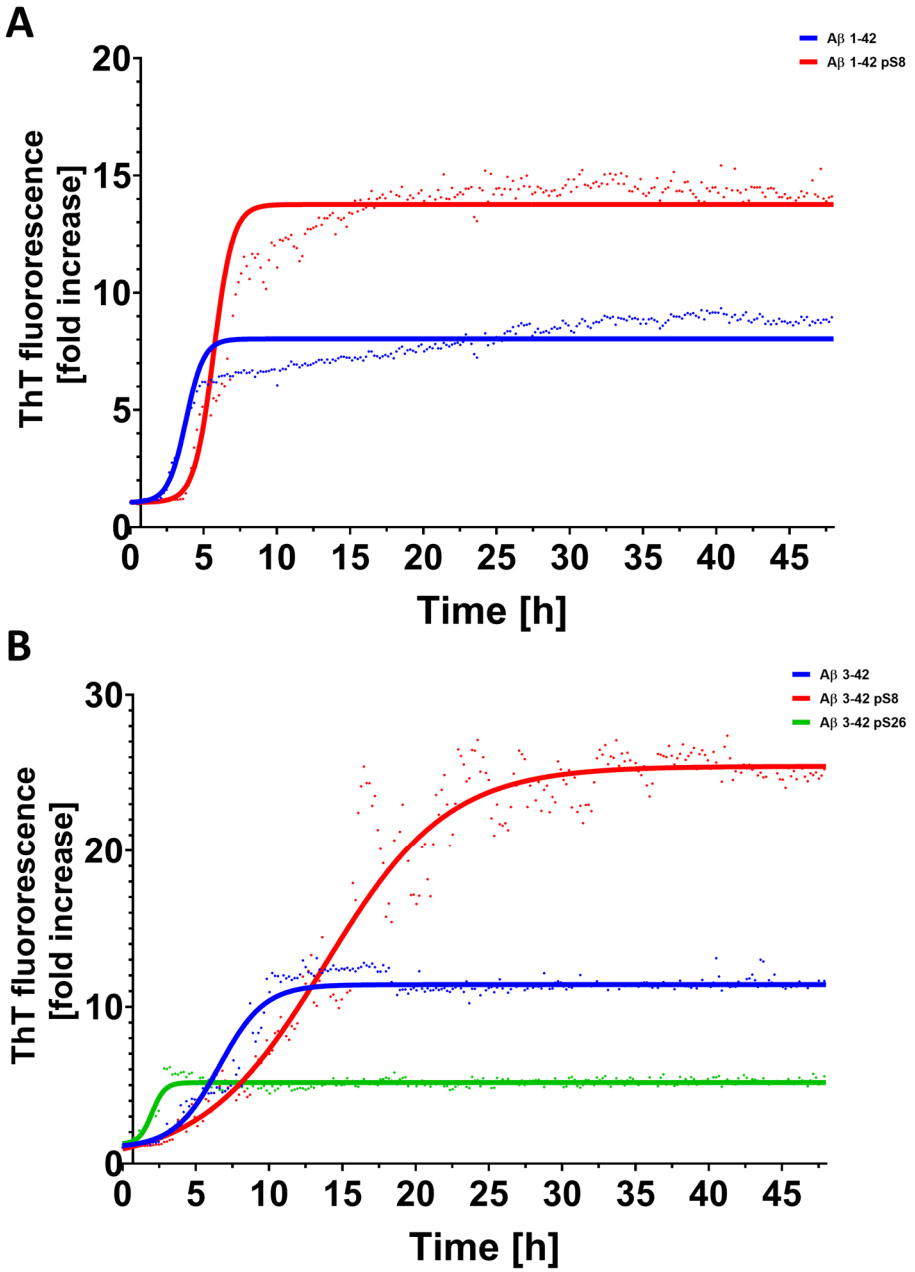

Supplementary 1 Absolute changes in aggregation of post-translationally modified Aβ species.

Monitoring the fold-increase of ThT fluorescence of 5 µM Aβ over a time course of 48 h shows that phosphorylation at serine 26 of Aβ 3-42 drastically shortens the time till a stable plateau is reached compared to non-modified Aβ, but also exhibits very little change in overall fluorescence. In contrast, phosphorylation of Aβ at serine 8 both in the 1-42 as well as the 3-42 background elongated the time till the plateau was reached but presented with a much higher overall change in fluorescence.

Supplementary 2

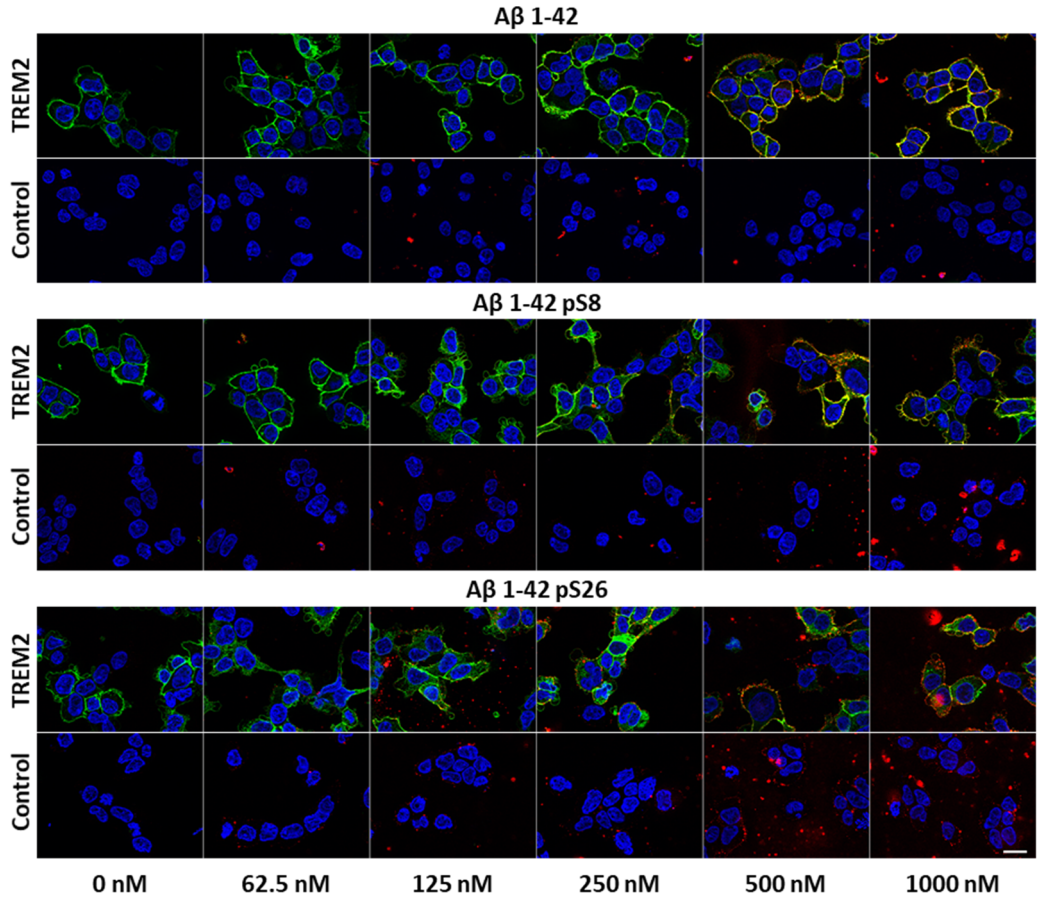

Supplementary 2 Binding of differentially modified Aβ in a TREM2 expressing cell system.

Binding of the three different variants Aβ 1-42, Aβ 1-42 pS8, and Aβ 1-42 pS26 was compared by incubation of HEK293 cells or HEK293 cells with bicistronic expression of TREM2 and DAP12 (Ibach, Mathews et al. 2021) for 2 h on ice. Immunocytochemical analysis after fixation by staining nuclei with DAPI (blue), TREM2 with the anti-TREM2 antibody (AF1828, green), and Aβ with the generic anti-Aβ antibody 82E1 (red) revealed a concentration-dependent increase in the binding of Aβ to cells, especially in the TREM2-expressing system. The interaction of TREM2 and Aβ is further confirmed by the overlapping staining signal.

Supplementary 3

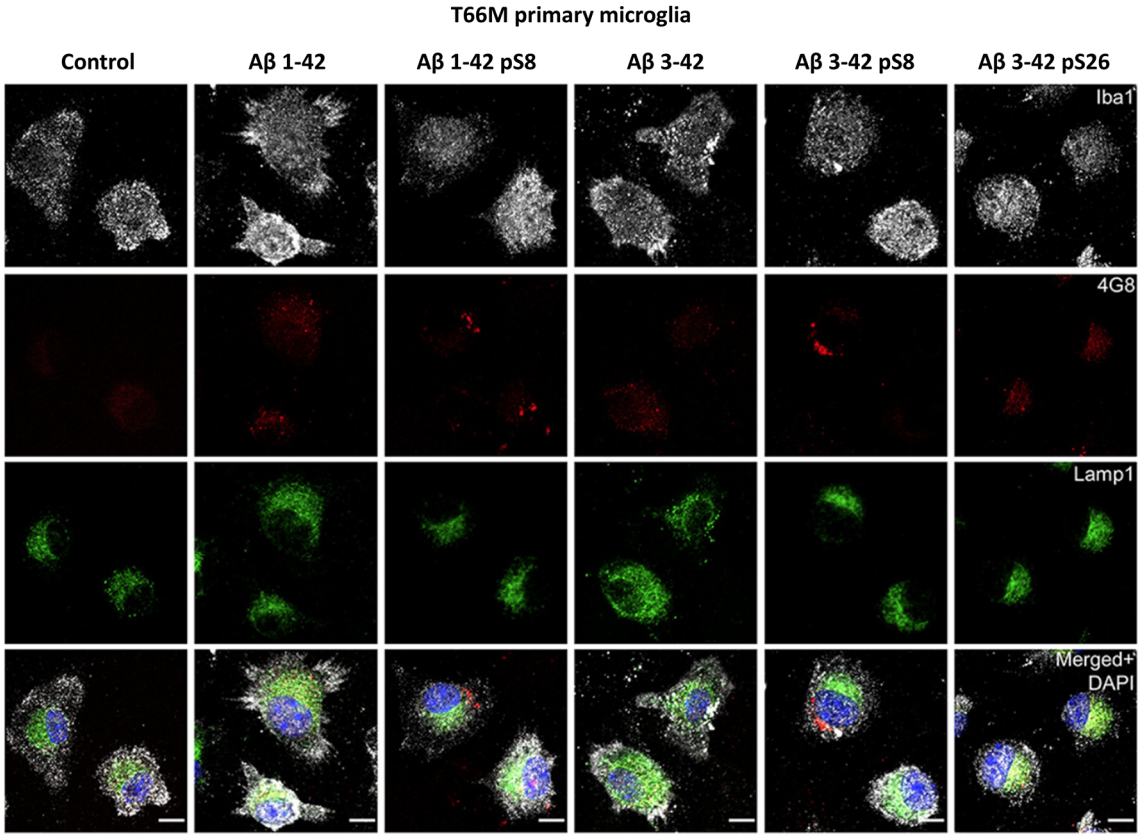

Supplementary 3 T66M-primary microglia differential uptake of Aβ variants.

Exemplary immunocytochemical staining of primary microglia from TREM2^{T66M} knock-in mice after treatment with 1 µM oligomer-rich Aβ for 2 hours at 37 °C. Microglial cells were stained using the Iba1 antibody (white) while Aβ was stained via the generic antibody 4G8 (red). The Lamp1 antibody was employed as a lysosomal marker. (scale bar = 10µm)

Data adapted from already published results (Joshi, Riffel et al. 2021, Joshi 2022).

Supplementary 4

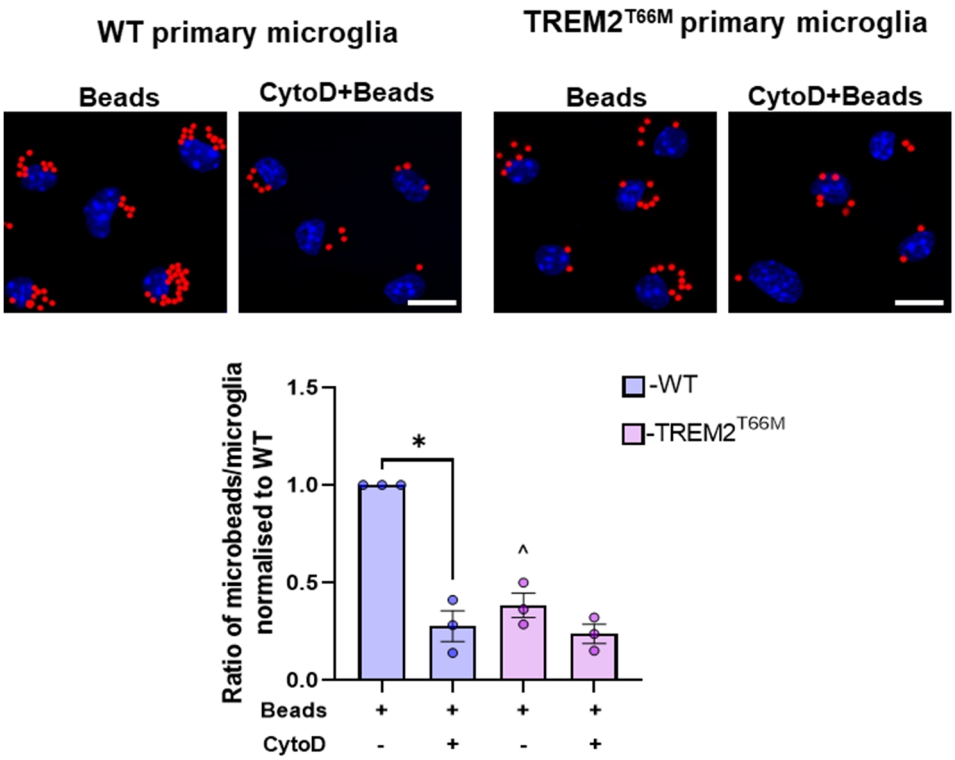

***Supplementary 4 Uptake of fluorescent latex beads by primary microglia**.*

Uptake of fluorescent latex beads by primary microglia from WT and Trem2^{T66M} mice at 37 °C for 2 h. Values were calculated by randomly selecting bead-positive cells: 10 cells/image, 50 cells/coverslip, 100 cells/experiment and hence total of 300 cells/group (n = 3, unpaired t-test with Welch correction). Data represent mean ± SD.

**p < 0.05; for comparison CytoD treated to non-treated cells*
^p < 0.05; for comparison WT to T66M

Data adapted from already published results (Joshi, Riffel et al. 2021).

Supplementary 5

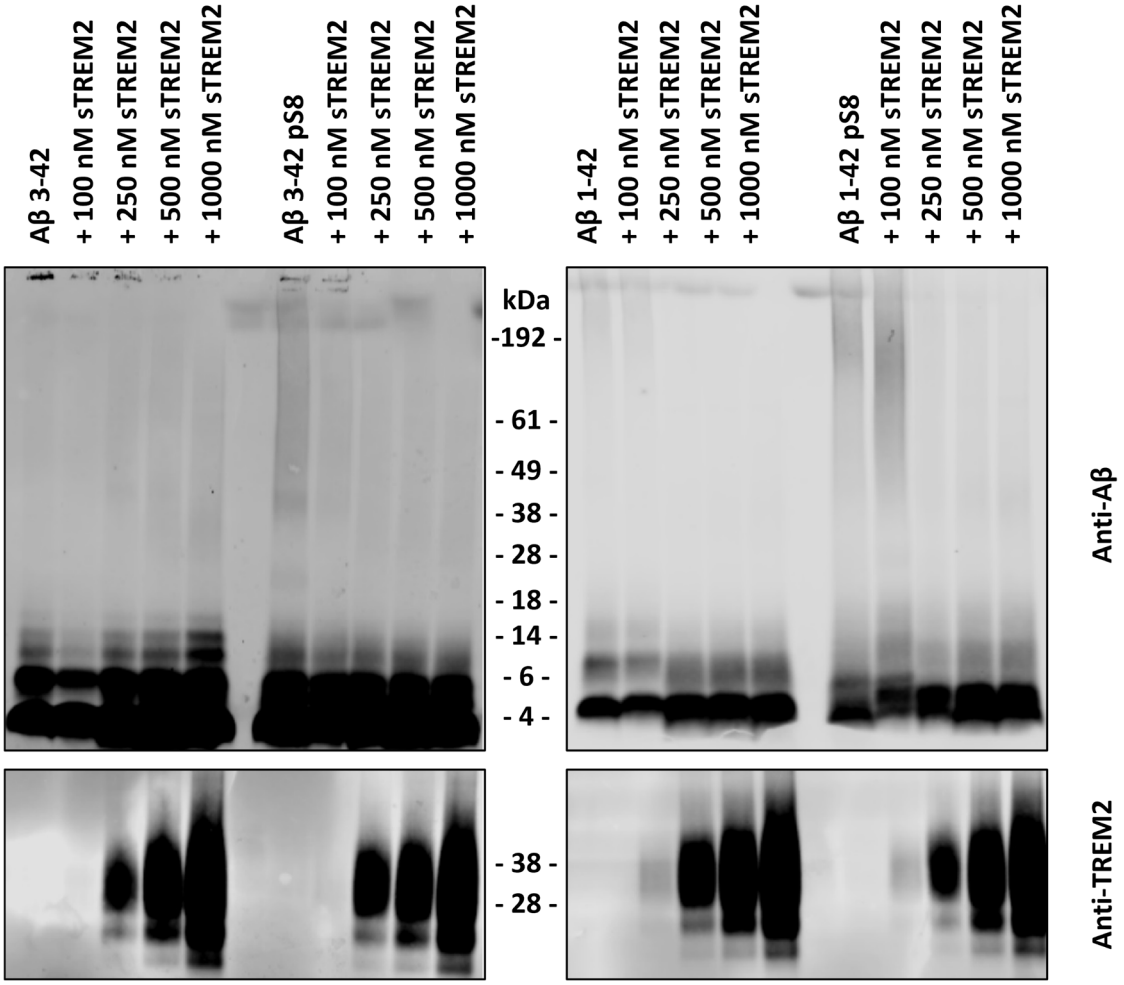

Supplementary 5 Western blot of Aβ samples from thioflavin T aggregation analysis.

Western blot analysis of Aβ 3-42 and 1-42 samples after aggregation for 15 h in the presence of increasing concentrations of sTREM2. Detection of Aβ with the generic anti-Aβ antibody (4G8) as well as of sTREM2 with an antibody against human TREM2 (AF1828) shows a dose-dependent increase in monomers and a simultaneous decrease of high molecular weight Aβ.

6 LITERATURE

Alzheimer, A. (1906). "Uber einen eigenartigen schweren Erkrankungsprozess der Hirninde." Neurologisches Centralblatt **25**: 1134.

Anttila, J. E., K. W. Whitaker, E. S. Wires, B. K. Harvey and M. Airavaara (2017). "Role of microglia in ischemic focal stroke and recovery: focus on Toll-like receptors." Prog Neuropsychopharmacol Biol Psychiatry **79**(Pt A): 3-14.

Arosio, P., T. P. J. Knowles and S. Linse (2015). "On the lag phase in amyloid fibril formation." Physical Chemistry Chemical Physics **17**(12): 7606-7618.

Atagi, Y., C. C. Liu, M. M. Painter, X. F. Chen, C. Verbeeck, H. Zheng, X. Li, R. Rademakers, S. S. Kang, H. Xu, S. Younkin, P. Das, J. D. Fryer and G. Bu (2015). "Apolipoprotein E Is a Ligand for Triggering Receptor Expressed on Myeloid Cells 2 (TREM2)." J Biol Chem **290**(43): 26043-26050.

Backliwal, G., M. Hildinger, S. Chenuet, S. Wulhfard, M. De Jesus and F. M. Wurm (2008). "Rational vector design and multi-pathway modulation of HEK 293E cells yield recombinant antibody titers exceeding 1 g/l by transient transfection under serum-free conditions." Nucleic Acids Res **36**(15): e96.

Backliwal, G., M. Hildinger, V. Hasija and F. M. Wurm (2008). "High-density transfection with HEK-293 cells allows doubling of transient titers and removes need for a priori DNA complex formation with PEI." **99**(3): 721-727.

Bailey, C. C., L. B. DeVaux and M. Farzan (2015). "The Triggering Receptor Expressed on Myeloid Cells 2 Binds Apolipoprotein E." J Biol Chem **290**(43): 26033-26042.

Bakker, A. B., J. Wu, J. H. Phillips and L. L. Lanier (2000). "NK cell activation: distinct stimulatory pathways counterbalancing inhibitory signals." Hum Immunol **61**(1): 18-27.

Ball, K. A., A. H. Phillips, P. S. Nerenberg, N. L. Fawzi, D. E. Wemmer and T. Head-Gordon (2011). "Homogeneous and heterogeneous tertiary structure ensembles of amyloid-β peptides." Biochemistry **50**(35): 7612-7628.

Barcia, C., C. M. Ros, F. Ros-Bernal, A. Gómez, V. Annese, M. A. Carrillo-de Sauvage, J. E. Yuste, C. M. Campuzano, V. de Pablos, E. Fernández-Villalba and M. T. Herrero (2013). "Persistent phagocytic characteristics of microglia in the substantia nigra of long-term Parkinsonian macaques." J Neuroimmunol **261**(1-2): 60-66.

Bateman, R. J., C. Xiong, T. L. Benzinger, A. M. Fagan, A. Goate, N. C. Fox, D. S. Marcus, N. J. Cairns, X. Xie, T. M. Blazey, D. M. Holtzman, A. Santacruz, V.

Buckles, A. Oliver, K. Moulder, P. S. Aisen, B. Ghetti, W. E. Klunk, E. McDade, R. N. Martins, C. L. Masters, R. Mayeux, J. M. Ringman, M. N. Rossor, P. R. Schofield, R. A. Sperling, S. Salloway and J. C. Morris (2012). "Clinical and biomarker changes in dominantly inherited Alzheimer's disease." N Engl J Med **367**(9): 795-804.

Beck, A. and J. M. Reichert (2011). "Therapeutic Fc-fusion proteins and peptides as successful alternatives to antibodies." MAbs **3**(5): 415-416.

Beck, A., E. Wagner-Rousset, M.-C. Bussat, M. Lokteff, C. Klinguer-Hamour, J.-F. Haeuw, L. Goetsch, T. Wurch, V. A. Dorsselaer and N. Corvaia (2008). "Trends in Glycosylation, Glycoanalysis and Glycoengineering of Therapeutic Antibodies and Fc-Fusion Proteins." Current Pharmaceutical Biotechnology **9**(6): 482-501.

Belsare, K. D., H. Wu, D. Mondal, A. Bond, E. Castillo, J. Jin, H. Jo, A. E. Roush, K. B. Pilla, A. Sali, C. Condello and W. F. DeGrado (2022). "Soluble TREM2 inhibits secondary nucleation of Aβ fibrillization and enhances cellular uptake of fibrillar Aβ." **119**(5): e2114486119.

Benitez, B. A., B. Cooper, P. Pastor, S. C. Jin, E. Lorenzo, S. Cervantes and C. Cruchaga (2013). "TREM2 is associated with the risk of Alzheimer's disease in Spanish population." Neurobiol Aging **34**(6): 1711.e1715-1717.

Berner, D. K., L. Wessolowski, F. Armbrust, J. Schneppenheim, K. Schlepckow, T. Koudelka, F. Scharfenberg, R. Lucius, A. Tholey, G. Kleinberger, C. Haass, P. Arnold and C. Becker-Pauly (2020). "Meprin β cleaves TREM2 and controls its phagocytic activity on macrophages." Faseb j **34**(5): 6675-6687.

Boillée, S., K. Yamanaka, C. S. Lobsiger, N. G. Copeland, N. A. Jenkins, G. Kassiotis, G. Kollias and D. W. Cleveland (2006). "Onset and progression in inherited ALS determined by motor neurons and microglia." Science **312**(5778): 1389-1392.

Boussif, O., F. Lezoualc'h, M. A. Zanta, M. D. Mergny, D. Scherman, B. Demeneix and J. P. Behr (1995). "A versatile vector for gene and oligonucleotide transfer into cells in culture and in vivo: polyethylenimine." Proc Natl Acad Sci U S A **92**(16): 7297-7301.

Budd Haeberlein, S., P. S. Aisen, F. Barkhof, S. Chalkias, T. Chen, S. Cohen, G. Dent, O. Hansson, K. Harrison, C. von Hehn, T. Iwatsubo, C. Mallinckrodt, C. J. Mummery, K. K. Muralidharan, I. Nestorov, L. Nisenbaum, R. Rajagovindan, L. Skordos, Y. Tian, C. H. van Dyck, B. Vellas, S. Wu, Y. Zhu and A. Sandrock (2022). "Two Randomized Phase 3 Studies of Aducanumab in Early Alzheimer's Disease." The Journal of Prevention of Alzheimer's Disease **9**(2): 197-210.

Burnett, G. and E. P. Kennedy (1954). "The enzymatic phosphorylation of proteins." J Biol Chem **211**(2): 969-980.

Campbell, K. S. and M. Colonna (1999). "DAP12: a key accessory protein for relaying signals by natural killer cell receptors." Int J Biochem Cell Biol **31**(6): 631-636.

Chen, Z. and P. A. Cole (2015). "Synthetic approaches to protein phosphorylation." Current Opinion in Chemical Biology **28**: 115-122.

Chiti, F. and C. M. Dobson (2006). "Protein misfolding, functional amyloid, and human disease." Annu Rev Biochem **75**: 333-366.

Chiti, F., P. Webster, N. Taddei, A. Clark, M. Stefani, G. Ramponi and C. M. Dobson (1999). "Designing conditions for in vitro formation of amyloid protofilaments and fibrils." Proc Natl Acad Sci U S A **96**(7): 3590-3594.

Choong, X. Y., J. L. Tosh, L. J. Pulford and E. M. C. Fisher (2015). "Dissecting Alzheimer disease in Down syndrome using mouse models." **9**.

Ciechanover, A. (2005). "Proteolysis: from the lysosome to ubiquitin and the proteasome." Nat Rev Mol Cell Biol **6**(1): 79-87.

Cleary, J. P., D. M. Walsh, J. J. Hofmeister, G. M. Shankar, M. A. Kuskowski, D. J. Selkoe and K. H. Ashe (2005). "Natural oligomers of the amyloid-beta protein specifically disrupt cognitive function." Nat Neurosci **8**(1): 79-84.

Corder, E. H., A. M. Saunders, W. J. Strittmatter, D. E. Schmechel, P. C. Gaskell, G. W. Small, A. D. Roses, J. L. Haines and M. A. Pericak-Vance (1993). "Gene dose of apolipoprotein E type 4 allele and the risk of Alzheimer's disease in late onset families." Science **261**(5123): 921-923.

Czajkowsky, D. M., J. Hu, Z. Shao and R. J. Pleass (2012). "Fc-fusion proteins: new developments and future perspectives." EMBO Mol Med **4**(10): 1015-1028.

D'Andrea, M. R., G. M. Cole and M. D. Ard (2004). "The microglial phagocytic role with specific plaque types in the Alzheimer disease brain." Neurobiol Aging **25**(5): 675-683.

Dammers, C., M. Schwarten, A. K. Buell and D. Willbold (2017). "Pyroglutamate-modified Aβ(3-42) affects aggregation kinetics of Aβ(1-42) by accelerating primary and secondary pathways." Chemical Science **8**(7): 4996-5004.

De-Paula, V. J., M. Radanovic, B. S. Diniz and O. V. Forlenza (2012). "Alzheimer's disease." Subcell Biochem **65**: 329-352.

de Groot, N. S., F. X. Aviles, J. Vendrell and S. Ventura (2006). "Mutagenesis of the central hydrophobic cluster in Abeta42 Alzheimer's peptide. Side-chain properties correlate with aggregation propensities." Febs j **273**(3): 658-668.

Del-Aguila, J. L., B. A. Benitez, Z. Li, U. Dube, K. A. Mihindukulasuriya, J. P. Budde, F. H. G. Farias, M. V. Fernández, L. Ibanez, S. Jiang, R. J. Perrin, N. J. Cairns, J. C. Morris, O. Harari and C. Cruchaga (2019). "TREM2 brain transcript-

specific studies in AD and TREM2 mutation carriers." Mol Neurodegener **14**(1): 18.

Deng, H. X., A. Hentati, J. A. Tainer, Z. Iqbal, A. Cayabyab, W. Y. Hung, E. D. Getzoff, P. Hu, B. Herzfeldt, R. P. Roos and et al. (1993). "Amyotrophic lateral sclerosis and structural defects in Cu,Zn superoxide dismutase." Science **261**(5124): 1047-1051.

Deribe, Y. L., T. Pawson and I. Dikic (2010). "Post-translational modifications in signal integration." Nat Struct Mol Biol **17**(6): 666-672.

Desai, D., K. Zhang, S. Barik, A. Srivastava, M. E. Bolander and G. Sarkar (2004). "Intragenic codon bias in a set of mouse and human genes." J Theor Biol **230**(2): 215-225.

DiFiglia, M., E. Sapp, K. O. Chase, S. W. Davies, G. P. Bates, J. P. Vonsattel and N. Aronin (1997). "Aggregation of huntingtin in neuronal intranuclear inclusions and dystrophic neurites in brain." Science **277**(5334): 1990-1993.

Elgundi, Z., V. Sifniotis, M. Reslan, E. Cruz and V. Kayser (2017). "Laboratory Scale Production and Purification of a Therapeutic Antibody." J Vis Exp(119).

Faller, P. and C. Hureau (2021). "Reproducibility Problems of Amyloid-β Self-Assembly and How to Deal With Them." **8**.

Fang, X. T., D. Sehlin, L. Lannfelt, S. Syvänen and G. Hultqvist (2017). "Efficient and inexpensive transient expression of multispecific multivalent antibodies in Expi293 cells." Biological Procedures Online **19**(1): 11.

Ferrer, I., E. Bernet, E. Soriano, T. del Rio and M. Fonseca (1990). "Naturally occurring cell death in the cerebral cortex of the rat and removal of dead cells by transitory phagocytes." Neuroscience **39**(2): 451-458.

Feuerbach, D., P. Schindler, C. Barske, S. Joller, E. Beng-Louka, K. A. Worringer, S. Kommineni, A. Kaykas, D. J. Ho, C. Ye, K. Welzenbach, G. Elain, L. Klein, I. Brzak, A. K. Mir, C. J. Farady, R. Aichholz, S. Popp, N. George and U. Neumann (2017). "ADAM17 is the main sheddase for the generation of human triggering receptor expressed in myeloid cells (hTREM2) ectodomain and cleaves TREM2 after Histidine 157." Neuroscience Letters **660**: 109-114.

Fortea, J., S. H. Zaman, S. Hartley, M. S. Rafii, E. Head and M. Carmona-Iragui (2021). "Alzheimer's disease associated with Down syndrome: a genetic form of dementia." The Lancet Neurology **20**(11): 930-942.

Frank, S., G. J. Burbach, M. Bonin, M. Walter, W. Streit, I. Bechmann and T. Deller (2008). "TREM2 is upregulated in amyloid plaque-associated microglia in aged APP23 transgenic mice." Glia **56**(13): 1438-1447.

Frautschy, S. A., F. Yang, M. Irrizarry, B. Hyman, T. C. Saido, K. Hsiao and G. M. Cole (1998). "Microglial response to amyloid plaques in APPsw transgenic mice." Am J Pathol **152**(1): 307-317.

Frutiger, A., A. Tanno, S. Hwu, R. F. Tiefenauer, J. Vörös and N. Nakatsuka (2021). "Nonspecific Binding—Fundamental Concepts and Consequences for Biosensing Applications." Chemical Reviews **121**(13): 8095-8160.

Fu, X. X., S. Y. Chen, H. W. Lian, Y. Deng, R. Duan, Y. D. Zhang and T. Jiang (2023). "The TREM2 H157Y Variant Influences Microglial Phagocytosis, Polarization, and Inflammatory Cytokine Release." Brain Sci **13**(4).

Fuller, J. P., J. B. Stavenhagen and J. L. Teeling (2014). "New roles for Fc receptors in neurodegeneration-the impact on Immunotherapy for Alzheimer's Disease." **8**.

Galante, D., A. Corsaro, T. Florio, S. Vella, A. Pagano, F. Sbrana, M. Vassalli, A. Perico and C. D'Arrigo (2012). "Differential toxicity, conformation and morphology of typical initial aggregation states of Aβ1-42 and Aβpy3-42 beta-amyloids." Int J Biochem Cell Biol **44**(11): 2085-2093.

Ganat, Y. M., J. Silbereis, C. Cave, H. Ngu, G. M. Anderson, Y. Ohkubo, L. R. Ment and F. M. Vaccarino (2006). "Early Postnatal Astroglial Cells Produce Multilineage Precursors and Neural Stem Cells In Vivo." **26**(33): 8609-8621.

Gao, Z., Q. Zhu, Y. Zhang, Y. Zhao, L. Cai, C. B. Shields and J. Cai (2013). "Reciprocal modulation between microglia and astrocyte in reactive gliosis following the CNS injury." Mol Neurobiol **48**(3): 690-701.

Gibson, D. G., L. Young, R.-Y. Chuang, J. C. Venter, C. A. Hutchison and H. O. Smith (2009). "Enzymatic assembly of DNA molecules up to several hundred kilobases." Nature Methods **6**(5): 343-345.

Giulian, D. and T. J. Baker (1986). "Characterization of ameboid microglia isolated from developing mammalian brain." J Neurosci **6**(8): 2163-2178.

Glebov, K., P. Wunderlich, I. Karaca and J. Walter (2016). "Functional involvement of γ-secretase in signaling of the triggering receptor expressed on myeloid cells-2 (TREM2)." Journal of Neuroinflammation **13**(1): 17.

Glenner, G. G. and C. W. Wong (1984). "Alzheimer's disease: initial report of the purification and characterization of a novel cerebrovascular amyloid protein." Biochem Biophys Res Commun **120**(3): 885-890.

Goate, A., M. C. Chartier-Harlin, M. Mullan, J. Brown, F. Crawford, L. Fidani, L. Giuffra, A. Haynes, N. Irving, L. James and et al. (1991). "Segregation of a missense mutation in the amyloid precursor protein gene with familial Alzheimer's disease." Nature **349**(6311): 704-706.

Goedert, M., S. S. Sisodia and D. L. Price (1991). "Neurofibrillary tangles and beta-amyloid deposits in Alzheimer's disease." Curr Opin Neurobiol **1**(3): 441-447.

Graham, W. V., A. Bonito-Oliva and T. P. Sakmar (2017). "Update on Alzheimer's Disease Therapy and Prevention Strategies." **68**(1): 413-430.

Gratuze, M., C. E. G. Leyns and D. M. Holtzman (2018). "New insights into the role of TREM2 in Alzheimer's disease." Mol Neurodegener **13**(1): 66.

Grundke-Iqbal, I., K. Iqbal, Y. C. Tung, M. Quinlan, H. M. Wisniewski and L. I. Binder (1986). "Abnormal phosphorylation of the microtubule-associated protein tau (tau) in Alzheimer cytoskeletal pathology." Proc Natl Acad Sci U S A **83**(13): 4913-4917.

Guerreiro, R., A. Wojtas, J. Bras, M. Carrasquillo, E. Rogaeva, E. Majounie, C. Cruchaga, C. Sassi, J. S. K. Kauwe, S. Younkin, L. Hazrati, J. Collinge, J. Pocock, T. Lashley, J. Williams, J.-C. Lambert, P. Amouyel, A. Goate, R. Rademakers, K. Morgan, J. Powell, P. St. George-Hyslop, A. Singleton and J. Hardy (2013). "TREM2 Variants in Alzheimer's Disease." New England Journal of Medicine **368**(2): 117-127.

Haass, C. and D. J. Selkoe (2007). "Soluble protein oligomers in neurodegeneration: lessons from the Alzheimer's amyloid β-peptide." Nature Reviews Molecular Cell Biology **8**(2): 101-112.

Hammond, C. and A. Helenius (1994). "Quality control in the secretory pathway: retention of a misfolded viral membrane glycoprotein involves cycling between the ER, intermediate compartment, and Golgi apparatus." J Cell Biol **126**(1): 41-52.

Hardy, J. and D. Allsop (1991). "Amyloid deposition as the central event in the aetiology of Alzheimer's disease." Trends Pharmacol Sci **12**(10): 383-388.

Healy, L. M., G. Perron, S. Y. Won, M. A. Michell-Robinson, A. Rezk, S. K. Ludwin, C. S. Moore, J. A. Hall, A. Bar-Or and J. P. Antel (2016). "MerTK Is a Functional Regulator of Myelin Phagocytosis by Human Myeloid Cells." J Immunol **196**(8): 3375-3384.

Henjum, K., I. S. Almdahl, V. Arskog, L. Minthon, O. Hansson, T. Fladby and L. N. Nilsson (2016). "Cerebrospinal fluid soluble TREM2 in aging and Alzheimer's disease." Alzheimers Res Ther **8**(1): 17.

Hickman, S., S. Izzy, P. Sen, L. Morsett and J. El Khoury (2018). "Microglia in neurodegeneration." Nat Neurosci **21**(10): 1359-1369.

Hickman, S. E., E. K. Allison and J. El Khoury (2008). "Microglial dysfunction and defective beta-amyloid clearance pathways in aging Alzheimer's disease mice." J Neurosci **28**(33): 8354-8360.

Hickman, S. E., N. D. Kingery, T. K. Ohsumi, M. L. Borowsky, L.-c. Wang, T. K. Means and J. El Khoury (2013). "The microglial sensome revealed by direct RNA sequencing." Nature Neuroscience **16**(12): 1896-1905.

Hoover, B. R., M. N. Reed, J. Su, R. D. Penrod, L. A. Kotilinek, M. K. Grant, R. Pitstick, G. A. Carlson, L. M. Lanier, L. L. Yuan, K. H. Ashe and D. Liao (2010). "Tau mislocalization to dendritic spines mediates synaptic dysfunction independently of neurodegeneration." Neuron **68**(6): 1067-1081.

Hortega, P. R. J. T. L. I. B. U. M. (1918). "Noticia de un nuevo y fácil método para la coloración de la neuroglia y el tejido conjuntivo." **15**: 367-378.

Howie, A. J. and M. P. Owen-Casey (2010). "Discrepancies between descriptions and illustrations of colours in Congo red-stained amyloid, and explanation of discrepant colours." Amyloid **17**(3-4): 109-117.

Hsieh, C. L., M. Koike, S. C. Spusta, E. C. Niemi, M. Yenari, M. C. Nakamura and W. E. Seaman (2009). "A role for TREM2 ligands in the phagocytosis of apoptotic neuronal cells by microglia." **109**(4): 1144-1156.

Hu, Y. S., J. Do, C. R. Edamakanti, A. R. Kini, M. Martina, S. I. Stupp and P. Opal (2019). "Self-assembling vascular endothelial growth factor nanoparticles improve function in spinocerebellar ataxia type 1." Brain **142**(2): 312-321.

Huang, Y., T. Ma, P. K. Lau, J. Wang, T. Zhao, S. Du, M. M. T. Loy and Y. Guo (2019). "Visualization of Protein Sorting at the Trans-Golgi Network and Endosomes Through Super-Resolution Imaging." **7**.

Hunter, T. (2009). "Tyrosine phosphorylation: thirty years and counting." Curr Opin Cell Biol **21**(2): 140-146.

Hutton, M., C. L. Lendon, P. Rizzu, M. Baker, S. Froelich, H. Houlden, S. Pickering-Brown, S. Chakraverty, A. Isaacs, A. Grover, J. Hackett, J. Adamson, S. Lincoln, D. Dickson, P. Davies, R. C. Petersen, M. Stevens, E. de Graaff, E. Wauters, J. van Baren, M. Hillebrand, M. Joosse, J. M. Kwon, P. Nowotny, L. K. Che, J. Norton, J. C. Morris, L. A. Reed, J. Trojanowski, H. Basun, L. Lannfelt, M. Neystat, S. Fahn, F. Dark, T. Tannenberg, P. R. Dodd, N. Hayward, J. B. Kwok, P. R. Schofield, A. Andreadis, J. Snowden, D. Craufurd, D. Neary, F. Owen, B. A. Oostra, J. Hardy, A. Goate, J. van Swieten, D. Mann, T. Lynch and P. Heutink (1998). "Association of missense and 5'-splice-site mutations in tau with the inherited dementia FTDP-17." Nature **393**(6686): 702-705.

Ibach, M., M. Mathews, B. Linnartz-Gerlach, S. Theil, S. Kumar, R. Feederle, O. Brüstle, H. Neumann and J. Walter (2021). "A reporter cell system for the triggering receptor expressed on myeloid cells 2 reveals differential effects of disease-associated variants on receptor signaling and activation by antibodies against the stalk region." Glia **69**(5): 1126-1139.

Ibach, M. S. (2021). A reporter cell system for TREM2 reveals differential effects of disease-associated variants on receptor signaling and activation by antibodies against the stalk region Dissertation, Rheinische Friedrich-Wilhelms-Universität Bonn.

Jawhar, S., O. Wirths and T. A. Bayer (2011). "Pyroglutamate amyloid-β (Aβ): a hatchet man in Alzheimer disease." J Biol Chem **286**(45): 38825-38832.

Jay, T. R., A. M. Hirsch, M. L. Broihier, C. M. Miller, L. E. Neilson, R. M. Ransohoff, B. T. Lamb and G. E. Landreth (2017). "Disease Progression-Dependent Effects of TREM2 Deficiency in a Mouse Model of Alzheimer's Disease." **37**(3): 637-647.

Jay, T. R., C. M. Miller, P. J. Cheng, L. C. Graham, S. Bemiller, M. L. Broihier, G. Xu, D. Margevicius, J. C. Karlo, G. L. Sousa, A. C. Cotleur, O. Butovsky, L. Bekris, S. M. Staugaitis, J. B. Leverenz, S. W. Pimplikar, G. E. Landreth, G. R. Howell, R. M. Ransohoff and B. T. Lamb (2015). "TREM2 deficiency eliminates TREM2+ inflammatory macrophages and ameliorates pathology in Alzheimer's disease mouse models." J Exp Med **212**(3): 287-295.

Jiang, T., L. Tan, X. C. Zhu, Q. Q. Zhang, L. Cao, M. S. Tan, L. Z. Gu, H. F. Wang, Z. Z. Ding, Y. D. Zhang and J. T. Yu (2014). "Upregulation of TREM2 ameliorates neuropathology and rescues spatial cognitive impairment in a transgenic mouse model of Alzheimer's disease." Neuropsychopharmacology **39**(13): 2949-2962.

Jin, S. C., B. A. Benitez, C. M. Karch, B. Cooper, T. Skorupa, D. Carrell, J. B. Norton, S. Hsu, O. Harari, Y. Cai, S. Bertelsen, A. M. Goate and C. Cruchaga (2014). "Coding variants in TREM2 increase risk for Alzheimer's disease." Hum Mol Genet **23**(21): 5838-5846.

Jonsson, T., J. K. Atwal, S. Steinberg, J. Snaedal, P. V. Jonsson, S. Bjornsson, H. Stefansson, P. Sulem, D. Gudbjartsson, J. Maloney, K. Hoyte, A. Gustafson, Y. Liu, Y. Lu, T. Bhangale, R. R. Graham, J. Huttenlocher, G. Bjornsdottir, O. A. Andreassen, E. G. Jönsson, A. Palotie, T. W. Behrens, O. T. Magnusson, A. Kong, U. Thorsteinsdottir, R. J. Watts and K. Stefansson (2012). "A mutation in APP protects against Alzheimer's disease and age-related cognitive decline." Nature **488**(7409): 96-99.

Jonsson, T., H. Stefansson, S. Steinberg, I. Jonsdottir, P. V. Jonsson, J. Snaedal, S. Bjornsson, J. Huttenlocher, A. I. Levey, J. J. Lah, D. Rujescu, H. Hampel, I. Giegling, O. A. Andreassen, K. Engedal, I. Ulstein, S. Djurovic, C. Ibrahim-Verbaas, A. Hofman, M. A. Ikram, C. M. van Duijn, U. Thorsteinsdottir, A. Kong and K. Stefansson (2013). "Variant of TREM2 associated with the risk of Alzheimer's disease." N Engl J Med **368**(2): 107-116.

Joshi, P., F. Riffel, S. Kumar, N. Villacampa, S. Theil, S. Parhizkar, C. Haass, M. Colonna, M. T. Heneka, T. Arzberger, J. Herms and J. Walter (2021). "TREM2 modulates differential deposition of modified and non-modified Aβ species in extracellular plaques and intraneuronal deposits." Acta Neuropathol Commun **9**(1): 168.

Joshi, P., F. Riffel, K. Satoh, M. Enomoto, S. Qamar, H. Scheiblich, N. Villacampa, S. Kumar, S. Theil, S. Parhizkar, C. Haass, M. T. Heneka, P. E.

Fraser, P. St George-Hyslop and J. Walter (2021). "Differential interaction with TREM2 modulates microglial uptake of modified Aβ species." **69**(12): 2917-2932.

Joshi, P., F. Riffel, K. Satoh, M. Enomoto, S. Qamar, H. Scheiblich, N. Villacampa, S. Kumar, S. Theil, S. Parhizkar, C. Haass, M. T. Heneka, P. E. Fraser, P. St George-Hyslop and J. Walter (2021). "Differential interaction with TREM2 modulates microglial uptake of modified Aβ species." Glia **69**(12): 2917-2932.

Joshi, P. C. (2022). TREM2 modulates differential deposition of post-translationally modified Aβ variants in the brain parenchyma and the vasculature Dissertation, Rheinische Friedrich-Wilhelms-Universität Bonn.

Karran, E. and B. De Strooper (2016). "The amyloid cascade hypothesis: are we poised for success or failure?" J Neurochem **139 Suppl 2**: 237-252.

Karran, E., M. Mercken and B. D. Strooper (2011). "The amyloid cascade hypothesis for Alzheimer's disease: an appraisal for the development of therapeutics." Nature Reviews Drug Discovery **10**(9): 698-712.

Karsak, M., K. Glebov, M. Scheffold, T. Bajaj, A. Kawalia, I. Karaca, S. Rading, J. Kornhuber, O. Peters, M. Diez-Fairen, L. Frölich, M. Hüll, J. Wiltfang, M. Scherer, S. Riedel-Heller, A. Schneider, M. T. Heneka, K. Fliessbach, A. Sharaf, H. Thiele, M. Lennarz, F. Jessen, W. Maier, C. Kubisch, Z. Ignatova, P. Nürnberg, P. Pastor, J. Walter and A. Ramirez (2020). "A rare heterozygous TREM2 coding variant identified in familial clustering of dementia affects an intrinsically disordered protein region and function of TREM2." Hum Mutat **41**(1): 169-181.

Kinney, J. W., S. M. Bemiller, A. S. Murtishaw, A. M. Leisgang, A. M. Salazar and B. T. Lamb (2018). "Inflammation as a central mechanism in Alzheimer's disease." Alzheimer's & Dementia: Translational Research & Clinical Interventions **4**: 575-590.

Kleinberger, G., M. Brendel, E. Mracsko, B. Wefers, L. Groeneweg, X. Xiang, C. Focke, M. Deußing, M. Suárez-Calvet, F. Mazaheri, S. Parhizkar, N. Pettkus, W. Wurst, R. Feederle, P. Bartenstein, T. Mueggler, T. Arzberger, I. Knuesel, A. Rominger and C. Haass (2017). "The FTD-like syndrome causing TREM2 T66M mutation impairs microglia function, brain perfusion, and glucose metabolism." **36**(13): 1837-1853.

Kleinberger, G., M. Brendel, E. Mracsko, B. Wefers, L. Groeneweg, X. Xiang, C. Focke, M. Deußing, M. Suárez-Calvet, F. Mazaheri, S. Parhizkar, N. Pettkus, W. Wurst, R. Feederle, P. Bartenstein, T. Mueggler, T. Arzberger, I. Knuesel, A. Rominger and C. Haass (2017). "The FTD-like syndrome causing TREM2 T66M mutation impairs microglia function, brain perfusion, and glucose metabolism." The EMBO Journal: e201796516.

Kleinberger, G., Y. Yamanishi, M. Suárez-Calvet, E. Czirr, E. Lohmann, E. Cuyvers, H. Struyfs, N. Pettkus, A. Wenninger-Weinzierl, F. Mazaheri, S.

Tahirovic, A. Lleó, D. Alcolea, J. Fortea, M. Willem, S. Lammich, J. L. Molinuevo, R. Sánchez-Valle, A. Antonell, A. Ramirez, M. T. Heneka, K. Sleegers, J. van der Zee, J. J. Martin, S. Engelborghs, A. Demirtas-Tatlidede, H. Zetterberg, C. Van Broeckhoven, H. Gurvit, T. Wyss-Coray, J. Hardy, M. Colonna and C. Haass (2014). "TREM2 mutations implicated in neurodegeneration impair cell surface transport and phagocytosis." Sci Transl Med **6**(243): 243ra286.

Kober, D. L., J. M. Alexander-Brett, C. M. Karch, C. Cruchaga, M. Colonna, M. J. Holtzman and T. J. Brett (2016). "Neurodegenerative disease mutations in TREM2 reveal a functional surface and distinct loss-of-function mechanisms." eLife **5**: e20391.

Kober, D. L., M. D. Stuchell-Brereton, C. E. Kluender, H. B. Dean, M. R. Strickland, D. F. Steinberg, S. S. Nelson, B. Baban, D. M. Holtzman, C. Frieden, J. Alexander-Brett, E. D. Roberson, Y. Song and T. J. Brett (2020). "Functional insights from biophysical study of TREM2 interactions with apoE and Aβ(1-42)." Alzheimers Dement.

Kumar, S., A. Kapadia, S. Theil, P. Joshi, F. Riffel, M. T. Heneka and J. Walter (2021). "Novel Phosphorylation-State Specific Antibodies Reveal Differential Deposition of Ser26 Phosphorylated Aβ Species in a Mouse Model of Alzheimer's Disease." **13**.

Kumar, S., C. A. Lemere and J. Walter (2020). "Phosphorylated Aβ peptides in human Down syndrome brain and different Alzheimer's-like mouse models." Acta Neuropathologica Communications **8**(1): 118.

Kumar, S., N. Rezaei-Ghaleh, D. Terwel, D. R. Thal, M. Richard, M. Hoch, J. M. Mc Donald, U. Wüllner, K. Glebov, M. T. Heneka, D. M. Walsh, M. Zweckstetter and J. Walter (2011). "Extracellular phosphorylation of the amyloid β-peptide promotes formation of toxic aggregates during the pathogenesis of Alzheimer's disease." **30**(11): 2255-2265.

Kumar, S., S. Singh, D. Hinze, M. Josten, H. G. Sahl, M. Siepmann and J. Walter (2012). "Phosphorylation of amyloid-β peptide at serine 8 attenuates its clearance via insulin-degrading and angiotensin-converting enzymes." J Biol Chem **287**(11): 8641-8651.

Kumar, S., O. Wirths, K. Stüber, P. Wunderlich, P. Koch, S. Theil, N. Rezaei-Ghaleh, M. Zweckstetter, T. A. Bayer, O. Brüstle, D. R. Thal and J. Walter (2016). "Phosphorylation of the amyloid β-peptide at Ser26 stabilizes oligomeric assembly and increases neurotoxicity." Acta Neuropathologica **131**(4): 525-537.

Kummer, M. P. and M. T. Heneka (2014). "Truncated and modified amyloid-beta species." Alzheimer's Research & Therapy **6**(3): 28.

Kuo, Y. M., S. Webster, M. R. Emmerling, N. De Lima and A. E. Roher (1998). "Irreversible dimerization/tetramerization and post-translational modifications

inhibit proteolytic degradation of A beta peptides of Alzheimer's disease." Biochim Biophys Acta **1406**(3): 291-298.

Lambert, J.-C., C. A. Ibrahim-Verbaas, D. Harold, A. C. Naj, R. Sims, C. Bellenguez, G. Jun, A. L. DeStefano, J. C. Bis, G. W. Beecham, B. Grenier-Boley, G. Russo, T. A. Thornton-Wells, N. Jones, A. V. Smith, V. Chouraki, C. Thomas, M. A. Ikram, D. Zelenika, B. N. Vardarajan, Y. Kamatani, C.-F. Lin, A. Gerrish, H. Schmidt, B. Kunkle, M. L. Dunstan, A. Ruiz, M.-T. Bihoreau, S.-H. Choi, C. Reitz, F. Pasquier, P. Hollingworth, A. Ramirez, O. Hanon, A. L. Fitzpatrick, J. D. Buxbaum, D. Campion, P. K. Crane, C. Baldwin, T. Becker, V. Gudnason, C. Cruchaga, D. Craig, N. Amin, C. Berr, O. L. Lopez, P. L. De Jager, V. Deramecourt, J. A. Johnston, D. Evans, S. Lovestone, L. Letenneur, F. J. Morón, D. C. Rubinsztein, G. Eiriksdottir, K. Sleegers, A. M. Goate, N. Fiévet, M. J. Huentelman, M. Gill, K. Brown, M. I. Kamboh, L. Keller, P. Barberger-Gateau, B. McGuinness, E. B. Larson, R. Green, A. J. Myers, C. Dufouil, S. Todd, D. Wallon, S. Love, E. Rogaeva, J. Gallacher, P. St George-Hyslop, J. Clarimon, A. Lleo, A. Bayer, D. W. Tsuang, L. Yu, M. Tsolaki, P. Bossù, G. Spalletta, P. Proitsi, J. Collinge, S. Sorbi, F. Sanchez-Garcia, N. C. Fox, J. Hardy, M. C. D. Naranjo, P. Bosco, R. Clarke, C. Brayne, D. Galimberti, M. Mancuso, F. Matthews, S. Moebus, P. Mecocci, M. Del Zompo, W. Maier, H. Hampel, A. Pilotto, M. Bullido, F. Panza, P. Caffarra, B. Nacmias, J. R. Gilbert, M. Mayhaus, L. Lannfelt, H. Hakonarson, S. Pichler, M. M. Carrasquillo, M. Ingelsson, D. Beekly, V. Alvarez, F. Zou, O. Valladares, S. G. Younkin, E. Coto, K. L. Hamilton-Nelson, W. Gu, C. Razquin, P. Pastor, I. Mateo, M. J. Owen, K. M. Faber, P. V. Jonsson, O. Combarros, M. C. O'Donovan, L. B. Cantwell, H. Soininen, D. Blacker, S. Mead, T. H. Mosley, D. A. Bennett, T. B. Harris, L. Fratiglioni, C. Holmes, R. F. A. G. de Bruijn, P. Passmore, T. J. Montine, K. Bettens, J. I. Rotter, A. Brice, K. Morgan, T. M. Foroud, W. A. Kukull, D. Hannequin, J. F. Powell, M. A. Nalls, K. Ritchie, K. L. Lunetta, J. S. K. Kauwe, E. Boerwinkle, M. Riemenschneider, M. Boada, M. Hiltunen, E. R. Martin, R. Schmidt, D. Rujescu, L.-S. Wang, J.-F. Dartigues, R. Mayeux, C. Tzourio, A. Hofman, M. M. Nöthen, C. Graff, B. M. Psaty, L. Jones, J. L. Haines, P. A. Holmans, M. Lathrop, M. A. Pericak-Vance, L. J. Launer, L. A. Farrer, C. M. van Duijn, C. Van Broeckhoven, V. Moskvina, S. Seshadri, J. Williams, G. D. Schellenberg, P. Amouyel, I. European Alzheimer's Disease, Genetic, D. Environmental Risk in Alzheimer's, C. Alzheimer's Disease Genetic, H. Cohorts for and E. Aging Research in Genomic (2013). "Meta-analysis of 74,046 individuals identifies 11 new susceptibility loci for Alzheimer's disease." Nature Genetics **45**(12): 1452-1458.

Lambert, M. P., A. K. Barlow, B. A. Chromy, C. Edwards, R. Freed, M. Liosatos, T. E. Morgan, I. Rozovsky, B. Trommer, K. L. Viola, P. Wals, C. Zhang, C. E. Finch, G. A. Krafft and W. L. Klein (1998). "Diffusible, nonfibrillar ligands derived from Abeta1-42 are potent central nervous system neurotoxins." Proc Natl Acad Sci U S A **95**(11): 6448-6453.

Lamptey, R. N. L., B. Chaulagain, R. Trivedi, A. Gothwal, B. Layek and J. Singh (2022). "A Review of the Common Neurodegenerative Disorders: Current Therapeutic Approaches and the Potential Role of Nanotherapeutics." Int J Mol Sci **23**(3).

Latousakis, D. and N. Juge (2018). "How Sweet Are Our Gut Beneficial Bacteria? A Focus on Protein Glycosylation in Lactobacillus." Int J Mol Sci **19**(1).

Lawson, L. J., V. H. Perry, P. Dri and S. Gordon (1990). "Heterogeneity in the distribution and morphology of microglia in the normal adult mouse brain." Neuroscience **39**(1): 151-170.

Lehner, R., X. Wang and P. Hunziker (2013). "Plasmid linearization changes shape and efficiency of transfection complexes." **5**(4): 205-212.

Lessard, C. B., S. L. Malnik, Y. Zhou, T. B. Ladd, P. E. Cruz, Y. Ran, T. E. Mahan, P. Chakrabaty, D. M. Holtzman, J. D. Ulrich, M. Colonna and T. E. Golde (2018). "High-affinity interactions and signal transduction between Aβ oligomers and TREM2." EMBO molecular medicine **10**(11): e9027.

Levene, P. A. and C. L. Alsberg (1906). "The Cleavage Products of Vitellin." Journal of Biological Chemistry **2**(1): 127-133.

Levy-Lahad, E., W. Wasco, P. Poorkaj, D. M. Romano, J. Oshima, W. H. Pettingell, C. E. Yu, P. D. Jondro, S. D. Schmidt, K. Wang and et al. (1995). "Candidate gene for the chromosome 1 familial Alzheimer's disease locus." Science **269**(5226): 973-977.

Liddelow, S. A., K. A. Guttenplan, L. E. Clarke, F. C. Bennett, C. J. Bohlen, L. Schirmer, M. L. Bennett, A. E. Münch, W.-S. Chung, T. C. Peterson, D. K. Wilton, A. Frouin, B. A. Napier, N. Panicker, M. Kumar, M. S. Buckwalter, D. H. Rowitch, V. L. Dawson, T. M. Dawson, B. Stevens and B. A. Barres (2017). "Neurotoxic reactive astrocytes are induced by activated microglia." Nature **541**(7638): 481-487.

Lin, H. P., B. Singla, P. Ghoshal, J. L. Faulkner, M. Cherian-Shaw, P. M. O'Connor, J. X. She, E. J. Belin de Chantemele and G. Csányi (2018). "Identification of novel macropinocytosis inhibitors using a rational screen of Food and Drug Administration-approved drugs." Br J Pharmacol **175**(18): 3640-3655.

Liu, L. (2018). "Pharmacokinetics of monoclonal antibodies and Fc-fusion proteins." Protein Cell **9**(1): 15-32.

Longo, P. A., J. M. Kavran, M. S. Kim and D. J. Leahy (2013). "Transient mammalian cell transfection with polyethylenimine (PEI)." Methods Enzymol **529**: 227-240.

Ma, L., M. Allen, N. Sakae, N. Ertekin-Taner, N. R. Graff-Radford, D. W. Dickson, S. G. Younkin and D. Sevlever (2016). "Expression and processing

analyses of wild type and p.R47H TREM2 variant in Alzheimer's disease brains." Mol Neurodegener **11**(1): 72.

Ma, Q., J. Y. Hu, J. Chen and Y. Liang (2013). "The role of crowded physiological environments in prion and prion-like protein aggregation." Int J Mol Sci **14**(11): 21339-21352.

Malhotra, J. D. and R. J. Kaufman (2007). "The endoplasmic reticulum and the unfolded protein response." Semin Cell Dev Biol **18**(6): 716-731.

Masters, C. L., G. Multhaup, G. Simms, J. Pottgiesser, R. N. Martins and K. Beyreuther (1985). "Neuronal origin of a cerebral amyloid: neurofibrillary tangles of Alzheimer's disease contain the same protein as the amyloid of plaque cores and blood vessels." Embo j **4**(11): 2757-2763.

Masters, C. L., G. Simms, N. A. Weinman, G. Multhaup, B. L. McDonald and K. Beyreuther (1985). "Amyloid plaque core protein in Alzheimer disease and Down syndrome." Proc Natl Acad Sci U S A **82**(12): 4245-4249.

Meisl, G., J. B. Kirkegaard, P. Arosio, T. C. T. Michaels, M. Vendruscolo, C. M. Dobson, S. Linse and T. P. J. Knowles (2016). "Molecular mechanisms of protein aggregation from global fitting of kinetic models." Nature Protocols **11**(2): 252-272.

Meisl, G., X. Yang, E. Hellstrand, B. Frohm, J. B. Kirkegaard, S. I. Cohen, C. M. Dobson, S. Linse and T. P. Knowles (2014). "Differences in nucleation behavior underlie the contrasting aggregation kinetics of the Aβ40 and Aβ42 peptides." Proc Natl Acad Sci U S A **111**(26): 9384-9389.

Mohamed, H. A., D. R. Mosier, L. L. Zou, L. Siklós, M. E. Alexianu, J. I. Engelhardt, D. R. Beers, W.-d. Le and S. H. Appel (2002). "Immunoglobulin Fcγ receptor promotes immunoglobulin uptake, immunoglobulin-mediated calcium increase, and neurotransmitter release in motor neurons." **69**(1): 110-116.

Moore, B. D., P. Chakrabarty, Y. Levites, T. L. Kukar, A. M. Baine, T. Moroni, T. B. Ladd, P. Das, D. W. Dickson and T. E. Golde (2012). "Overlapping profiles of Aβ peptides in the Alzheimer's disease and pathological aging brains." Alzheimers Res Ther **4**(3): 18.

Mortada, I., R. Farah, S. Nabha, D. M. Ojcius, Y. Fares, W. Y. Almawi and N. S. Sadier (2021). "Immunotherapies for Neurodegenerative Diseases." **12**.

Mucke, L., E. Masliah, G. Q. Yu, M. Mallory, E. M. Rockenstein, G. Tatsuno, K. Hu, D. Kholodenko, K. Johnson-Wood and L. McConlogue (2000). "High-level neuronal expression of abeta 1-42 in wild-type human amyloid protein precursor transgenic mice: synaptotoxicity without plaque formation." J Neurosci **20**(11): 4050-4058.

Neumann, H. and K. Takahashi (2007). "Essential role of the microglial triggering receptor expressed on myeloid cells-2 (TREM2) for central nervous tissue immune homeostasis." J Neuroimmunol **184**(1-2): 92-99.

Neumann, M., D. M. Sampathu, L. K. Kwong, A. C. Truax, M. C. Micsenyi, T. T. Chou, J. Bruce, T. Schuck, M. Grossman, C. M. Clark, L. F. McCluskey, B. L. Miller, E. Masliah, I. R. Mackenzie, H. Feldman, W. Feiden, H. A. Kretzschmar, J. Q. Trojanowski and V. M. Lee (2006). "Ubiquitinated TDP-43 in frontotemporal lobar degeneration and amyotrophic lateral sclerosis." Science **314**(5796): 130-133.

Noël, S., S. Cadet, E. Gras and C. Hureau (2013). "The benzazole scaffold: a SWAT to combat Alzheimer's disease." Chemical Society Reviews **42**(19): 7747-7762.

Pagano, K., S. Tomaselli, H. Molinari and L. Ragona (2020). "Natural Compounds as Inhibitors of Aβ Peptide Aggregation: Chemical Requirements and Molecular Mechanisms." **14**.

Paloneva, J., T. Manninen, G. Christman, K. Hovanes, J. Mandelin, R. Adolfsson, M. Bianchin, T. Bird, R. Miranda, A. Salmaggi, L. Tranebjaerg, Y. Konttinen and L. Peltonen (2002). "Mutations in two genes encoding different subunits of a receptor signaling complex result in an identical disease phenotype." Am J Hum Genet **71**(3): 656-662.

Pan, X. D., Y. G. Zhu, N. Lin, J. Zhang, Q. Y. Ye, H. P. Huang and X. C. Chen (2011). "Microglial phagocytosis induced by fibrillar β-amyloid is attenuated by oligomeric β-amyloid: implications for Alzheimer's disease." Mol Neurodegener **6**: 45.

Parhizkar, S., T. Arzberger, M. Brendel, G. Kleinberger, M. Deussing, C. Focke, B. Nuscher, M. Xiong, A. Ghasemigharagoz, N. Katzmarski, S. Krasemann, S. F. Lichtenthaler, S. A. Muller, A. Colombo, L. S. Monasor, S. Tahirovic, J. Herms, M. Willem, N. Pettkus, O. Butovsky, P. Bartenstein, D. Edbauer, A. Rominger, A. Erturk, S. A. Grathwohl, J. J. Neher, D. M. Holtzman, M. Meyer-Luehmann and C. Haass (2019). "Loss of TREM2 function increases amyloid seeding but reduces plaque-associated ApoE." Nat Neurosci **22**(2): 191-204.

Park, J. S., I. J. Ji, D. H. Kim, H. J. An and S. Y. Yoon (2016). "The Alzheimer's Disease-Associated R47H Variant of TREM2 Has an Altered Glycosylation Pattern and Protein Stability." Front Neurosci **10**: 618.

Parks, T. D., K. K. Leuther, E. D. Howard, S. A. Johnston and W. G. Dougherty (1994). "Release of proteins and peptides from fusion proteins using a recombinant plant virus proteinase." Anal Biochem **216**(2): 413-417.

Pascoal, T. A., A. L. Benedet, N. J. Ashton, M. S. Kang, J. Therriault, M. Chamoun, M. Savard, F. Z. Lussier, C. Tissot, T. K. Karikari, J. Ottoy, S. Mathotaarachchi, J. Stevenson, G. Massarweh, M. Schöll, M. J. de Leon, J. P. Soucy, P. Edison, K. Blennow, H. Zetterberg, S. Gauthier and P. Rosa-Neto (2021). "Microglial activation and tau propagate jointly across Braak stages." Nat Med **27**(9): 1592-1599.

Peferoen, L., D. Vogel, M. Breur, W. Gerritsen, C. Dijkstra and S. J. G. Amor (2013). "Do stressed oligodendrocytes trigger microglia activation in pre-active MS lesion." **61**: S164-164.

Perez, S. E., M. Nadeem, B. He, J. C. Miguel, M. H. Malek-Ahmadi, K. Chen and E. J. Mufson (2017). "Neocortical and hippocampal TREM2 protein levels during the progression of Alzheimer's disease." Neurobiol Aging **54**: 133-143.

Piccio, L., C. Buonsanti, M. Cella, I. Tassi, R. E. Schmidt, C. Fenoglio, J. Rinker, 2nd, R. T. Naismith, P. Panina-Bordignon, N. Passini, D. Galimberti, E. Scarpini, M. Colonna and A. H. Cross (2008). "Identification of soluble TREM-2 in the cerebrospinal fluid and its association with multiple sclerosis and CNS inflammation." Brain **131**(Pt 11): 3081-3091.

Pike, C. J., A. J. Walencewicz, C. G. Glabe and C. W. Cotman (1991). "In vitro aging of beta-amyloid protein causes peptide aggregation and neurotoxicity." Brain Res **563**(1-2): 311-314.

Popov, I. A., M. I. Indeikina, S. I. Pekov, N. L. Starodubtseva, A. S. Kononikhin, M. I. Nikolaeva, E. N. Kukaev, Y. I. Kostyukevich, S. A. Kozin, A. A. Makarov and E. N. Nikolaev (2014). "Estimation of phosphorylation level of amyloid-beta isolated from human blood plasma: Ultrahigh-resolution mass spectrometry." Molecular Biology **48**(4): 607-614.

Prasher, V. P., M. J. Farrer, A. M. Kessling, E. M. C. Fisher, R. J. West, P. C. Barber and A. C. Butler (1998). "Molecular mapping of alzheimer-type dementia in Down's syndrome." **43**(3): 380-383.

Prince, M. J., A. Wimo, M. M. Guerchet, G. C. Ali, Y.-T. Wu and M. Prina (2015). "World Alzheimer Report 2015-The Global Impact of Dementia: An analysis of prevalence, incidence, cost and trends."

Rauchmann, B. S., A. Sadlon and R. Perneczky (2020). "Soluble TREM2 and Inflammatory Proteins in Alzheimer's Disease Cerebrospinal Fluid." J Alzheimers Dis **73**(4): 1615-1626.

Raymond, C., R. Tom, S. Perret, P. Moussouami, D. L'Abbé, G. St-Laurent and Y. Durocher (2011). "A simplified polyethylenimine-mediated transfection process for large-scale and high-throughput applications." Methods **55**(1): 44-51.

Ree, R., S. Varland and T. Arnesen (2018). "Spotlight on protein N-terminal acetylation." Exp Mol Med **50**(7): 1-13.

Ripoli, C., S. Cocco, D. D. Li Puma, R. Piacentini, A. Mastrodonato, F. Scala, D. Puzzo, M. D'Ascenzo and C. Grassi (2014). "Intracellular accumulation of amyloid-β (Aβ) protein plays a major role in Aβ-induced alterations of glutamatergic synaptic transmission and plasticity." J Neurosci **34**(38): 12893-12903.

Roberts, C. J. (2007). "Non-native protein aggregation kinetics." **98**(5): 927-938.

Rogers, J., J. Luber-Narod, S. D. Styren and W. H. Civin (1988). "Expression of immune system-associated antigens by cells of the human central nervous system: Relationship to the pathology of Alzheimer's disease." Neurobiology of Aging **9**: 339-349.

Roopenian, D. C. and S. Akilesh (2007). "FcRn: the neonatal Fc receptor comes of age." Nat Rev Immunol **7**(9): 715-725.

Saido, T. C., T. Iwatsubo, D. M. A. Mann, H. Shimada, Y. Ihara and S. Kawashima (1995). "Dominant and differential deposition of distinct β-amyloid peptide species, AβN3(pE), in senile plaques." Neuron **14**(2): 457-466.

Schilling, S., T. Lauber, M. Schaupp, S. Manhart, E. Scheel, G. Böhm and H.-U. Demuth (2006). "On the Seeding and Oligomerization of pGlu-Amyloid Peptides (in vitro)." Biochemistry **45**(41): 12393-12399.

Schlepckow, K., G. Kleinberger, A. Fukumori, R. Feederle, S. F. Lichtenthaler, H. Steiner and C. Haass (2017). "An Alzheimer-associated TREM2 variant occurs at the ADAM cleavage site and affects shedding and phagocytic function." EMBO Molecular Medicine **9**(10): 1356-1365.

Schlepckow, K., K. M. Monroe, G. Kleinberger, L. Cantuti-Castelvetri, S. Parhizkar, D. Xia, M. Willem, G. Werner, N. Pettkus, B. Brunner, A. Sülzen, B. Nuscher, H. Hampel, X. Xiang, R. Feederle, S. Tahirovic, J. I. Park, R. Prorok, C. Mahon, C.-C. Liang, J. Shi, D. J. Kim, H. Sabelström, F. Huang, G. Di Paolo, M. Simons, J. W. Lewcock and C. Haass (2020). "Enhancing protective microglial activities with a dual function TREM2 antibody to the stalk region." **12**(4): e11227.

Schmid, C. D., L. N. Sautkulis, P. E. Danielson, J. Cooper, K. W. Hasel, B. S. Hilbush, J. G. Sutcliffe and M. J. Carson (2002). "Heterogeneous expression of the triggering receptor expressed on myeloid cells-2 on adult murine microglia." J Neurochem **83**(6): 1309-1320.

Selkoe, D. J. and J. Hardy (2016). "The amyloid hypothesis of Alzheimer's disease at 25 years." **8**(6): 595-608.

Sergeant, N., S. Bombois, A. Ghestem, H. Drobecq, V. Kostanjevecki, C. Missiaen, A. Wattez, J. P. David, E. Vanmechelen, C. Sergheraert and A. Delacourte (2003). "Truncated beta-amyloid peptide species in pre-clinical Alzheimer's disease as new targets for the vaccination approach." J Neurochem **85**(6): 1581-1591.

Sherrington, R., E. I. Rogaev, Y. Liang, E. A. Rogaeva, G. Levesque, M. Ikeda, H. Chi, C. Lin, G. Li, K. Holman, T. Tsuda, L. Mar, J. F. Foncin, A. C. Bruni, M. P. Montesi, S. Sorbi, I. Rainero, L. Pinessi, L. Nee, I. Chumakov, D. Pollen, A. Brookes, P. Sanseau, R. J. Polinsky, W. Wasco, H. A. Da Silva, J. L. Haines, M. A. Perkicak-Vance, R. E. Tanzi, A. D. Roses, P. E. Fraser, J. M. Rommens and P. H. St George-Hyslop (1995). "Cloning of a gene bearing missense mutations in early-onset familial Alzheimer's disease." Nature **375**(6534): 754-760.

Sonawane, N. D., F. C. Szoka, Jr. and A. S. Verkman (2003). "Chloride accumulation and swelling in endosomes enhances DNA transfer by polyamine-DNA polyplexes." J Biol Chem **278**(45): 44826-44831.

Song, W., B. Hooli, K. Mullin, S. C. Jin, M. Cella, T. K. Ulland, Y. Wang, R. E. Tanzi and M. Colonna (2017). "Alzheimer's disease-associated TREM2 variants exhibit either decreased or increased ligand-dependent activation." Alzheimers Dement **13**(4): 381-387.

Spillantini, M. G., R. A. Crowther, R. Jakes, M. Hasegawa and M. Goedert (1998). "alpha-Synuclein in filamentous inclusions of Lewy bodies from Parkinson's disease and dementia with lewy bodies." Proc Natl Acad Sci U S A **95**(11): 6469-6473.

Sudom, A., S. Talreja, J. Danao, E. Bragg, R. Kegel, X. Min, J. Richardson, Z. Zhang, N. Sharkov, E. Marcora, S. Thibault, J. Bradley, S. Wood, A. C. Lim, H. Chen, S. Wang, I. N. Foltz, S. Sambashivan and Z. Wang (2018). "Molecular basis for the loss-of-function effects of the Alzheimer's disease-associated R47H variant of the immune receptor TREM2." J Biol Chem **293**(32): 12634-12646.

Sun, M., M. Zhu, K. Chen, X. Nie, Q. Deng, L. D. Hazlett, Y. Wu, M. Li, M. Wu and X. Huang (2013). "TREM-2 promotes host resistance against Pseudomonas aeruginosa infection by suppressing corneal inflammation via a PI3K/Akt signaling pathway." Invest Ophthalmol Vis Sci **54**(5): 3451-3462.

Sun, S. W., H. F. Liang, K. Trinkaus, A. H. Cross, R. C. Armstrong and S. K. Song (2006). "Noninvasive detection of cuprizone induced axonal damage and demyelination in the mouse corpus callosum." Magn Reson Med **55**(2): 302-308.

Sunde, M., L. C. Serpell, M. Bartlam, P. E. Fraser, M. B. Pepys and C. C. Blake (1997). "Common core structure of amyloid fibrils by synchrotron X-ray diffraction." J Mol Biol **273**(3): 729-739.

Takahashi, K., C. D. Rochford and H. Neumann (2005). "Clearance of apoptotic neurons without inflammation by microglial triggering receptor expressed on myeloid cells-2." J Exp Med **201**(4): 647-657.

Takahashi, R. H., T. A. Milner, F. Li, E. E. Nam, M. A. Edgar, H. Yamaguchi, M. F. Beal, H. Xu, P. Greengard and G. K. Gouras (2002). "Intraneuronal Alzheimer abeta42 accumulates in multivesicular bodies and is associated with synaptic pathology." Am J Pathol **161**(5): 1869-1879.

Talafous, J., K. J. Marcinowski, G. Klopman and M. G. Zagorski (1994). "Solution structure of residues 1-28 of the amyloid beta-peptide." Biochemistry **33**(25): 7788-7796.

Taylor, J. P., J. Hardy and K. H. Fischbeck (2002). "Toxic proteins in neurodegenerative disease." Science **296**(5575): 1991-1995.

Terry, A. V. and J. J. Buccafusco (2003). "The Cholinergic Hypothesis of Age and Alzheimer's Disease-Related Cognitive Deficits: Recent Challenges and Their Implications for Novel Drug Development." **306**(3): 821-827.

Thornton, P., J. Sevalle, M. J. Deery, G. Fraser, Y. Zhou, S. Ståhl, E. H. Franssen, R. B. Dodd, S. Qamar, B. Gomez Perez-Nievas, L. S. Nicol, S. Eketjäll, J. Revell, C. Jones, A. Billinton, P. H. St George-Hyslop, I. Chessell and D. C. Crowther (2017). "TREM2 shedding by cleavage at the H157-S158 bond is accelerated for the Alzheimer's disease-associated H157Y variant." EMBO Molecular Medicine **9**(10): 1366-1378.

Thorsness, P. E. and D. E. J. J. o. B. C. Koshland (1987). "Inactivation of isocitrate dehydrogenase by phosphorylation is mediated by the negative charge of the phosphate." **262**(22): 10422-10425.

Ting-Beall, H. P., A. S. Lee and R. M. Hochmuth (1995). "Effect of cytochalasin D on the mechanical properties and morphology of passive human neutrophils." Ann Biomed Eng **23**(5): 666-671.

Turnbull, I. R., S. Gilfillan, M. Cella, T. Aoshi, M. Miller, L. Piccio, M. Hernandez and M. Colonna (2006). "Cutting Edge: TREM-2 Attenuates Macrophage Activation1." The Journal of Immunology **177**(6): 3520-3524.

Uddin, M. S., M. T. Kabir, M. S. Rahman, T. Behl, P. Jeandet, G. M. Ashraf, A. Najda, M. N. Bin-Jumah, H. R. El-Seedi and M. M. Abdel-Daim (2020). "Revisiting the Amyloid Cascade Hypothesis: From Anti-Aβ Therapeutics to Auspicious New Ways for Alzheimer's Disease." **21**(16): 5858.

Uhlén, M., L. Fagerberg, B. M. Hallström, C. Lindskog, P. Oksvold, A. Mardinoglu, Å. Sivertsson, C. Kampf, E. Sjöstedt, A. Asplund, I. Olsson, K. Edlund, E. Lundberg, S. Navani, C. A. Szigyarto, J. Odeberg, D. Djureinovic, J. O. Takanen, S. Hober, T. Alm, P. H. Edqvist, H. Berling, H. Tegel, J. Mulder, J. Rockberg, P. Nilsson, J. M. Schwenk, M. Hamsten, K. von Feilitzen, M. Forsberg, L. Persson, F. Johansson, M. Zwahlen, G. von Heijne, J. Nielsen and F. Pontén (2015). "Proteomics. Tissue-based map of the human proteome." Science **347**(6220): 1260419.

Ulland, T. K., W. M. Song, S. C.-C. Huang, J. D. Ulrich, A. Sergushichev, W. L. Beatty, A. A. Loboda, Y. Zhou, N. J. Cairns, A. Kambal, E. Loginicheva, S. Gilfillan, M. Cella, H. W. Virgin, E. R. Unanue, Y. Wang, M. N. Artyomov, D. M. Holtzman and M. Colonna (2017). "TREM2 Maintains Microglial Metabolic Fitness in Alzheimer's Disease." Cell **170**(4): 649-663.e613.

Utsumi, T., M. Sato, K. Nakano, D. Takemura, H. Iwata and R. Ishisaka (2001). "Amino acid residue penultimate to the amino-terminal gly residue strongly affects two cotranslational protein modifications, N-myristoylation and N-acetylation." J Biol Chem **276**(13): 10505-10513.

Venegas, C., S. Kumar, B. S. Franklin, T. Dierkes, R. Brinkschulte, D. Tejera, A. Vieira-Saecker, S. Schwartz, F. Santarelli, M. P. Kummer, A. Griep, E. Gelpi, M.

Beilharz, D. Riedel, D. T. Golenbock, M. Geyer, J. Walter, E. Latz and M. T. Heneka (2017). "Microglia-derived ASC specks cross-seed amyloid-β in Alzheimer's disease." Nature **552**(7685): 355-361.

Vilalta, A., Y. Zhou, J. Sevalle, J. K. Griffin, K. Satoh, D. H. Allendorf, S. De, M. Puigdellívol, A. Bruzas, M. A. Burguillos, R. B. Dodd, F. Chen, Y. Zhang, P. Flagmeier, L. M. Needham, M. Enomoto, S. Qamar, J. Henderson, J. Walter, P. E. Fraser, D. Klenerman, S. F. Lee, P. St George-Hyslop and G. C. Brown (2021). "Wild-type sTREM2 blocks Aβ aggregation and neurotoxicity, but the Alzheimer's R47H mutant increases Aβ aggregation." J Biol Chem **296**: 100631.

Vlastaridis, P., P. Kyriakidou, A. Chaliotis, Y. Van de Peer, S. G. Oliver and G. D. Amoutzias (2017). "Estimating the total number of phosphoproteins and phosphorylation sites in eukaryotic proteomes." Gigascience **6**(2): 1-11.

Walsh, D. M., I. Klyubin, J. V. Fadeeva, W. K. Cullen, R. Anwyl, M. S. Wolfe, M. J. Rowan and D. J. Selkoe (2002). "Naturally secreted oligomers of amyloid beta protein potently inhibit hippocampal long-term potentiation in vivo." Nature **416**(6880): 535-539.

Walsh, D. M. and D. J. Selkoe (2007). "A beta oligomers - a decade of discovery." J Neurochem **101**(5): 1172-1184.

Walter, J. (2016). "The Triggering Receptor Expressed on Myeloid Cells 2: A Molecular Link of Neuroinflammation and Neurodegenerative Diseases." J Biol Chem **291**(9): 4334-4341.

Wang, Y., M. Cella, K. Mallinson, J. D. Ulrich, K. L. Young, M. L. Robinette, S. Gilfillan, G. M. Krishnan, S. Sudhakar, B. H. Zinselmeyer, D. M. Holtzman, J. R. Cirrito and M. Colonna (2015). "TREM2 lipid sensing sustains the microglial response in an Alzheimer's disease model." Cell **160**(6): 1061-1071.

Wang, Y., T. K. Ulland, J. D. Ulrich, W. Song, J. A. Tzaferis, J. T. Hole, P. Yuan, T. E. Mahan, Y. Shi, S. Gilfillan, M. Cella, J. Grutzendler, R. B. DeMattos, J. R. Cirrito, D. M. Holtzman and M. Colonna (2016). "TREM2-mediated early microglial response limits diffusion and toxicity of amyloid plaques." J Exp Med **213**(5): 667-675.

Wang, Y., R. Yang, J. Gu, X. Yin, N. Jin, S. Xie, Y. Wang, H. Chang, W. Qian, J. Shi, K. Iqbal, C. X. Gong, C. Cheng and F. Liu (2015). "Cross talk between PI3K-AKT-GSK-3β and PP2A pathways determines tau hyperphosphorylation." Neurobiol Aging **36**(1): 188-200.

Wang, Y. C., S. E. Peterson and J. F. Loring (2014). "Protein post-translational modifications and regulation of pluripotency in human stem cells." Cell Res **24**(2): 143-160.

Ward, R. J., F. A. Zucca, J. H. Duyn, R. R. Crichton and L. Zecca (2014). "The role of iron in brain ageing and neurodegenerative disorders." The Lancet. Neurology **13**(10): 1045-1060.

Weids, A. J., S. Ibstedt, M. J. Tamás and C. M. Grant (2016). "Distinct stress conditions result in aggregation of proteins with similar properties." Scientific Reports **6**(1): 24554.

Weissmann, C. (1999). "Molecular genetics of transmissible spongiform encephalopathies." J Biol Chem **274**(1): 3-6.

Wirths, O., G. Multhaup, C. Czech, V. Blanchard, S. Moussaoui, G. Tremp, L. Pradier, K. Beyreuther and T. A. Bayer (2001). "Intraneuronal Abeta accumulation precedes plaque formation in beta-amyloid precursor protein and presenilin-1 double-transgenic mice." Neurosci Lett **306**(1-2): 116-120.

Wulhfard, S., L. Baldi, D. L. Hacker and F. Wurm (2010). "Valproic acid enhances recombinant mRNA and protein levels in transiently transfected Chinese hamster ovary cells." J Biotechnol **148**(2-3): 128-132.

Wunderlich, P., K. Glebov, N. Kemmerling, N. T. Tien, H. Neumann and J. Walter (2013). "Sequential proteolytic processing of the triggering receptor expressed on myeloid cells-2 (TREM2) protein by ectodomain shedding and gamma-secretase-dependent intramembranous cleavage." J Biol Chem **288**(46): 33027-33036.

Yan, S. D., X. Chen, J. Fu, M. Chen, H. Zhu, A. Roher, T. Slattery, L. Zhao, M. Nagashima, J. Morser, A. Migheli, P. Nawroth, D. Stern and A. M. Schmidt (1996). "RAGE and amyloid-β peptide neurotoxicity in Alzheimer's disease." Nature **382**(6593): 685-691.

Yin, Z., S. Wang, B. Shen, C. Deng, Q. Tu, Y. Jin, L. Shen, B. Jiao and J. Xiang (2019). "Coimmunocapture and Electrochemical Quantitation of Total and Phosphorylated Amyloid-β(40) Monomers." Anal Chem **91**(5): 3539-3545.

Yu, Y., D. C. Jans, B. Winblad, L. O. Tjernberg and S. Schedin-Weiss (2018). "Neuronal Aβ42 is enriched in small vesicles at the presynaptic side of synapses." Life Sci Alliance **1**(3): e201800028.

Zhan, Y., R. C. Paolicelli, F. Sforazzini, L. Weinhard, G. Bolasco, F. Pagani, A. L. Vyssotski, A. Bifone, A. Gozzi, D. Ragozzino and C. T. Gross (2014). "Deficient neuron-microglia signaling results in impaired functional brain connectivity and social behavior." Nature Neuroscience **17**(3): 400-406.

Zhang, S., K. Iwata, M. J. Lachenmann, J. W. Peng, S. Li, E. R. Stimson, Y. Lu, A. M. Felix, J. E. Maggio and J. P. Lee (2000). "The Alzheimer's peptide a beta adopts a collapsed coil structure in water." J Struct Biol **130**(2-3): 130-141.

Zhao, Y., X. Wu, X. Li, L.-L. Jiang, X. Gui, Y. Liu, Y. Sun, B. Zhu, J. C. Piña-Crespo, M. Zhang, N. Zhang, X. Chen, G. Bu, Z. An, T. Y. Huang and H. Xu (2018). "TREM2 Is a Receptor for β-Amyloid that Mediates Microglial Function." Neuron **97**(5): 1023-1031.e1027.

Zhao, Y., X. Wu, X. Li, L. L. Jiang, X. Gui, Y. Liu, Y. Sun, B. Zhu, J. C. Pina-Crespo, M. Zhang, N. Zhang, X. Chen, G. Bu, Z. An, T. Y. Huang and H. Xu

(2018). "TREM2 Is a Receptor for beta-Amyloid that Mediates Microglial Function." Neuron **97**(5): 1023-1031.e1027.

Zhong, L., X.-F. Chen, T. Wang, Z. Wang, C. Liao, Z. Wang, R. Huang, D. Wang, X. Li, L. Wu, L. Jia, H. Zheng, M. Painter, Y. Atagi, C.-C. Liu, Y.-W. Zhang, J. D. Fryer, H. Xu and G. Bu (2017). "Soluble TREM2 induces inflammatory responses and enhances microglial survival." The Journal of experimental medicine **214**(3): 597-607.

Zhong, L., X. F. Chen, T. Wang, Z. Wang, C. Liao, Z. Wang, R. Huang, D. Wang, X. Li, L. Wu, L. Jia, H. Zheng, M. Painter, Y. Atagi, C. C. Liu, Y. W. Zhang, J. D. Fryer, H. Xu and G. Bu (2017). "Soluble TREM2 induces inflammatory responses and enhances microglial survival." J Exp Med **214**(3): 597-607.

Zhong, L., Z. Wang, D. Wang, Z. Wang, Y. A. Martens, L. Wu, Y. Xu, K. Wang, J. Li, R. Huang, D. Can, H. Xu, G. Bu and X.-F. Chen (2018). "Amyloid-beta modulates microglial responses by binding to the triggering receptor expressed on myeloid cells 2 (TREM2)." Molecular Neurodegeneration **13**(1): 15.

Zhong, L., Y. Xu, R. Zhuo, T. Wang, K. Wang, R. Huang, D. Wang, Y. Gao, Y. Zhu, X. Sheng, K. Chen, N. Wang, L. Zhu, D. Can, Y. Marten, M. Shinohara, C.-C. Liu, D. Du, H. Sun, L. Wen, H. Xu, G. Bu and X.-F. Chen (2019). "Soluble TREM2 ameliorates pathological phenotypes by modulating microglial functions in an Alzheimer's disease model." Nature Communications **10**(1): 1365.

Zitzmann, J., C. Schreiber, J. Eichmann, R. O. Bilz, D. Salzig, T. Weidner and P. Czermak (2018). "Single-cell cloning enables the selection of more productive Drosophila melanogaster S2 cells for recombinant protein expression." Biotechnol Rep (Amst) **19**: e00272.